Strål
säkerhets
myndigheten
Swedish Radiation Safety Authority

Authors: Peter Robinson
Philip Maul
Claire Watson

Research

2010:18

Radionuclide Transport: Preparation During 2009 for the SR-Site Review

Report number: 2010:18 ISSN: 2000-0456
Available at www.stralsakerhetsmyndigheten.se

Title: Radionuclide Transport: Preparation During 2009 for the SR-Site Review.
Report number: 2010:18
Author: Peter Robinson, Philip Maul and Claire Watson
Quintessa Ltd. UK
Date: December 2009

This report concerns a study which has been conducted for the Swedish Radiation Safety Authority, SSM. The conclusions and viewpoints presented in the report are those of the author/authors and do not necessarily coincide with those of the SSM.

SSM Perspective

Background

Post-closure safety assessments for nuclear waste repositories involve radioecological modelling for an underground source term. Following several decades of research and development, the Swedish Nuclear Waste Management Company (SKB) is approaching a phase of license application. According to SKB's plans, an application to construct a geological repository will be submitted by the end of 2010. The application will be supported by a post-closure safety assessment. In order to prepare for the review of the oncoming license application the Swedish Radiation Safety Authority (SSM), has performed research and development projects in the area of performance assessment (PA) modelling during recent years. Independent modelling teams have been established, including both "in house" as well as consultant's competences.

Quintessa have undertaken research and development for the Swedish regulatory authorities over many years. This has included the development of approaches and models for consequence analysis (radionuclide transport) that can be used to support the review of submissions from SKB.

Objectives of the project

SSM held a workshop at Rånäs Castle from 18 – 20 February 2009 to discuss the status of Consequence Analysis capabilities and to plan for preparatory work in the current year. Out of this meeting and subsequent discussions, four areas were identified where further research during 2009 would be beneficial:

1. spatially varying transport properties;
2. choices of PDFs (probability density functions) and parameter correlations;
3. SKB's approach to quantifying the role of the various barriers; and
4. combining scenarios.

This report documents the research that was undertaken.

Project information

Project manager: Shulan Xu
Project reference: SSM 2009/2090
Project number: 1692

Summary

SSM held a workshop at Rånäs Castle in February 2009 to discuss the status of Consequence Analysis capabilities and to plan for preparatory work in the current year. Out of this meeting and subsequent discussions, four areas were identified where further research during 2009 would be beneficial:

- spatially varying transport properties;
- choices of PDFs (probability density functions) and parameter correlations;
- combining scenarios; and
- SKB's approach to quantifying the role of the various barriers.

This report documents the research that was undertaken.

The most important findings for consequence analysis and the conduct of the SR Site review are listed here.

In the study of spatially varying properties, the following conclusions were made.

- The SKB F-factor approach is exact only in the case of a single nuclide, constant matrix properties and no dispersion. Compared to other sensitivities, the effect of dispersion for Peclet numbers 10 and higher is small.
- Output fluxes are highly sensitive to the F-factor itself, but not to the water travel time. Matrix penetration depth can be important if it is small, (less than about 10 cm in the cases considered here). The retention and porosity in the matrix have a direct proportional effect on peak releases for the single sorbed nuclide.
- Varying matrix retention properties along a flow path can be handled exactly for a single nuclide, a result that SKB may be unaware of.
- The main approximation that can occur with the F-factor approach is in the use of constant matrix retention properties for a chain case. When there are short-lived daughters, their output fluxes are strongly influenced by the matrix retention properties at the end of the path rather than by any overall average.
- Cases using path lines generated using SSM's independent discrete feature model showed that the EDZ can dominate the F-factor for many release points. In such cases, the properties of this EDZ control the output flux. The approach that SKB take to the EDZ in SR Site should be a focus for review. The relevance of such

issues will depend on which canister failure scenarios are considered – if failures can only occur by buffer erosion then this is likely to be where flows are at their highest and path lines from such location may not pass through the EDZ.

For the study of PDFs, key parameters have been reviewed for the source-term, near-field and geosphere. The following conclusions were reached.

- A key issue for the release overall is the resistance of the buffer-fracture interface. The importance of this process is well-known and must continue to be a focus for the review. It is more important than the transport resistance offered by the buffer as a diffusive barrier. In particular, results are rather insensitive to details of the near-field sorption properties.

- Of the near-field parameters, the initial release fractions (IRFs) had the biggest impact on the result; using the alternative conservative values resulted in an order of magnitude increase in the peak dose (both near-field and total).

- Fuel dissolution rates are significant for later releases. Near-field doses are more sensitive to the fuel dissolution rate distributions than to solubility limit distributions.

- The use of uncorrelated radionuclide solubilities had no discernable effect on the dose; and the use of sorption coefficients for bentonite in saline and non-saline groundwaters caused approximately a factor of 2 reduction in the peak dose.

- In the far-field, the uncertainty is likely to be dominated by conceptual model uncertainty (e.g. different discrete feature models) leading to different flow distributions.

- The effects of reducing the matrix K_d value for Ra were considered for both a small and a sampled (effectively infinite) matrix penetration depth. In both cases the smaller sorption coefficient led to a smaller total dose.

The SKB calculations for the role of the various barriers presented in SR-Can have been satisfactorily reproduced, confirming that the basis for these calculations is adequately understood. In particular, the following conclusions were reached.

- The calculations emphasise the key role played by the copper shells in SKB's safety case, but this depends on the calculated slow rate of copper corrosion in repository conditions.

- As previously documented, the role of the buffer as a barrier to radionuclide transport is minor compared with the other barriers. The case presented has just

the transport resistance of the buffer neglected; a case with no buffer would behave very differently.

- With other barriers in place radionuclide retention in the geosphere is less important than other barriers, but when other barriers fail, this can be important in keeping calculated consequences to levels that are comparable with background radiation. In these cases, modelling of fuel dissolution can become much more important.

Looking at the impact of combined scenarios, the following conclusion was reached.

- A combined pinhole and erosion scenario could give spike releases of a factor 3 higher than pinhole alone.

Contents

1 Introduction

Quintessa have undertaken research and development for the Swedish regulatory authorities over many years. This has included the development of approaches and models for consequence analysis (radionuclide transport) that can be used to support the review of submissions from SKB. Independent calculations in support of the regulatory review of SKB's SR-Can assessment (SKB, 2006, henceforth referred to as the SR-Can main report) using the AMBER software are described in Maul et al. (2008). Further work undertaken in 2008 was reported by Maul and Robinson (2008); this included the use of software based on Quintessa's general purpose modelling code QPAC, referred to as QPAC-TRAN.

With the expected submission of SKB's SR-Site documentation in support of a licence application at the end of 2010, the focus for consequence analysis in 2009 has been further preparation for SSM's review.

SSM held a workshop (Wilmot, 2009) at Rånäs Castle from 18 – 20 February 2009 to discuss the status of Consequence Analysis capabilities and to plan for preparatory work in the current year. Out of this meeting and subsequent discussions, four areas were identified where further research during 2009 would be beneficial:

1. spatially varying transport properties;
2. choices of PDFs (probability density functions) and parameter correlations;
3. SKB's approach to quantifying the role of the various barriers; and
4. combining scenarios.

This report documents the research that was undertaken.

In Section 2 some previously undertaken radionuclide transport calculations relevant to the present work are summarised. Progress in each of the four technical areas is discussed in turn in Sections 3 to 6. Section 7 brings together some conclusions.

2 Previous AMBER and QPAC-TRAN Calculations

2.1 The SR-Can Calculations

Maul et al. (2008) described two types of calculation, mainly using the AMBER code: calculations aimed at reproducing SKB's radionuclide transport calculations, and calculations using independent geosphere data. The first set of calculations is most relevant for the topics considered in the present report.

2.1.1 The Pinhole Failure Mode

The Pinhole Failure mode is not considered likely to occur by SKB, but it has been studied in detail in previous assessments (including SR-97) and provided information that is relevant to calculations for other potential failure modes. In effect the pinhole failure mode provided a 'reference' set of calculations.

Figure 1 gives details of the modelling blocks used in the near field, some of which are broken down into a number of compartments. The pathway Q4 was not considered by SKB in the SR-Can assessment, as it was assumed to be less important than the other pathways.

Figure 1: Discretisation of the Near Field

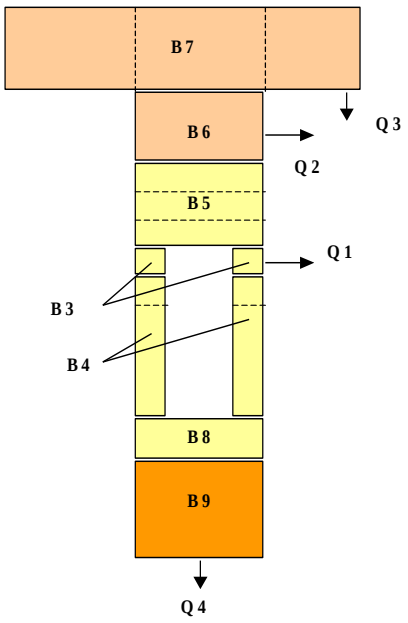

Some of the issues noted in implementing the SKB model in AMBER included:

- Some of the flow resistances were defined as the reciprocal of **equivalent flow rates**. Due to lack of clarity in the SKB documentation it was not clear whether the AMBER implementation was totally compatible with the calculations presented in SR-Can, particularly for the Q3 pathway.

- It is understood that the **diffusive transport resistance** at the buffer/rock interface was neglected by SKB when spalling takes place, although it was not clear why this was considered to be appropriate.

- **Advective flows** were included in the **tunnel** (only diffusive flows were included in the Quintessa SR-97 Case File). The details of the parameter values used by SKB to represent this process were not totally clear from the SR-Can documentation, so it is not clear whether the approach taken in the AMBER implementation mirrored that employed by SKB.

- SKB used **data 'triples'** for the correlated parameters F, t_w and Q_{eq} . Sample files proved by SKB were used directly for probabilistic calculations. It is understood that the data in these sample files did not include a factor of 10 division referred to on page 407 of the main SR-Can report (SKB, 2006a) to account for channelling effects.

- SKB used **correlated sorption coefficients**. Values of K_d for elements (in a given redox state) in the same correlation group are correlated. The way that these correlations were implemented was not stated explicitly in the SR-Can documentation.

The following simplifications were made in the AMBER implementation:

1. The same geosphere transport parameters were taken for each of the transport pathways Q1, Q2 and Q3 when all the pathways are considered together. Alternatively, each pathway could be considered separately. To provide different geosphere parameters for the different pathways would require significant changes to the structure of the AMBER model. This issue can be addressed using QPAC-TRAN.

2. Reducing conditions were assumed throughout, and this determined the chemical form assumed for some elements that can be in more than one redox state.

The deterministic calculations presented by SKB were for Forsmark. Other than the biosphere dose factors, the only parameters that would differ between the two sites

would be the matrix porosity in the geosphere and the formation factors used in the calculation of effective diffusivities in the rock matrix. These differences are small, and so separate AMBER calculations were not been undertaken for Laxemar. Subsequently, Forsmark was chosen as SKB's preferred site.

Good agreement was obtained between the AMBER and SKB deterministic and probabilistic calculations, although some uncertainties remained because of the shortcomings in the SKB documentation and because associated deterministic calculations were not presented for each of the probabilistic calculations considered.

Because these calculations for Forsmark are later taken as 'reference' calculations, the probabilistic calculations with a log-triangular distribution for the fuel dissolution rate are summarised here.

Figure 2 shows AMBER probabilistic calculations obtained with 4000 samples with just pathway Q1 modelled. The run time for such calculations is about two days. This figure can be compared with Figure 10-20 in the SR-Can main report. The overall features are very similar for times up to about 10^4 y, but at longer timescales the AMBER values for the mean and 99th percentile are around an order of magnitude higher than the SR-Can values.

Figure 3 shows the contribution to the mean dose from the key radionuclides. This figure compares well with Figure 10-18 in the SR-Can main report, although the doses from Ra-226 and Pb-210 are somewhat higher at long times. The Pb-210 dose calculated by AMBER is not obtained in the SR-Can calculations because SKB do not model this radionuclide in the near field and geosphere; it is not clear that this will necessarily be an appropriate approximation for all possible parameter values in probabilistic calculations.

In Figure 10-19 of the SR-Can main report SKB gives dose calculations based on fluxes from the near field. Corresponding AMBER calculations are given in Figure 4, and the results compare very closely.

Figure 2: AMBER Probabilistic Calculations for Biosphere Doses for Forsmark

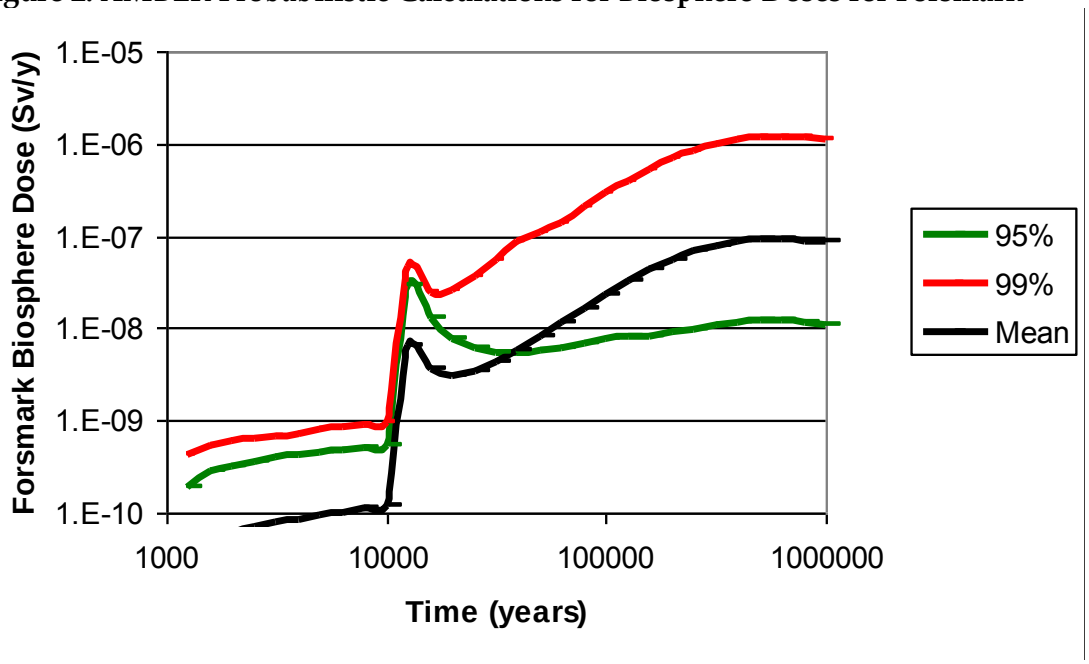

Figure 3: AMBER Probabilistic Calculations for Biosphere Doses for Forsmark - Key Radionuclides

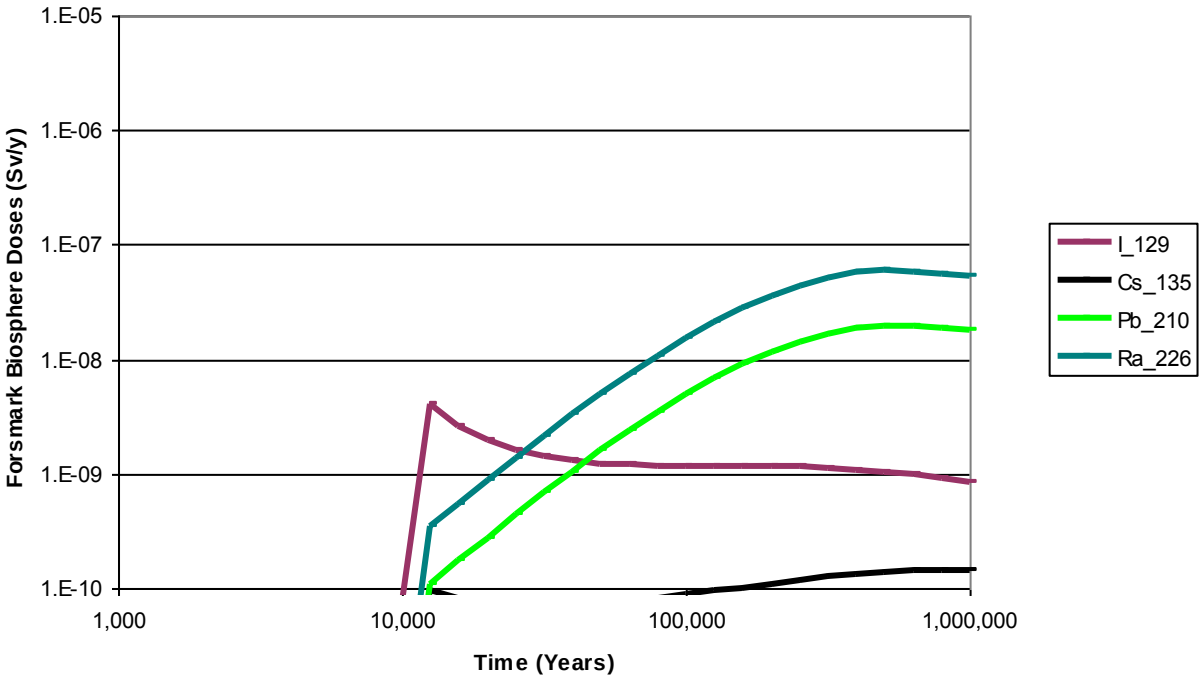

Figure 4: AMBER Probabilistic Calculations for "Near Field Doses" for Forsmark for Pathway Q1

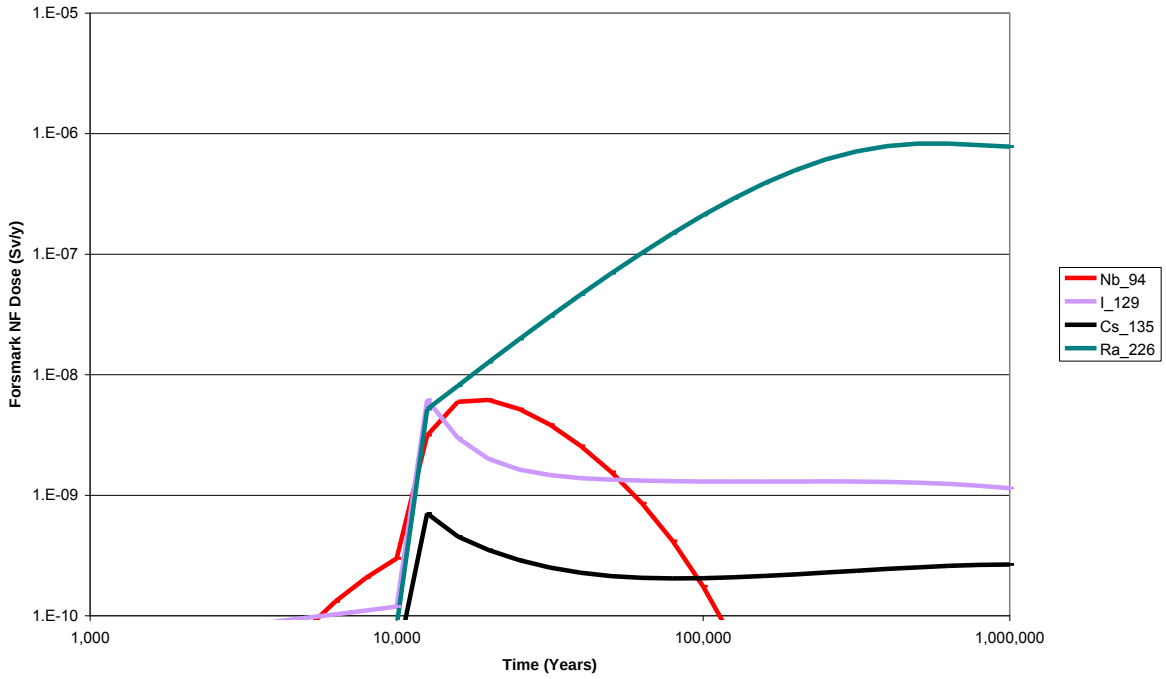

2.1.2 The Lost Buffer Failure Mode

In this failure mode the canister was assumed to fail at a specified time and there was then an additional delay before the resistance to radionuclide transport from the canister is assumed to fall to zero. The calculations for this failure mode were actually much simpler and quicker to reproduce in AMBER than for the pinhole failure mode because there is no radionuclide transport in the buffer.

The following issues arose in comparing the AMBER and SKB calculations:

- SKB spread the period over which the instantaneous release fractions for Ni-59 and Nb-94 left the canister once failure occurred. This change was not reproduced in the AMBER calculations.

- The calculations reported in the main SR-Can report were for a high equivalent flow rate, Q_{eq}, although this was not made clear in the documentation, and no value was given.

- Figure 10-41 of the SR-Can report gives modified (analytical) calculations with Th retained in the canister, and these were compared with the full numerical calculation in Figure B-1 of the same report. SKB indicated in Section 10.6.5 of the SR-Can report that radionuclide in-growth was not included for this failure mode

(although it is not clear why). As a result, if co-precipitation of Th occurs in the canister, more Ra-226 will be released. This is an example of where it is not straightforward to identify conservative assumptions in systems as complex as the one being modelled here. Effectively reducing the solubility of Th results in higher doses, which may not necessarily have been expected. AMBER calculations were undertaken where the solubility of all Th isotopes was reduced to effectively zero and the resulting calculations were similar, but not identical to the SKB calculations.

- Based on the discussion given in Appendix B of the SR-Can main report, it appears that SKB's probabilistic calculations for the lost buffer failure mode used the alternative model where Th-230 is retained in the canister, but this was not totally clear.

- The risks calculated from this failure mode depend critically on two key inputs: the specified canister failure times and the assumed fuel dissolution rate. The first failure time calculated by SKB was not until nearly 500, 000 years at Forsmark. By this time most of the original inventory has decayed, and this is the main reason why the calculated risks are compatible with the relevant regulatory criterion.

2.1.3 Mechanical Failure Modes

Two such modes were considered by SKB. AMBER calculations were not undertaken to reproduce the SR-Can calculations for the Shear Movement failure, because it was considered that little additional insight would be gained beyond that obtained for the pinhole and advective failure modes; the risk calculations depend primarily on the probabilities assumed for the event happening.

Similarly, the consequences of the Isostatic Load failure mode can be assessed from the calculations produced for the pinhole failure mode, so no additional AMBER calculations were undertaken.

2.2 Additional Calculations undertaken in 2008

The developments described by Maul and Robinson (2008) included:

- The use of the Quintessa's QPAC code with a radionuclide transport module (referred to as QPAC-TRAN). QPAC is able to represent a wider range of transport processes than is possible with AMBER and this broadens the range of issues that can be addressed. One important assumption in this module is that the interface area between two compartments is taken to be the area that is actually in common for the relevant faces of the compartments. This is considered to be the

most physically-appropriate assumption, but does not correspond to that employed in the SR-Can assessment (and the AMBER calculations that reproduced these calculations) where a transport resistance approach was used with the net resistance being taken to be the average for the two compartments; this can imply a different effective interface area from that employed in QPAC-TRAN, and this resulted in small differences between AMBER and QPAC-TRAN calculations.

- An improved approach to discretisation in the geosphere was described which should improve the accuracy of radionuclide transport calculations and reduce computing run times.

AMBER remains a convenient and powerful tool for many types of calculation, particularly where probabilistic calculations are required. It is anticipated, however, that the wider range of problems that can be addressed using codes based on QPAC, and the flexibility provided by the use of file-based input, will mean that this will increasingly be used for addressing detailed radionuclide transport issues.

2.3 Current Knowledge on Important Features of the PA

From the work described above and published work by, for example, Hedin (2003) the following key features of the performance of the KBS3_V are well understood:

- Once canister corrosion has taken place the transport of radionuclides into the geosphere is critically dependent on the characteristics of the buffer/rock interface; this is much more important than the characteristics of the buffer itself, such as bentonite sorption coefficients.

- The rate of transport through the geosphere depends critically on the conceptual model for the processes involved, particularly for the sorption of long-lived radionuclides in the rock matrix; very different results can be obtained with different models.

These topics are not the focus of the current work, but sensitivity to the buffer/rock interface transport resistance is discussed in Section 4.4 and the question of sorption in the rock matrix is consider in Sections 3.4.5 and 4.4.

3 Spatially Varying Transport Properties

3.1 Introduction

SKB have used a one-dimensional transport modelling approach for many years and it is expected that this will continue to be their main approach in SR-Site. This approach follows path-lines, calculated in a flow code, from a deposition hole to the near-surface environment.

Transport along this path is governed by advection and dispersion, radioactive decay and ingrowth, equilibrium sorption and matrix diffusion. SKB have argued that the matrix diffusion effects can be parameterised through the single F factor (Elert et al, 2004). The argument supporting this claim is quite restricted in its scope – being valid only for transport through homogeneous matrix material with constant penetration depth (i.e. varying fracture apertures and flow velocities along the path are allowed but not varying matrix properties). There are, however, many cases where parts of the flow path are through different materials, e.g. tunnel infill and/or near-surface soil layers. In these cases, the level of inaccuracy in taking averaged properties and a single F value is unclear. With the possible use of the MARFA code (as yet undocumented) in SR-Site, SKB will have the capability to undertake the radionuclide transport calculations more accurately, but this will not be their main assessment route.

The purpose of this task was to look at the sensitivity of transport calculations to the assumptions underlying the use of the F-factor. This was done by looking at the basic assumptions that underlie the F factor concept and by comparing solutions using the F factor approach to those obtained by splitting a path into separate parts for the different materials that it travels through.

3.2 The SKB Approach and Justification

The approach used for radionuclide transport in the geosphere in SR-Can is summarised in Section 10.4.2 of the main SR-Can report (SKB, 2006a). This refers to the documentation for the FARF31 code (Elert et al, 2004) for details. Figure 5 shows the modelled system as depicted by Elert et al. A very similar figure appears in the SKI Project-90 report (SKI, 1991, Figure 4.8.1). The CRYSTAL code was developed by SKI to calculate one-dimensional transport in these systems (Worgan and Robinson, 1995).

Figure 5: Matrix diffusion in the micro-fissures in the rock matrix (from Elert, 2004)

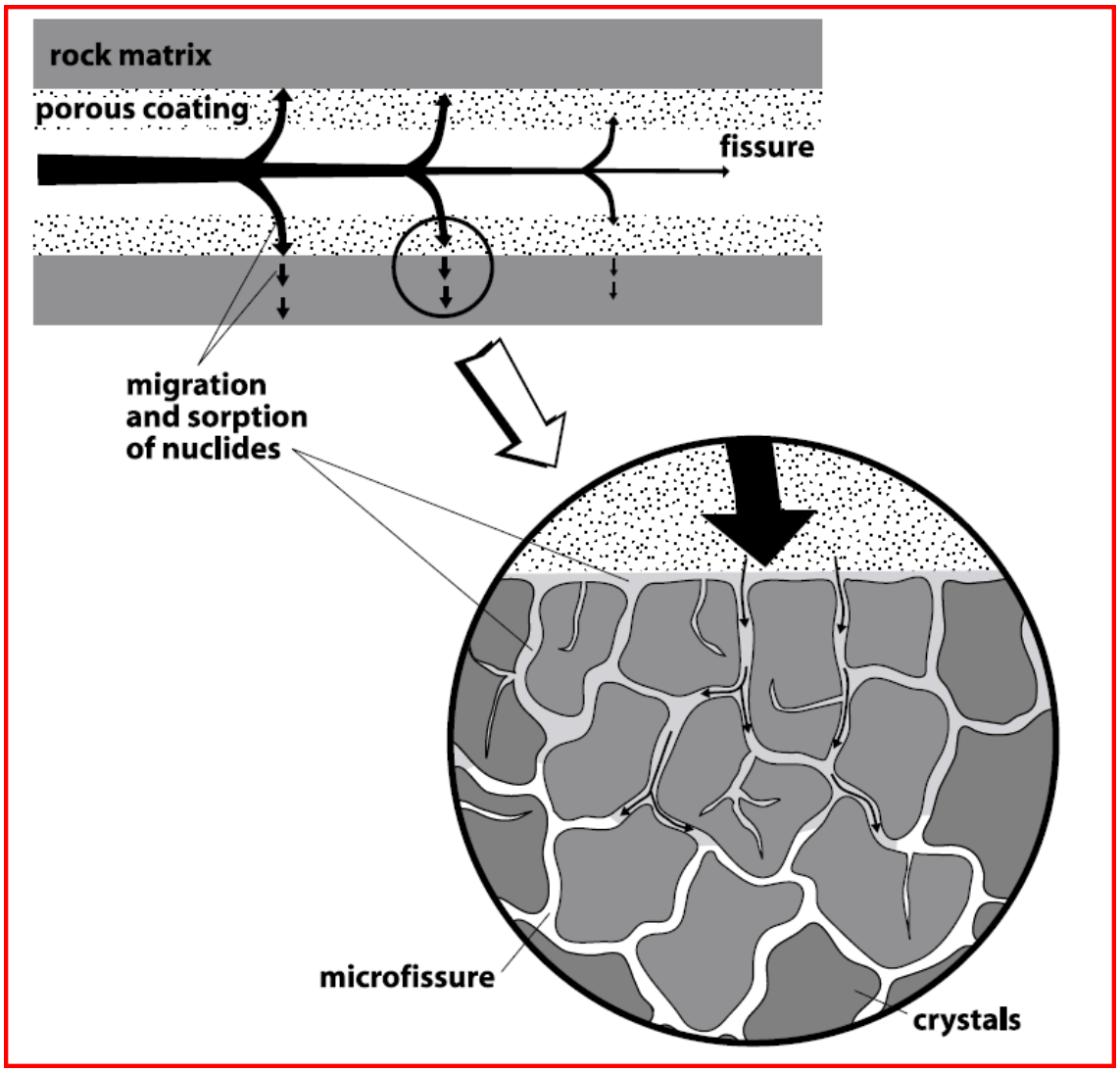

It is stated by Elert et al (2004) that the DFN (discrete fracture network) calculations calculate the advective travel time (t_w) and the transport resistance (F) and that FARF31 uses these inputs directly. The European RETROCK project (RETROCK, 2005) is quoted and provides a useful summary, noting that the Posiva and SKB definitions of F differ by a factor of 2. The F-factor is defined by SKB as the integral over time of the flow wetted surface (per unit volume of water) along the path line and hence has units of y m^{-1}.

Limitations of the migration path concept are said to be that it is restricted to time-invariant flow fields and that "*with the current utilisation of the F-factor integrated over the migration path as an input parameter the solution is formally correct for single-member decay chains only. For longer decay chains, use of the integrated parameter F is strictly not correct if the channel width to flow ratio varies in space.*"

The FARF31 report (Elert et al, 2004) gives the equations that are solved and indicates that averages are required along the path. It seems to take for granted that an appropriate average F value along the path can be calculated.

The SR-Can data report (SKB, 2006b) records how the F and t_w parameters are calculated, but does not discuss the assumptions that underlie this. This report also makes it clear that parts of the flow path in the tunnels or EDZ are excluded from the calculation.

For a discussion of the underlying assumptions it is necessary to go back to Andersson et al (1998) and Selroos and Cvetkovic (1996).

Andersson et al (1998) clearly state that "*for the simple case with no dispersion and matrix diffusion into an infinite matrix … the sum of the F-quotients determines the transport as long as $D_{m,i}$ [matrix diffusivity] and $K_{d,i}$ [matrix sorption] are constant*". They go on to state that "*In SR-97 this [the constant diffusion and matrix properties] will also be assumed to be the case*" but that "*generally also $D_{m,i}$ and $K_{d,i}$ vary along the flow path and the proper averaging must preserve the u value [a lumped parameter in the analytic solution] rather than the F-value*". Furthermore, "*the extension is less straight-forward for cases with important dispersion in the fracture or a finite penetration depth*".

Selroos and Cvetkovic (1996) provide a more technical analysis but take the same approach (they denote the F-factor as β).

Posiva have also adopted the F-factor approach, although they use the terminology WL/Q, where W is the fracture width (orthogonal to the flow), L is the path length and Q is the flow rate; this is equal to half of the F-factor as SKB would define it. A recent Posiva assessment (Smith et al, 2007) states that there has been no fundamental change in the Posiva approach since TILA-99.

In summary, the limitations of the F-factor approach were clear when it was first introduced. However, the approach is now used without comment for situations where these limitations are not respected. Although the approach may well remain a good approximation (particularly in the context of the uncertainties that exist in the precise values of the relevant geosphere properties) this has not been demonstrated. The purpose of the current work is to explore whether there are any significant errors that arise when using the F-factor approach for a general system.

In the following section, the governing equations are stated and some analytic results are derived to show where the F-factor arises and when it is valid to integrate along a flow path. Some numerical calculations are then performed to indicate the level of approximation that arises when the F-factor is used beyond where it is strictly valid.

3.3 Mathematical Basis

The various reports that have been referred to above all use slightly different notations. Here, we endeavour to define all the terms that we use as they are introduced and summarise them in a table in Appendix A.

We start by defining the general system of governing equations that we will consider. Simplified versions of these will then be considered.

3.3.1 The Full Set of Transport Equations

Conceptually, we consider transport along a one-dimensional flow tube. The water velocity along the flow tube can vary, but the total flow rate along the tube is constant. There is exchange between neighbouring flow paths which manifests itself as longitudinal dispersion within the flow tube of interest. Moreover, this exchange ensures a constant concentration across a fracture and each flow tube sees its share of the rock matrix surfaces for sorption and matrix diffusion. In practice this means that we can assume that the flow tube extends across the full aperture of each fracture but is of varying width, consistent with the local pore velocity in the fracture. We assume that the fractures are open and planar.

The governing equation for transport along the flow tube can then be written

$$R_f^n \frac{\partial C_f^n}{\partial t} = D_f^n \frac{\partial^2 C_f^n}{\partial x^2} - v \frac{\partial C_f^n}{\partial x} - \lambda^n R_f^n C_f^n + \lambda^{n-1} R_f^{n-1} C_f^{n-1} + \delta_f D_m^n \frac{dC_m^n}{dz}\bigg|_{z=0} \qquad (3.1)$$

where

t is the time [y]

x is the distance along the flow tube [m]

C_f^n is the concentration of nuclide n in the flowing water [moles/m^3]

R_f^n is the retardation (due to surface sorption if any) of nuclide n [-]

D_f^n is the dispersion/diffusion coefficient for nuclide n. $D_f^n = \frac{vL}{Pe} + D_{eff}^n$ [m^2/y]

L is the path length [m]

Pe is the Peclet number, taken here to represent dispersion only [-]

D_{eff}^n is the effective diffusion coefficient for nuclide n, which in an open fracture would be equal to the pore water diffusion coeffcient [m²/year]

v is the water velocity [m/year]

λ^n is the decay constant for nuclide n [per year]

δ_f is the specific surface area of matrix (i.e. area per unit volume of flowing water) [m²/m³]

C_m^n is the concentration of nuclide n in the matrix water [moles/m³]

z is the distance into the rock matrix [m]

D_m^n is matrix effective diffusion coefficient for nuclide n [m²/y] .

The retardation can be calculated from the sorption parameters, using

$$R_f^n = 1 + \delta_f (1 - \varepsilon_m) K_{a,m}^n \tag{3.2}$$

where,

ε_m is the matrix porosity [-]

$K_{a,m}^n$ is the area-based sorption coefficient of nuclide n for the matrix [m³/m²].

For a planar fracture, the specific surface area is simply derived from the aperture:

$$\delta_f = \frac{2}{h} \tag{3.3}$$

where,

h is the fracture aperture [m].

Note that half-apertures are sometimes used in formulating these equations, with consequent changes by factors of 2. This is the source of the difference between SKB's and Posiva's definitions.

In general the parameters can be spatially varying.

Implicit in this formulation is the flow rate along the flow tube, Q [m³/y], from which the width of the flow tube, w [m] can be derived:

$$w = \frac{Q}{vh}. \tag{3.4}$$

Within the rock matrix, a diffusion equation applies

$$\varepsilon_m R_m^n \frac{\partial C_m^n}{\partial t} = D_m^n \frac{\partial^2 C_m^n}{\partial z^2} - \lambda^n \varepsilon_m R_m^n C_m^n + \lambda^{n-1} \varepsilon_m R_m^{n-1} C_m^{n-1} \tag{3.5}$$

where

R_m^n is the retention factor in the matrix of nuclide n [-]

The matrix retention of nuclide n can be calculated from the sorption parameters, using

$$R_m^n = 1 + \frac{(1-\varepsilon_m)}{\varepsilon_m} \rho_m K_{d,m}^n, \tag{3.6}$$

where

ρ_m is the matrix grain density [kg/m^3]

$K_{d,m}^n$ is the matrix sorption coefficient of nuclide n [m^3/kg].

To complete the equations initial and boundary conditions are required. Initially, all the concentrations are zero. The boundary conditions for the flow tube can take various forms, but we will assume that a flux is specified at x=0,

$$hw\left[vC_f^n - D_f^n \frac{dC_f^n}{dx} \right]_{x=0} = G_{in}^n. \tag{3.7}$$

Here G_{in}^n has units of mol/y. At the far end, L [m], either a zero concentration or zero gradient condition is assumed depending on the situation. No downstream condition is necessary if there is no diffusion or dispersion.

For the matrix, the concentration at the fracture equals that of the flowing water

$$\left[C_m^n\right]_{z=0} = C_f^n, \tag{3.8}$$

and there may be a limited penetration depth, a_m [m], for the diffusion where

$$\left[\frac{dC_m^n}{dz} \right]_{z=a_m} = 0, \tag{3.9}$$

which becomes redundant if an infinite matrix is assumed, being replaced by a condition that the concentration tends to zero at infinity.

The result of interest is the flux at the far end of the path:

$$G_{out}^{n} = hw\left[vC_f^n - D_f^n \frac{dC_f^n}{dx} \right]_{x=L}, \tag{3.10}$$

again with units of mol/y. Note that in practice the value of the total flow rate for the flow tube, Q, need not be specified. It cancels out because the equations are all linear and only fluxes are of interest.

3.3.2 Single Nuclide Advection with Constant Properties and Infinite Matrix

In the case of a single nuclide, the ingrowth terms in (3.1) and (3.5) are irrelevant. Disregarding diffusion and dispersion in the flow tube makes (3.1) first order and leaves no place for a downstream boundary condition. Assuming constant properties simplifies the solution. The assumption of an infinite matrix makes the solution particularly simple and is the starting point for seeing where the F-factor arises.

Here, and in later sections, we shall use a Laplace Transform approach to solving the equations. This is the approach used in FARF31 by SKB. When it is necessary to produce time-domain solutions, we will use Talbot's algorithm (Talbot, 1979; Robinson and Maul, 1991) to invert the Laplace Transform. This is also used by FARF31 and provides an essentially exact result.

The Laplace transformed simplified equations are:

$$R_f(\lambda + s)\overline{C}_f = -v\frac{d\overline{C}_f}{dx} + \delta_f D_m \frac{d\overline{C}_m}{dz}\bigg|_{z=0}, \tag{3.11}$$

$$\varepsilon_m R_m(\lambda + s)\overline{C}_m = D_m \frac{d^2\overline{C}_m}{dz^2}, \tag{3.12}$$

with boundary conditions

$$hw\left[v\overline{C}_f\right]_{x=0} = \overline{G}_{in}. \tag{3.13}$$

$$\left[\overline{C}_m\right]_{z=0} = \overline{C}_f. \tag{3.14}$$

Here, the over bar denotes the Laplace Transform and

s is the Laplace variable [y^{-1}]

The required result is

$$\overline{G}_{out} = hw\left[v\overline{C}_f\right]_{x=L}. \tag{3.10}$$

Note that this system, without the decay term, is analogous to the problem of heat exchangers discussed by Carslaw and Jaeger (1959).

The solution for the transformed matrix concentration is simply

$$\overline{C}_m = \overline{C}_f e^{-\phi x}, \tag{3.15}$$

where

$$\phi = \sqrt{\frac{\varepsilon_m R_m(\lambda + s)}{D_m}}. \tag{3.16}$$

Substitution into (3.11) gives

$$\left[R_f(\lambda + s) + \delta_f D_m \phi\right]\overline{C}_f = -v\frac{d\overline{C}_f}{dx}. \tag{3.17}$$

The solution is then

$$\overline{C}_f = \frac{\overline{G}_{in}}{hwv} e^{-\frac{x}{v}\left[R_f(\lambda + s) + \delta_f D_m \phi\right]}, \tag{3.18}$$

and the required result is

$$\overline{G}_{out} = \overline{G}_{in} \exp\left\{-\frac{L}{v}\left[R_f(\lambda + s) + \delta_f D_m \phi\right]\right\}. \tag{3.19}$$

We can now relate this to the F-factor and advective travel time.

In our notation, the F-factor is defined as

$$F = \frac{L\delta_f}{v}, \tag{3.20}$$

which corresponds to the formula given by SKB's SR-Can data report (SKB, 2006b, Section 6.6) $F = \frac{2wL}{Q}$ through the relationships given in (3.3) and (3.4).

The travel time is given by SKB as $t_w = \frac{hwL}{Q}$ which is simply equivalent to $t_w = \frac{L}{v}$. This is valid if it is assumed that there is no surface sorption ($R_f = 1$), but more generally we write

$$t'_w = \frac{LR_f}{v}. \tag{3.21}$$

Then, the required result can be written

$$\overline{G}_{out} = \overline{G}_{in} \exp\left\{-t'_w(\lambda + s) - FD_m\phi\right\}. \tag{3.22}$$

If we take the case where the input is a pulse of unit strength, then the Laplace Transform can be explicitly inverted to give

$$G_{out} = e^{-\lambda t}\sqrt{\frac{F^2\varepsilon_m R_m D_m}{4\pi(t-t'_w)^3}}\exp\left\{-\frac{F^2\varepsilon_m R_m D_m}{4(t-t'_w)}\right\}H(t-t'_w). \tag{3.23}$$

Thus, the F-factor and t'_w represent the fracture-dependent part of the solution while the matrix contribution is a product of three key matrix properties. This result agrees with that quoted by Selroos (1996).

3.3.3 Single Nuclide Advection with Varying Fracture Properties and Infinite Matrix

When the fracture properties vary it is clear from (3.22) that a summation (or integration) approach can be taken to deriving an F-factor and t'_w for the total path. In the case of piecwise-constant properties in N segments, the result simply becomes

$$\overline{G}_{out} = \overline{G}_{in}\prod_{i=1}^{N}\exp\left\{-t'_{w,i}(\lambda + s) - F_i D_m\phi\right\} = \overline{G}_{in}\exp\left\{-\sum_i t'_{w,i}(\lambda + s) - \sum_i F_i D_m\phi\right\}. \tag{3.24}$$

The result for a continuously varying property evidently turns the sums into integrals.

Thus, the assumption that is made about deriving the F-factor as a sum over the path is correct when there is no variation in matrix properties, the matrix is infinite and there is no dispersion/diffusion along the flow path.

3.3.4 Single Nuclide Advection with a Finite Matrix

If the matrix penetration depth is finite, so that (3.9) applies, the Laplace transform solution given in (3.22) changes slightly. It becomes

$$\overline{G}_{out} = \overline{G}_{in} \exp\left\{-t'_w(\lambda + s) - FD_m\phi\tanh(a_m\phi)\right\}. \tag{3.25}$$

This change makes no difference to the validity of the derivations of the F-factor and t'_w for the total path; the approach remains valid as long as all the matrix properties are constant.

Note that this also indicates that other matrix geometries would not change the validity – for example cylindrical diffusion from narrow channels, since they have very similar forms of transform – with the tanh replaced by, for example, Bessel functions.

Although direct inversion of this result to the time domain is intractable, it is straightforward to calculate the mean transport time for a pulse input. This is calculated from the derivative of the exponent in (3.25), evaluated at *s=0*. The result is

$$t_{mean} = t'_w + \frac{F\varepsilon_m R_m}{2\phi_0}\left\{\tanh(a_m\phi_0) + a_m\phi_0 \operatorname{sech}^2(a_m\phi_0)\right\}, \tag{3.26}$$

$$\phi_0 = \sqrt{\frac{\varepsilon_m R_m \lambda}{D_m}}\,. \tag{3.27}$$

This result can be useful in obtaining an indication of sensitivity to the various parameters.

3.3.5 Single Nuclide Advection with a Varying Matrix Properties

If the matrix properties vary along the path then the approach as it stands cannot be valid. There is a need to define suitable average matrix properties.

For the infinite matrix case this can be done quite simply. We rewrite (3.22) to emphasise the dependence on the matrix properties

$$\begin{aligned}\overline{G}_{out} &= \overline{G}_{in}\exp\left\{-t'_w(\lambda + s) - F\sqrt{\varepsilon_m R_m D_m}\sqrt{\lambda + s}\right\} \\ &= \overline{G}_{in}\exp\left\{-t'_w(\lambda + s) - F\beta_m\sqrt{\lambda + s}\right\}\end{aligned}. \tag{3.28}$$

where we have written $\beta_m = \sqrt{\varepsilon_m R_m D_m}$ as the only matrix property that is relevant. Then, for a series of paths with difference properties each $\overline{G}_{in}$ equals the previous $\overline{G}_{out}$ and the exponents are added together. Thus, a suitable average β must satisfy

$$F\beta_{m,ave} = \sum_{i=1}^{n} F_i\beta_{m,i}\,, \tag{3.29}$$

which implies that the F-factors act as weights in the averaging:

$$\beta_{m,ave} = \frac{\sum_{i=1}^{n} F_i\beta_{m,i}}{\sum_{i=1}^{n} F_i}\,. \tag{3.30}$$

With this definition of the average matrix properties the F-factor approach can still be used. The authors are not aware of this being exploited by SKB or similar organisations.

For a finite matrix, the requirement would be

$$F\beta_{m,ave}\sqrt{\lambda+s}\tanh\left(\frac{\beta_{m,ave}a_{m,ave}}{D_{m,ave}}\sqrt{\lambda+s}\right)=\sum_{i=1}^{n}F_i\beta_{m,i}\sqrt{\lambda+s}\tanh\left(\frac{\beta_{m,i}a_{m,i}}{D_{m,i}}\sqrt{\lambda+s}\right). \quad (3.31)$$

This would have to be satisfied for all values of s. This is impossible and the F-factor approach cannot therefore be extended to this case.

3.3.6 Dispersion

We now look at the effect of dispersion, starting by deriving the solution for the simplest case of a single nuclide, infinite matrix and constant properties.

When dispersion is present, a downstream boundary condition is required. Given that we expect the effects of dispersion to be small (i.e. transport in the fracture is dominantly advective), we take a zero gradient condition, so the resulting flux is purely advective at the boundary.

We write the solution in a form that makes the connection with the non-dispersive case clear. We assume no diffusion in the fracture and use the Peclet number to characterise the degree of dispersion; a high Peclet number indicates advective dominance (assuming that diffusion along the flow path is negligible).

To this end, define

$$\gamma_{adv}=t_w'(\lambda+s)+FD_m\phi. \quad (3.32)$$

so that

$$\overline{G}_{out}=\overline{G}_{in}\exp\{-\gamma_{adv}\}. \quad (3.33)$$

Then the solution with dispersion can be written as

$$\overline{G}_{out}=\overline{G}_{in}\exp\left\{-\gamma_{adv}\frac{2}{\mu+1}\right\}\left[\frac{(\mu+1)}{(\mu+1)+(\mu-1)e^{-\mu Pe}}\right], \quad (3.34)$$

where

$$\mu=\sqrt{1+4\gamma_{adv}/Pe}\,. \quad (3.35)$$

Clearly $\mu \to 1$ as $Pe \to \infty$ and the advective result is recovered. Clearly, the F-factor approach becomes invalid in the dispersive case, but can be expected to remain a good approximation for high Peclet numbers. Numerical experiments will quantify this.

An additional complication in the dispersive case is that continuity conditions are needed between each segment in a case with piecewise constant properties. The effect of these is to make the solution dependent on the order in which the segments arise. This means that it is not strictly valid to group segments that have common properties together unless they actually occur contiguously in the flow tube, as would be natural for the non-dispersive case; the effect of this will also be explored through numerical experiments.

3.3.7 Chain Decay in the Advection Case

We now look at the effect of decay chains.

We first note that cases where all members of a chain share the same transport properties can be treated as single nuclide cases, since the total concentration can be modelled and then the distribution between members applied retrospectively from solution of the Bateman equations for decay and ingrowth (Bateman, 1910). Therefore, we are interested in the general case when the chain members have different properties.

In the general case the solution becomes mathematically much more complicated, with the result for each member depending on the behaviour of all previous chain members. The solution for the first member is, of course, identical to the single nuclide case. The general case is dealt with in Appendix B.

Here we start by exploring the solution for the simplest case of a 2-member chain with an infinite matrix and constant properties. The result for the first member is unchanged:

$$\overline{G}_{out}^{(1)} = \overline{G}_{in}^{(1)} \exp\left\{-t_w'^{(1)}(\lambda^{(1)} + s) - FD_m^{(1)}\phi^{(1)}\right\}. \tag{3.36}$$

The second member result can be written as a sum over the basic single-nuclide response. Specifically,

$$\begin{aligned} \overline{G}_{out}^{(2)} = {} & K_{22} \exp\left\{-t_w'^{(2)}(\lambda^{(2)} + s) - FD_m^{(2)}\phi^{(2)}\right\} \\ & + K_{21} \exp\left\{-t_w'^{(1)}(\lambda^{(1)} + s) - FD_m^{(1)}\phi^{(1)}\right\}, \end{aligned} \tag{3.37}$$

where

$$
\begin{aligned}
K_{22} &= \overline{G}_{in}^{(2)} - K_{21} \\
K_{21} &= \frac{R_f^{(1)}\lambda^{(1)} + \delta_f D_m^{(2)} U_{21}\left(\phi^{(2)} - \phi^{(1)}\right)}{\left[R_f^{(2)}(\lambda^{(2)} + s) + \delta_f D_m^{(2)}\phi^{(2)}\right] - \left[R_f^{(1)}(\lambda^{(1)} + s) + \delta_f D_m^{(1)}\phi^{(1)}\right]} \\
U_{21} &= \frac{R_m^{(1)}\lambda^{(1)}}{\left[R_m^{(2)}(\lambda^{(2)} + s)\right] - \dfrac{D_m^{(2)}}{D_m^{(1)}}\left[R_m^{(1)}(\lambda^{(1)} + s)\right]}.
\end{aligned}
\tag{3.38}
$$

The later member results are better written in terms of recurrence relations, see Appendix B.

Thus, although the F-factor and t_w' still appear in these results, the introduction of chain decay causes complex coefficients to arise containing all the different properties.

It is clear that the summation of F-factors will not be strictly valid for decay chains, even in the simplest case of an infinite matrix and only advection in the fracture. Moreover, no suitable average matrix properties can be derived.

The analytic form does not make it easy to see how big an error in the breakthrough for later chain members is likely to be made if the F-factor approach is used. Section 3.4.6 examines this by by numerical experiment.

Also note that decay chain results depend on the ordering of the segments. This arises because the solution involves a product of matrices that are non-commutative.

3.3.8 Summary

The F-factor approach as used by SKB can be seen to be fully mathematically valid for advective transport of a single nuclide with constant matrix properties. This applies to both finite and infinite matrix diffusion.

If the matrix properties vary then a suitable averaging scheme exists for the case of infinite matrix diffusion, but it is not thought that SKB have exploited this. In cases of interest the matrix penetration depth may be sufficiently large for the infinite case to be an excellent approximation.

For decay chain members whose breakthroughs are significantly affected by ingrowth from precursor nuclides, the F-factor approach is invalid. If all chain members share the same transport properties then the approach would be valid, so it is to be expected that the approximation will be poorest when there are significantly different properties (sorption being the most likely case). The quality of the approximation may depend on the ordering of segments, this will be investigated numerically.

Similarly, when dispersion is present the F-factor approach fails. The approximation will become increasing poor as the level of dispersion increases. SKB use a fixed Peclet number of 10; numerical experiments are required to determine whether this is large enough to make the F-factor approach sufficiently accurate. There is potential for the order in which properties are encountered to be significant in in the dispersive case; this needs to be investigated numerically.

3.4 Numerical Study into Varying Properties

In this section the various issues that have been identified are explored numerically. A computer code was developed to calculate the solution for the general case, using the Laplace transform approach that is used by SKB in FARF31 based on Talbot's algorithm (Talbot, 1979). Talbot's algorithm uses a simple sum over the Laplace transform values along a contour in the complex plane to provide highly accurate approximations to the original time-domain function. The implementation was tested using transforms with known inverses. The same algorithm was used in the CRYSTAL code (Worgan and Robinson, 1995) and is used by SKB in FARF31.

The objective is first to confirm that the F factor approach is exactly valid in some cases and to explore the level of approximation that is introduced when it is used in other situations.

To this end we start with a set of base cases from which variants will be derived.

3.4.1 Base Cases

The base cases share the same flow and geometry, differing only in the nuclides involved. The three cases are for: a non-sorbed nuclide (I129); a sorbed nuclide (Se79) and a decay chain (Np237, U233, Th229). The base cases are for a single segment with advection only. A source term is used that injects 1 mol of the parent nuclide over a short period using a leaching source term with a leach rate of 1 per year.

The flux out of the end of the system is reported.

In the parameter tables F-value and travel time, t_w, are given along with physical properties (path length, velocity and aperture) that could lead to these values. From the analysis already presented it is clear that other values of the physical properties that correspond to the same F-value and travel time would give the same flux out of the system.

The parameters used for the base cases are given in Table 1and Table 2.

The output flux results for the three cases are presented in Figure 6 to Figure 8.

Table 1: Nuclide-independent Parameters for the Base Cases

Parameter	**Value**	**Units**
Path length	500	m
Flow velocity	10	m/y
Aperture	0.002	m
F value	50 000	y/m
Travel time	50	y
Peclet number	Infinite (advection only)	-
Rock porosity	0.001	-
Rock effective diffusion	6e-7	m^2/y
Maximum penetration depth	0.03	m
Source leach rate	1	y^{-1}

Table 2: Nuclide-independent Parameters for the Base Cases

Parameter	**I129**	**Se79**	**Np237**	**U233**	**Th229**	**Units**
Decay constant	4.415e-8	1.84e-6	3.24e-7	4.36e-6	9.44e-5	y^{-1}
Rock retention factor	1	2e3	2e5	1e6	2e5	-
Initial inventory (for source)	1	1	1	0	0	mol

Figure 6: Flux output for I129 Base Case

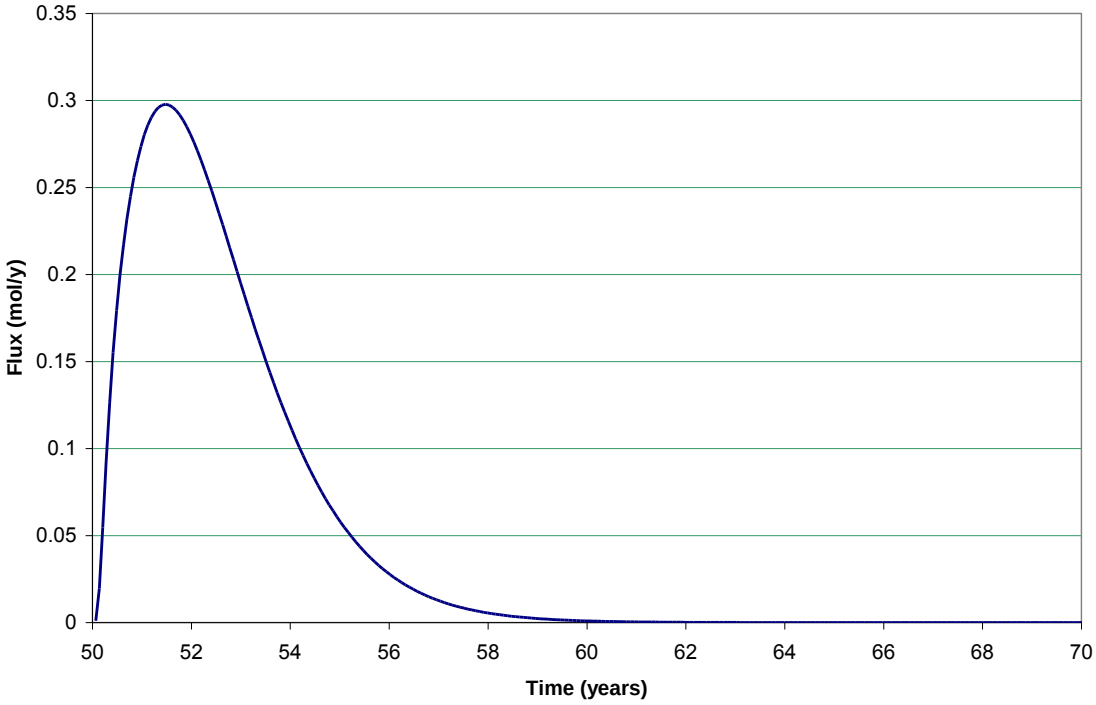

Figure 7: Flux output for Se79 Base Case

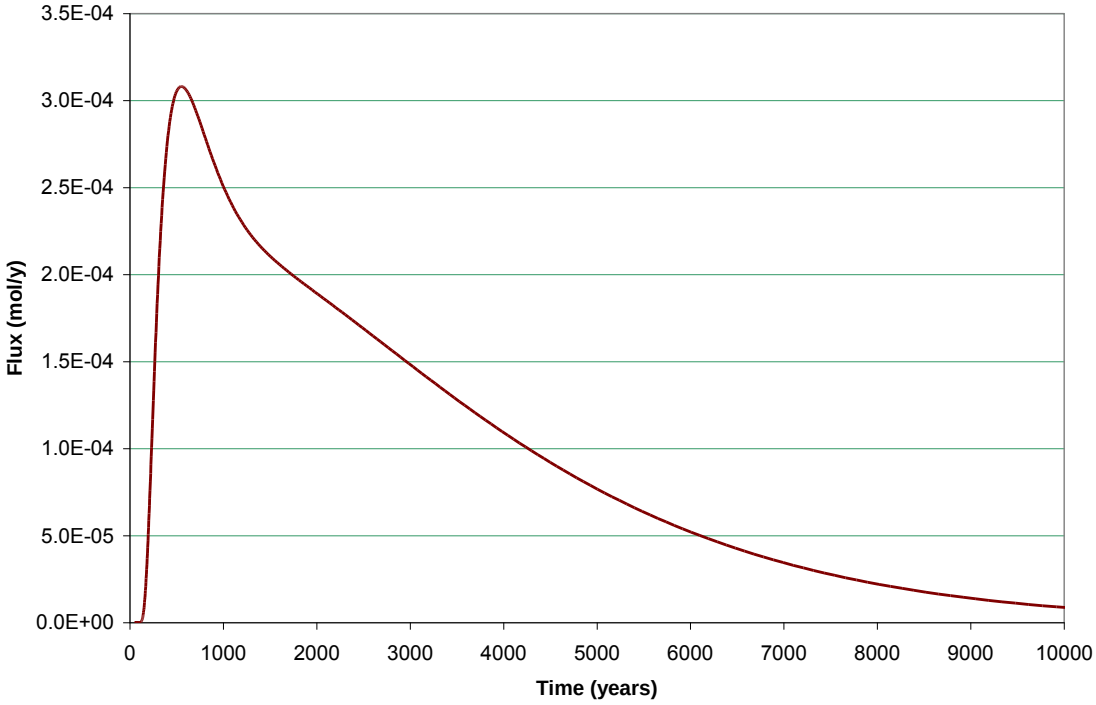

Figure 8: Flux output for Np237 Chain Base Case

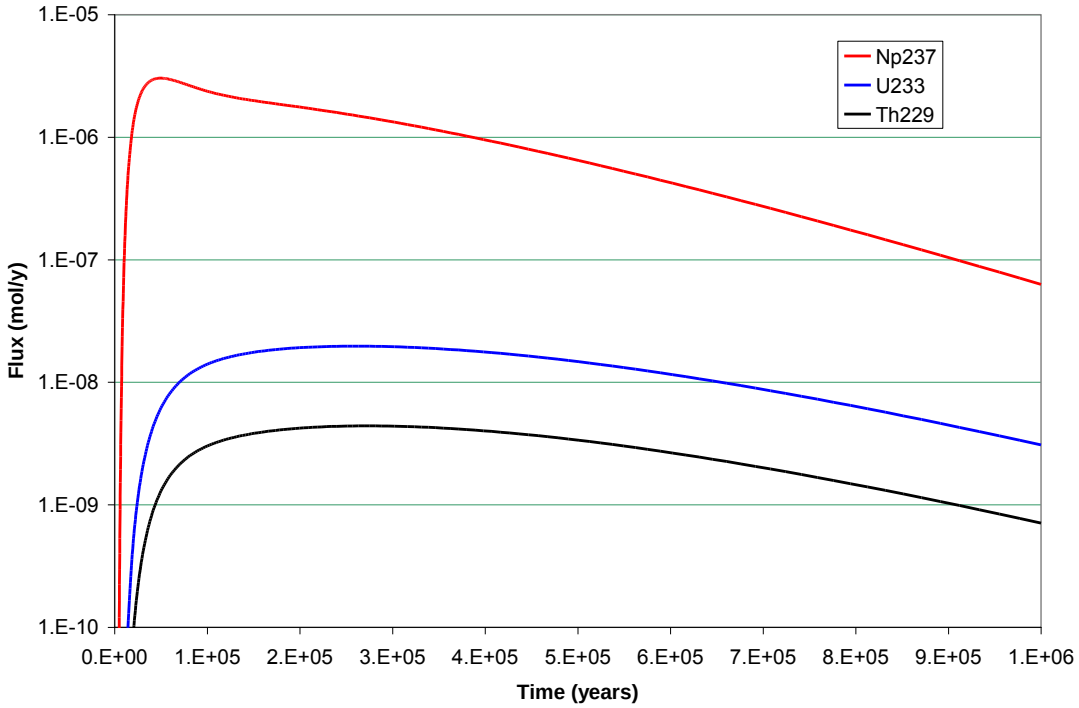

The I129 result shows a very rapid peak after the travel time of 50 years, indicating that the matrix diffusion has a very small effect.

The Se79 results show a peak after around 550 years; the shape of the curve is characteristic of a matrix diffusion case with the slowly falling flux after the initial peak caused by diffusion out of the matrix.

The Np237 chain result shows a peak for Np237 around 50000 years with the shape of the curve similar to the Se79 case. The daughter nuclides grow in during transport of the parent and show a later peak; the shorter-lived Th229 is in equilibrium with the U233 and the ratio of fluxes reflects the different decay constants and matrix retention.

3.4.2 Check on Exact Validity

In order to confirm the exact validity of the F-value approach in appropriate cases we have calculated the results for several cases that have the same F-value and travel time. This has been undertaken for the Se79 case as an example, noting that exact validity is not expected for the chain case and the I129 case shows too small an influence of the matrix diffusion to be of interest.

Different length and velocity

A case was run with the path length and velocity both reduced by a factor of 10. The results are identical to the base case as expected. Here, and in the subsequent comparisons, we treat the results as identical if they match precisely (to the reported 6 significant figures) over the non-trivial part of the range (where results are within 6 orders of magnitude of the peak); rounding errors in the calculations inevitably lead to minor difference outside this range.

Even split

A case was run with the path split into two segments, each contributing half of the travel time and F-factor. Different velocities and length were used in the two segments (400 m at 16 m/y for the first segment and 100 m at 4 m/y in the second). Again, the results are identical to the base case.

Uneven split

A case was run with the path split into two segments. The first segment had a travel time of 10 years and an F-factor contribution of 40000; the second segment had a travel time of 40 years and an F-factor contribution of 10000. The velocities and lengths used in the two segments were 100 m at 10 m/y for the first segment and 400 m at 10 m/y in the second. The apertures were 0.5 mm and 8 mm. Again, the results are identical to the base case.

Three-way split

A final case was run with the path split into three segments. The first segment had a travel time of 5 years and an F-factor contribution of 30000; the second segment had a travel time of 15 years and an F-factor contribution of 15000; and the third segment had a travel time of 30 years and an F-factor contribution of 5000. The velocities and lengths used in the three segments were 150 m at 30 m/y for the first segment, 200 m at 13.33 m/y in the second, and 150 m at 5 m/y in the third. The apertures were 0.333 mm, 2 mm and 12 mm. In this case too, the results are identical to the base case.

3.4.3 Sensitivity

We now look at the sensitivity of the results to the key parameters. This has two objectives. The first objective is to gain insight into the way the system behaves. The second objective is to get a measure of how significant approximations are in comparison with uncertainty in precise parameter values.

We look at sensitivity separately for five parameters: F-factor; travel time; matrix penetration depth; matrix retention (including porosity) and matrix diffusion. We continue to use the Se79 case, deferring discussion of sensitivity in the chain case until later.

F-factor

The F-factor characterises the degree of contact between the fracture and matrix. A higher F-factor corresponds to more contact and therefore to later and smaller peaks. We have run cases with a factor-of-two increase and decrease and with 20% increase and decrease. Figure 9 shows the results.

Figure 9: Sensitivity of flux output to varying F-factor for Se79 Case

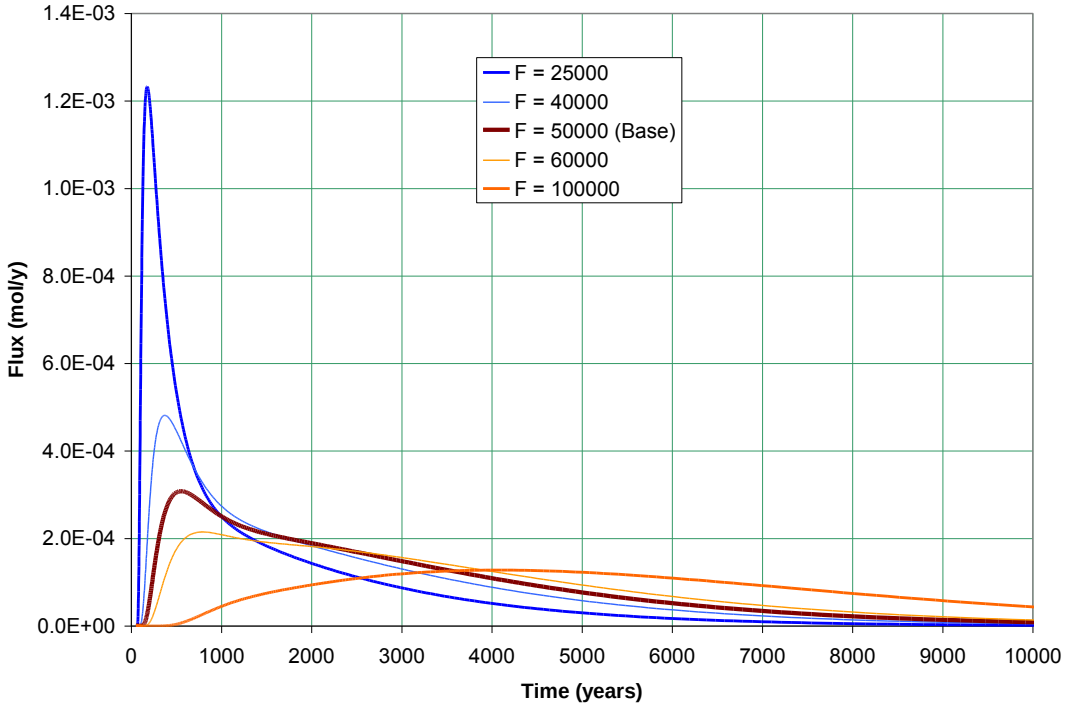

A factor-of-two reduction in F-factor leads to a factor-of-four increase in peak value for this case. The 20% reduction in F-factor changes the peak value by 60%, showing that this result is very sensitive to the F-value.

Travel time

The travel time corresponds to the time for water to pass through the system. In a case where matrix diffusion is significant, as it is here, the travel time itself is unlikely to be important, except through its indirect effect via the F-factor. We have run cases with a

factor-of-two increase and decrease and with 20% increase and decrease. Figure 10 shows the results.

Figure 10: Sensitivity of flux output to varying Travel Time, t_W, for Se79 Case

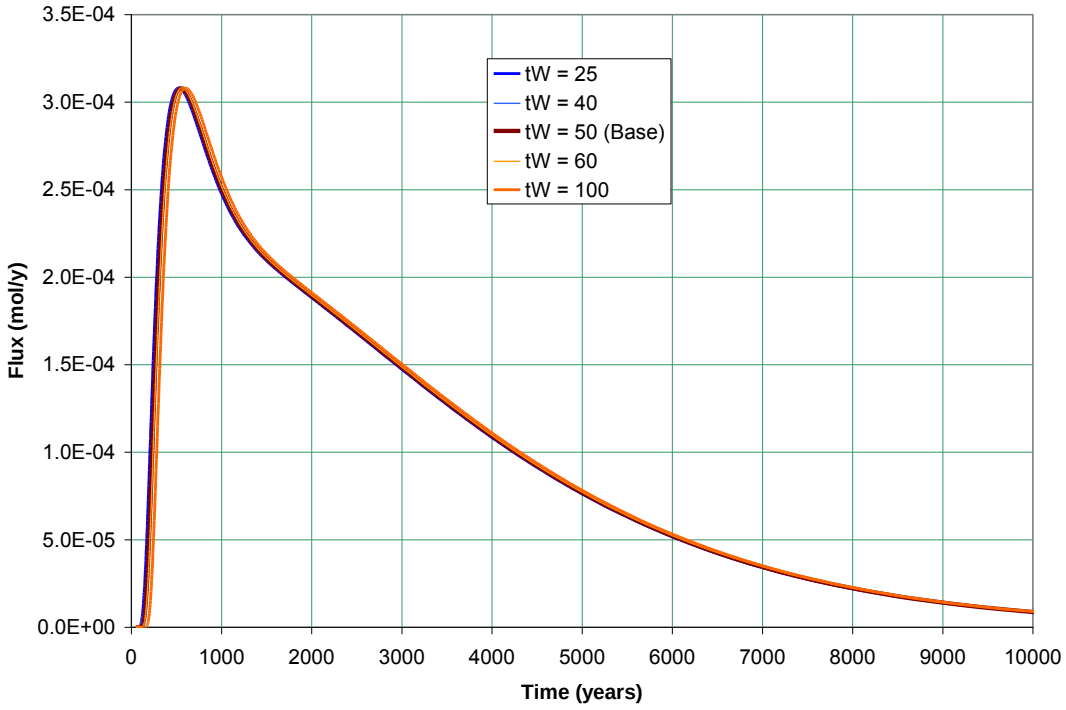

As expected, varying the travel time has almost no effect if the F-factor is unchanged. For a case where matrix diffusion is unimportant, such as the I129 base case, the travel time would have a direct influence on the result.

Matrix penetration depth

The matrix penetration depth controls the amount of sorptive capacity in the rock that is available. For small penetration depths this will directly control the flux, but for larger penetration depths it is the rate of diffusion into the matrix that controls the depth achieved and the result will tend towards a limit. We have run cases with a factor-of-three increase and decrease and with 20% increase and decrease. A case with infinite penetration depth was also run. Figure 11 shows the results.

Figure 11: Sensitivity of flux output to varying Maximum Penetration Depth, *a*, for Se79 Case

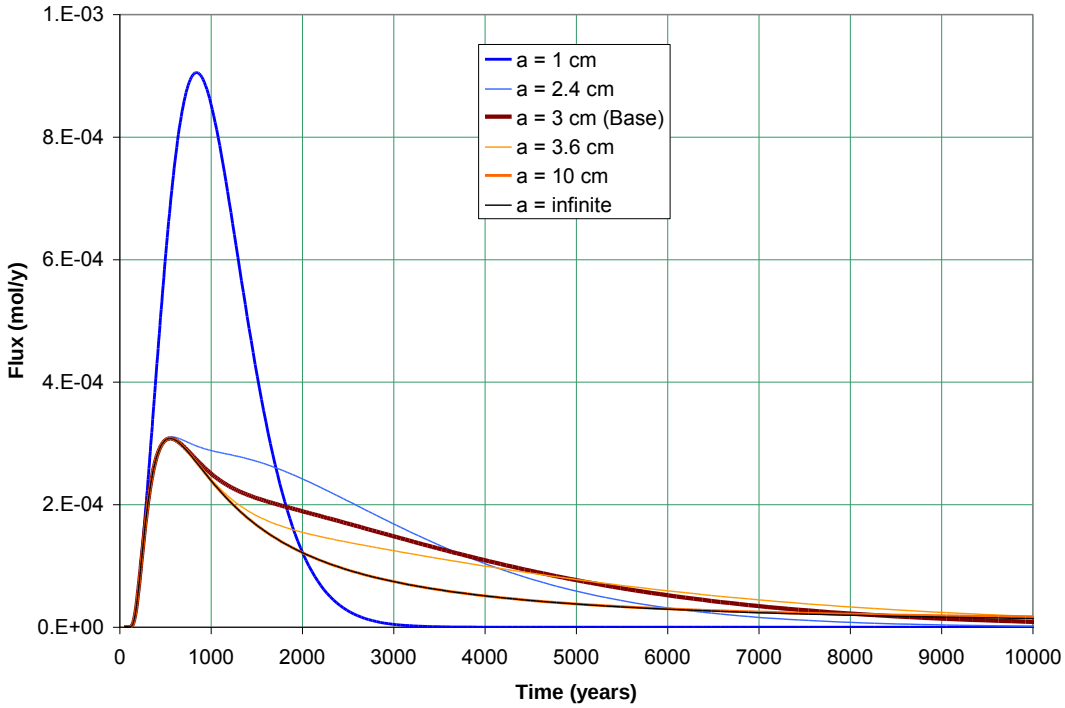

The infinite and 10 cm results are indistinguishable on this scale (they differ slightly at large times). In terms of the peak value, the result is the same for all the cases except the 1 cm case. This small penetration depth clearly allows for the rock matrix and fracture water to be in effective equilibrium, so that the overall effect is simply like that of retardation in the fracture.

Taking the formula given in (3.26), we can plot the extra average transport time (over the water travel time) as a function of the maximum penetration depth. This is shown in Figure 12, where the transition to the effectively infinite case can be seen to occur between 10 cm and 1 m. For depths less than around 20 cm the extra average transport time is linearly proportional to the maximum depth, but this measure does not provide information on the details of the peak response. The maximum extra travel time arises at a finite value of the depth because if the Se79 diffuses further than this then it decays before leaving the matrix and so does not contribute to the average travel time.

Figure 12: Extra Average Travel Time as a function of Maximum Penetration Depth, *a*, for Se79 Case

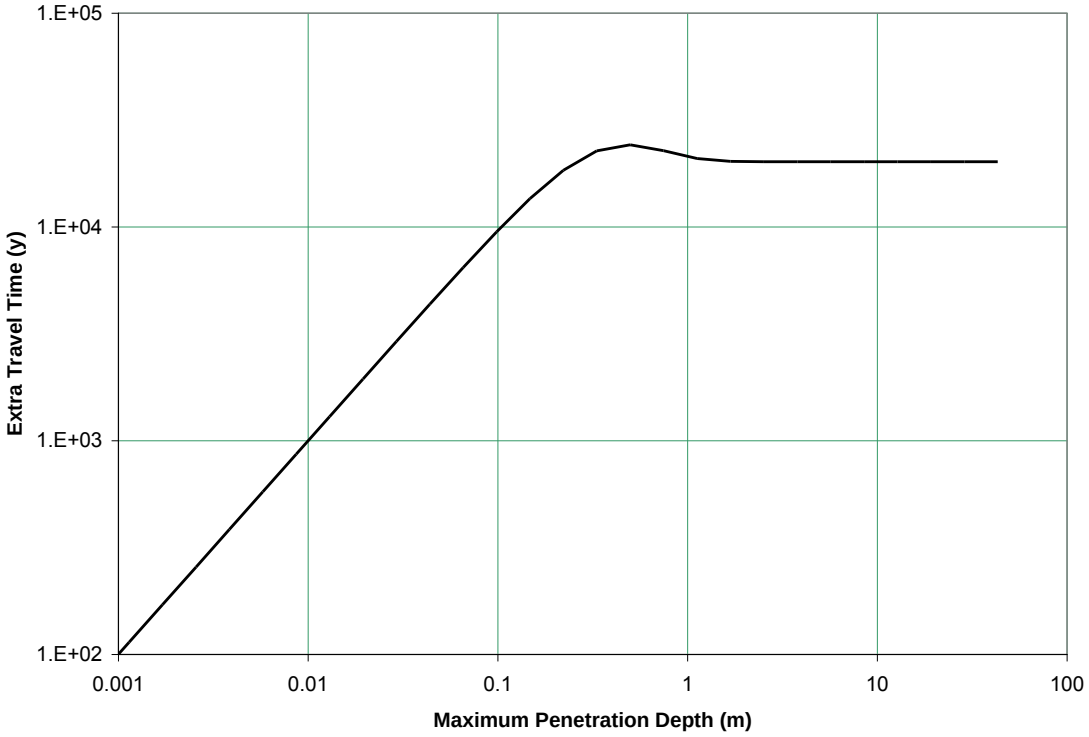

Matrix retention including porosity

Matrix retention and porosity always appear as a product in the solutions discussed earlier and represent a capacity of the matrix. The two uncertain parameters are the porosity itself and the Kd. For sorbed nuclides, the porosity component is negligible and the sorption dominates. The base case has a capacity factor of 2 (porosity 0.001, retention 2000). The capacity is expected to be important in directly controlling the amount of nuclide in the matrix compared to the fracture. We have run cases with a factor-of-two increase and decrease and with 20% increase and decrease. Figure 13 shows the results.

It is clear that the peak flux scales directly with the capacity factor in this range, due to the redistribution of material between stationary and flowing parts of the system.

Figure 13: Sensitivity of flux output to varying Rock Matrix Capacity, εR, for Se79 Case

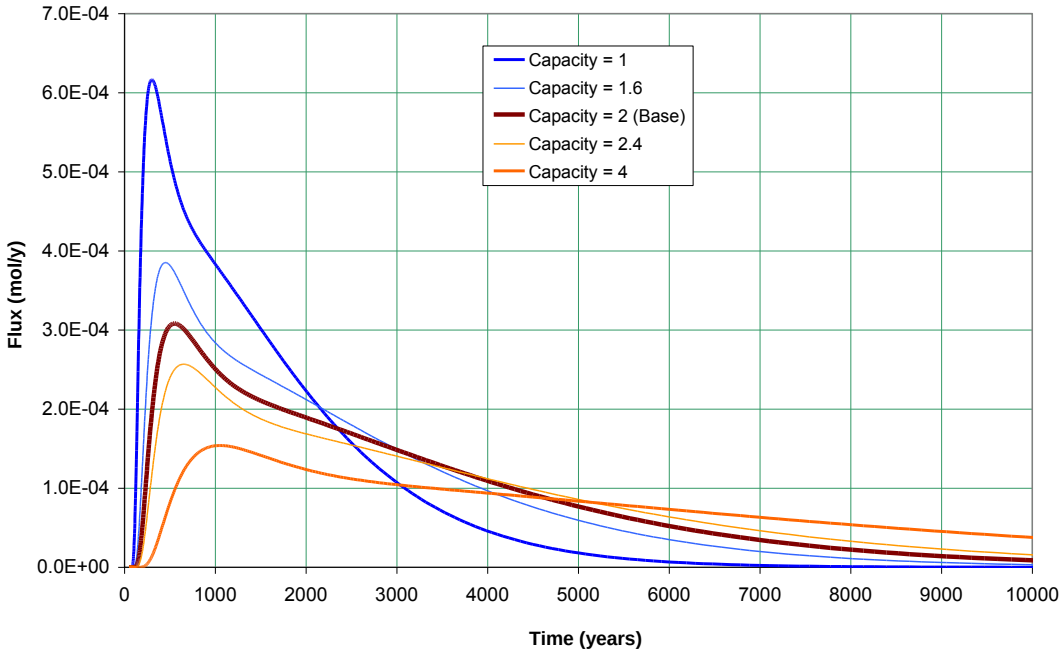

Matrix diffusion coefficient

The effective diffusion coefficient controls the rate at which material can enter and leave the matrix. Higher values allow diffusion further into the matrix which tends to increase transport times. Peaks may become tighter due to the faster diffusion out of the matrix. We have run cases with a factor-of-two increase and decrease and with 20% increase and decrease. Figure 14 shows the results.

For smaller values of the diffusion coefficient less material diffuses into the matrix and a sharper higher peak occurs. However, for larger values the increased rate of diffusion out of the matrix causes a more rapidly falling tail and therefore higher peaks. The value where the turnaround occurs will depend on the maximum penetration depth.

Figure 14: Sensitivity of flux output to varying Rock Matrix Effective Diffusion Coefficient, *D*, for Se79 Case

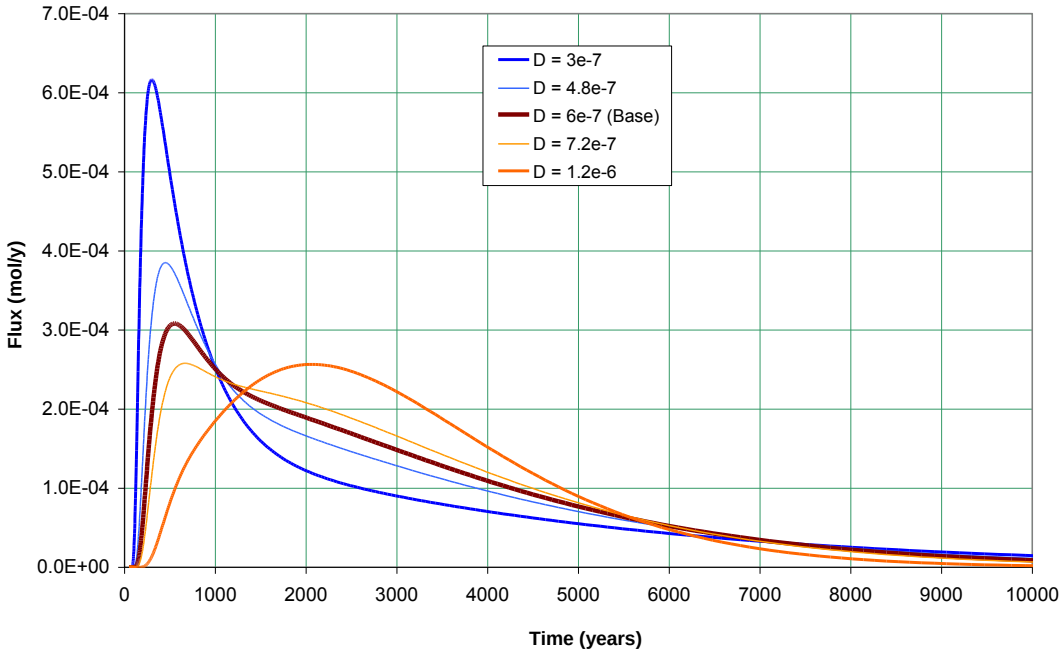

3.4.4 Effect of Dispersion

We now look at introducing dispersion. This is essentially a further sensitivity case, but with the base case being an infinite Peclet number. We have run cases with Peclet numbers down to a typical value of 10 (as used by SKB in SR Can). Figure 15 shows the results.

There is very little difference between the typical advective case of a Peclet number of 10 and the advection only case with the peak being 10% different. Peclet numbers above 20 differ from the infinite case by less than 5% at the peak.

The fact that the peak flux is higher for the more dispersive case is at first sight not what would be expected. Without matrix diffusion a lower Peclet number would lead to a more dispersed breakthrough and so a lower peak. When matrix diffusion is present, the early part of the breakthrough is less affected by the matrix, as it has had less contact time, and this has a stronger effect than dispersion in the fracture. This mechanism for some of the nuclide to avoid the matrix results in a higher peak for the more dispersive system.

The small difference seen here suggests that the approximation made in using the F-factor approach in cases with dispersion will not be important. To check this further,

we take the cases with a split path as in Section 3.4.2 but now with a Peclet number of 10.

First we confirm that using a path length and velocity both reduced by a factor of 10 gives identical results as implied by (3.25). This is as expected.

In the other cases, the Peclet number is used to give an overall dispersion length which is used in all segments. Splitting a path up and using the same Peclet number in each segment would not give the same results as the Peclet number is a characteristic of the whole path (i.e. the distance to the measuring position).

Figure 15: Sensitivity of flux output to varying Peclet Number, *Pe*, for Se79 Case

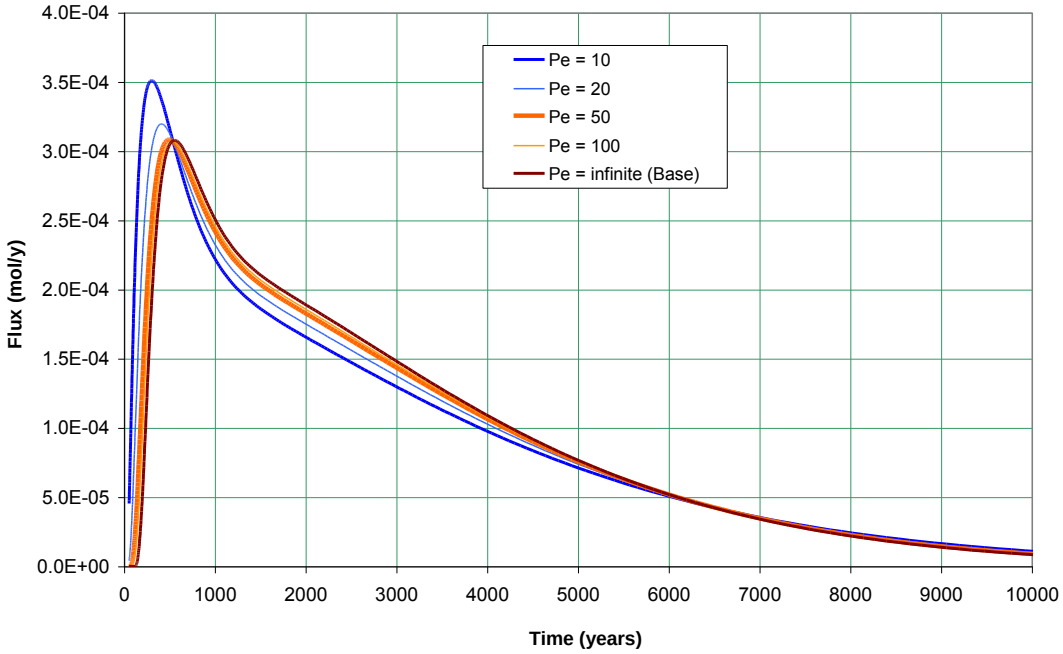

Even split

A case was run with the path split into two segments, each contributing half of the travel time and F-factor. Different velocities and length were used in the two segments (400 m at 16 m/y for the first segment and 100 m at 4 m/y in the second). The results differ as expected. To confirm that the coding of linked segments is correct a case was run where both segments are identical; this case does indeed match the dispersive base case.

It is expected that the ordering of segments is important when dispersion is present, so the case has also been run with the slower segment first. Figure 16 shows the results.

The ordering is not important in this case and the difference between the single segment and split segments is small, around 6% in peak value.

Figure 16: Impact on flux output of splitting path into two equal length segments for Se79 Case

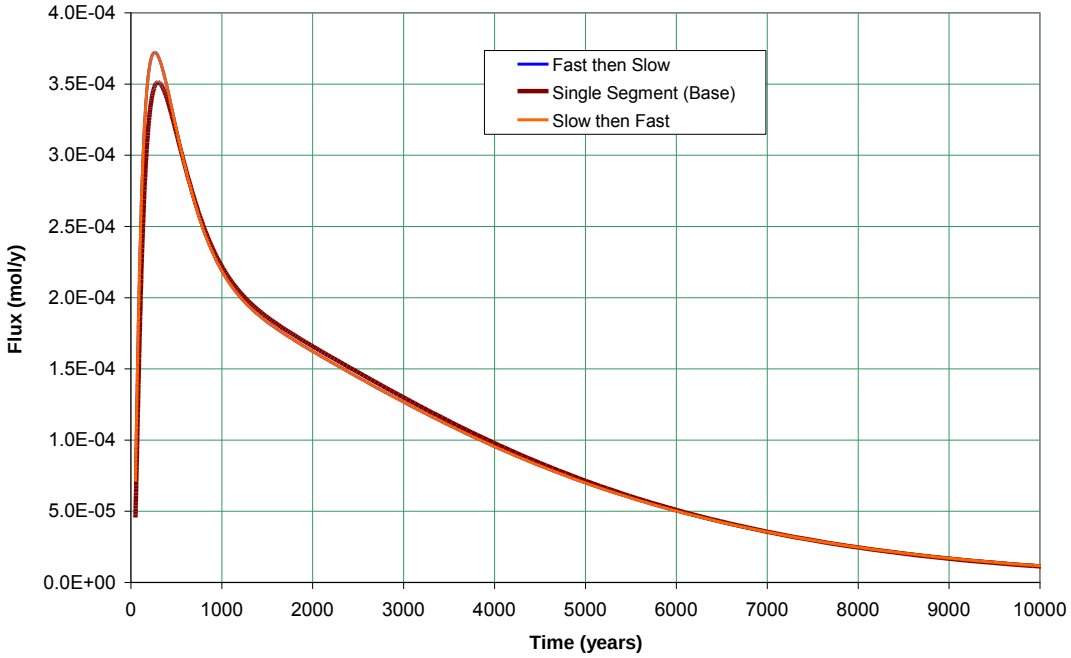

Uneven split

A case was run with the path split into two segments. The first segment had a travel time of 10 years and an F-factor contribution of 40000; the second segment had a travel time of 40 years and an F-factor contribution of 10000. The velocities and lengths used in the two segments were 100 m at 10 m/y for the first segment and 400 m at 10 m/y in the second. The apertures were 0.5 mm and 8 mm.

Again, two versions were run to check for order dependence.

Figure 17 shows that the ordering again makes no difference, but the unequal segment result gives a peak value 50% higher and rather earlier than the single segment case.

Figure 17: Impact on flux output of splitting path into two unequal length segments for Se79 Case

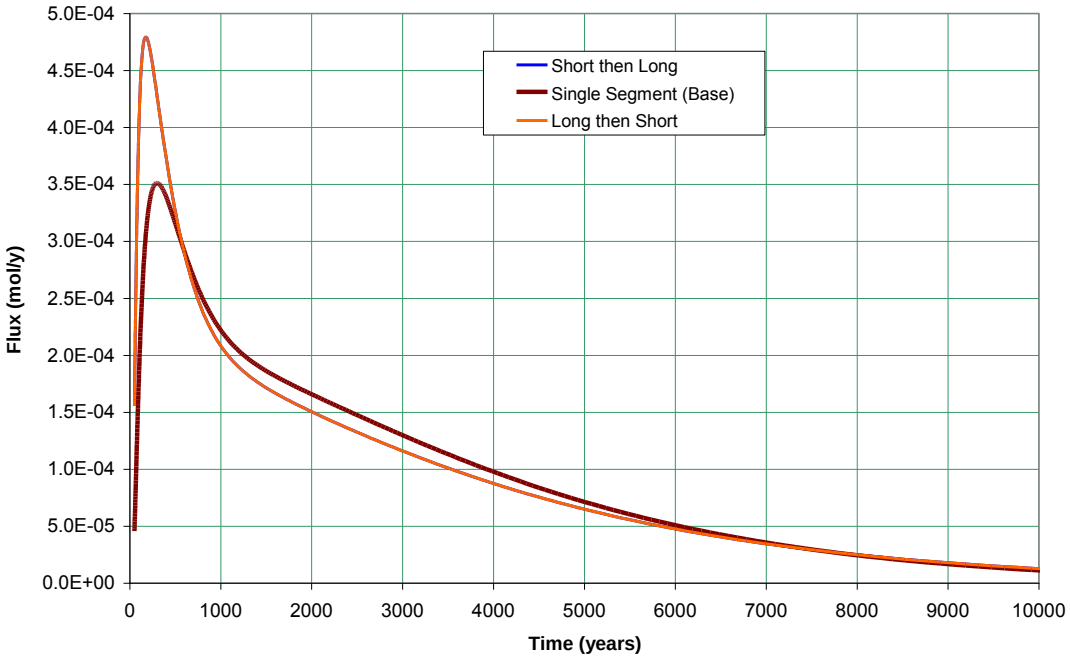

Three-way split

A final case was run with the path split into three segments. The first segment had a travel time of 5 years and an F-factor contribution of 30000; the second segment had a travel time of 15 years and an F-factor contribution of 15000; and the third segment had a travel time of 30 years and an F-factor contribution of 5000. The velocities and lengths used in the three segments were 150 m at 30 m/y for the first segment, 200 m at 13.33 m/y in the second, and 150 m at 5 m/y in the third. The apertures were 0.333 mm, 2 mm and 12 mm.

Six orders are possible. We call the original order ABC and look at all six possible ordering. The results are identical for certain pairs, where the ordering is precisely reversed (ABC=CBA, ACB=BCA, BAC=CAB). Figure 18 shows the flux results.

Although the results do depend on the ordering, the differences are small. In this case all the orderings give results within 10% of the single segment case.

The reason why the results are identical for pairs of orderings is that the same interfaces appear in ABC and CBA (i.e. A next to B and B next to C) and the overall result is controlled by averages at these interfaces as well as the individual segment properties.

Figure 18: Impact on flux output of splitting path into three unequal length segments for Se79 Case

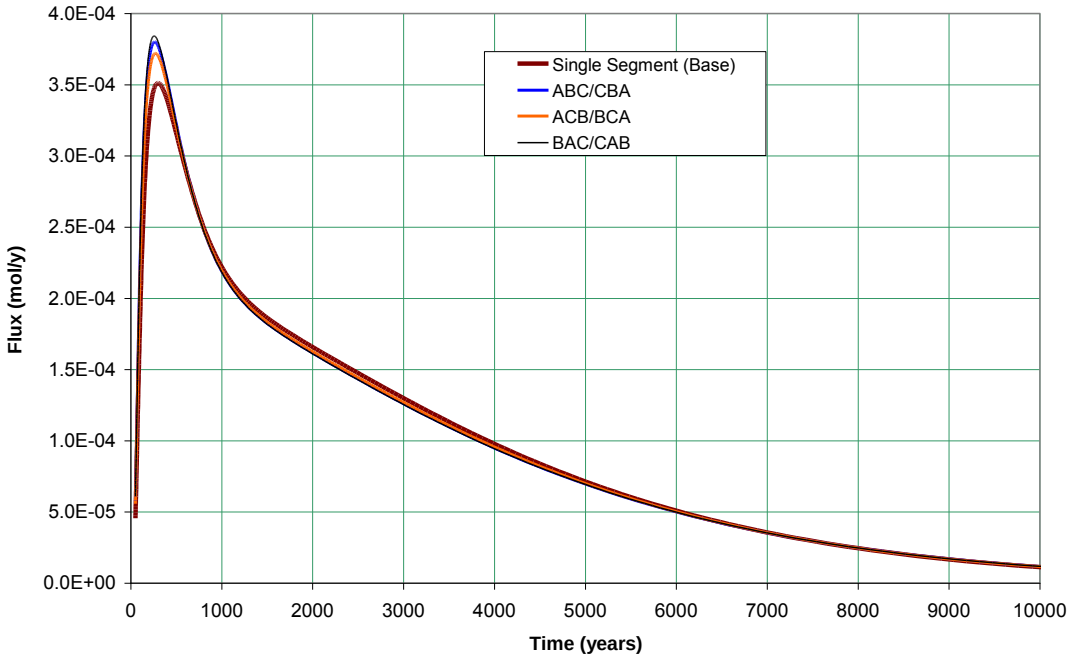

Conclusions

The effect of dispersion on the output flux and the effect of varying flow properties in this context are up to about 50%. This is equivalent to varying the key parameters by 20%. The use of a single segment gives lower peak results than multiple segments with differing F factors. The peak flux can be higher for more dispersive cases – showing how difficult it is to make conservative assumptions in these systems.

3.4.5 Varying Matrix Properties

In Section 3.3.5 the case of varying matrix properties was discussed. Here we check that the averaging approach suggested there does work correctly for the infinite matrix, advection only case and see if it remains a good approximation in the general case.

We focus on the matrix retention parameter, with results for varying the diffusion coefficient expected to be similar given the form of equation (3.30).

The base case for Se79 had a matrix retention factor of 2000. We take the even split case where the F-factor contributions are equal. Equation (3.30) suggests that an appropriate average retention factor in this case would satisfy $\sqrt{R_{ave}} = \left(\sqrt{R_1} + \sqrt{R_2}\right)/2$.

Thus, if we choose retention factors of 500 and 4500 for the two segments, the same result as the infinite penetration base case should be obtained.

This calculation was run and the results do indeed match exactly.

If we use the same approach for the finite penetration depth base case then exact agreement is not expected. Figure 19 shows the comparison. Although the peak has not changed very much, the shape of the curve is rather different suggesting that a more significant impact might be seen in other cases.

Figure 19: Impact on flux output of varying matrix retention for Se79 Case

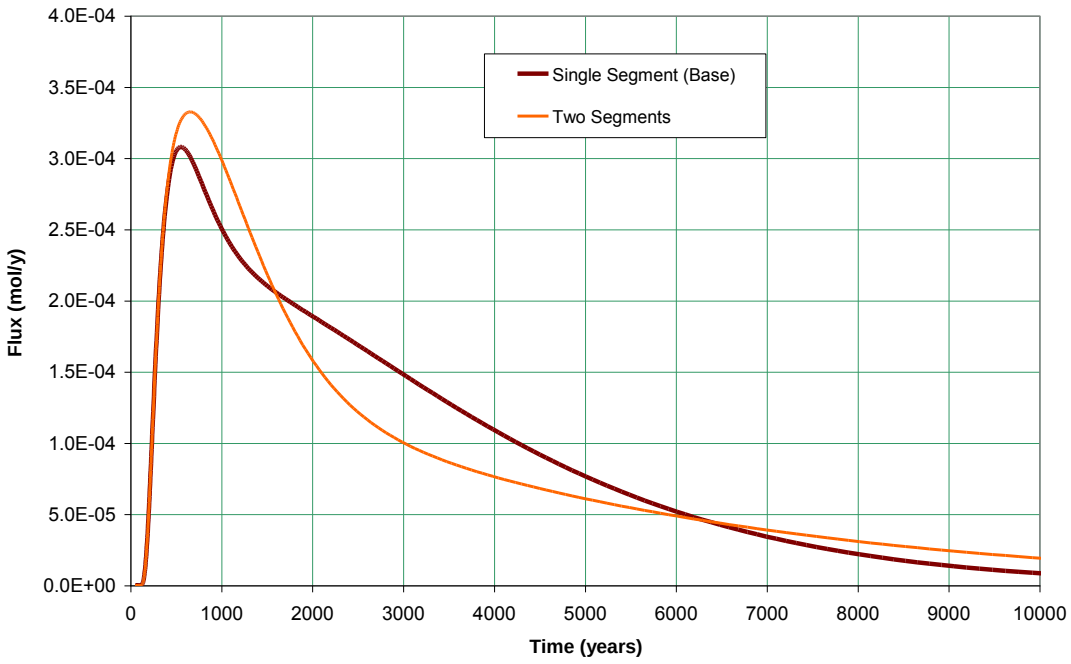

Figure 20 shows the comparison for a 1 cm maximum penetration depth, confirming that the averaging scheme becomes poorer as the penetration depth is reduced. The result for a single segment using the arithmetic average retention (2500) is also shown as this may be more appropriate for limited penetration depths.

Figure 20: Impact on flux output of varying matrix retention with 1 cm Maximum Penetration Depth for Se79 Case

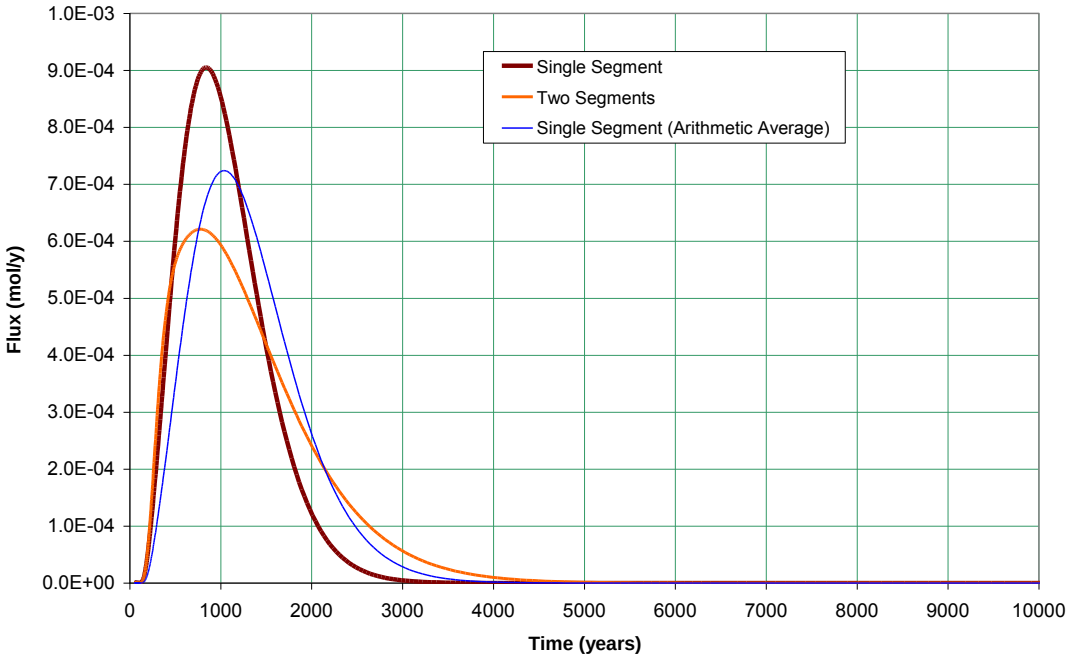

The other matrix parameter that might vary is the penetration depth. It is clear from the sensitivity calculations that this could be important, but there is no obvious way to define a suitable average penetration depth. Using a single segment with the smallest penetration depth would generally be conservative.

3.4.6 Decay Chains

So far, we have only looked at the results for single nuclides. These would apply equally to the top members of decay chains or to members where ingrowth was irrelevant. In this section we look at the impact on fluxes for daughter nuclides, using the Np237 chain as an example.

Split Cases

First, we look at the advective only case and revisit the split cases where the top chain member result will be exactly matched by the single segment. The cases are the same as those used in section 3.4.2 .

Even split

A case was run with the path split into two segments, each contributing half of the travel time and F-factor. Different velocities and length were used in the two segments

(400 m at 16 m/y for the first segment and 100 m at 4 m/y in the second). There is a precise match between the two-segment results and the single segment results.

Uneven split

A case was run with the path split into two segments. The first segment had a travel time of 10 years and an F-factor contribution of 40000; the second segment had a travel time of 40 years and an F-factor contribution of 10000. The velocities and lengths used in the two segments were 100 m at 10 m/y for the first segment and 400 m at 10 m/y in the second. The apertures were 0.5 mm and 8 mm. Although there are slight differences between the two-segment results and the single segment results, these are very small (fourth significant figure at the peak).

Three-way split

A final case was run with the path split into three segments. The first segment had a travel time of 5 years and an F-factor contribution of 30000; the second segment had a travel time of 15 years and an F-factor contribution of 15000; and the third segment had a travel time of 30 years and an F-factor contribution of 5000. The velocities and lengths used in the three segments were 150 m at 30 m/y for the first segment, 200 m at 13.33 m/y in the second, and 150 m at 5 m/y in the third. The apertures were 0.333 mm, 2 mm and 12 mm. Although there are slight differences between the two-segment results and the single segment results, these are very small (fourth significant figure at the peak).

Conclusions

Although the F-factor approach is not formally exact for daughters in a decay chain, the approximations involved are insignificant for the Np237 chain case which is typical of cases of interest.

Dispersion

The Pe = 10 case is compared to the advection only case here. Figure 21 shows the comparison. The effect is clear but not very large. The logarithmic scale makes the precise effects difficult to see, so the three individual nuclides are shown separately in Figure 22 to Figure 24. The effects are of the same scale as in the Se79 case – typically a 10% difference.

Figure 21: Impact on flux output of Dispersion with Peclet Number 10 for the Np237 Chain Case

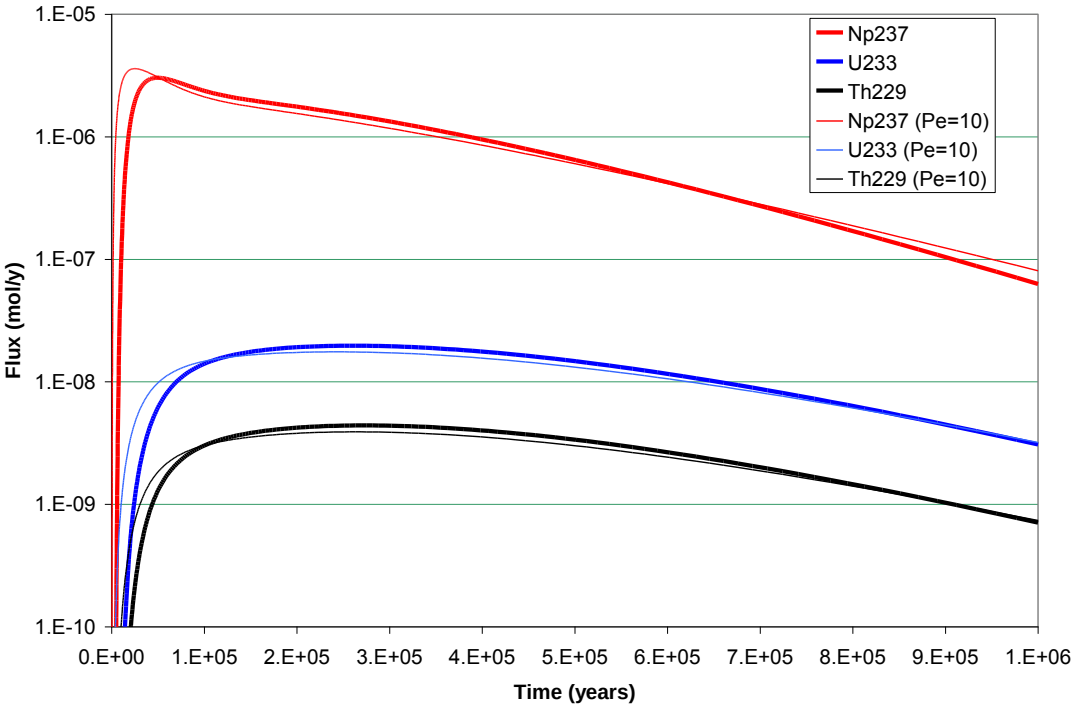

Figure 22: Impact on flux output of Dispersion with Peclet Number 10 for the Np237 Chain Case. Np237 Result.

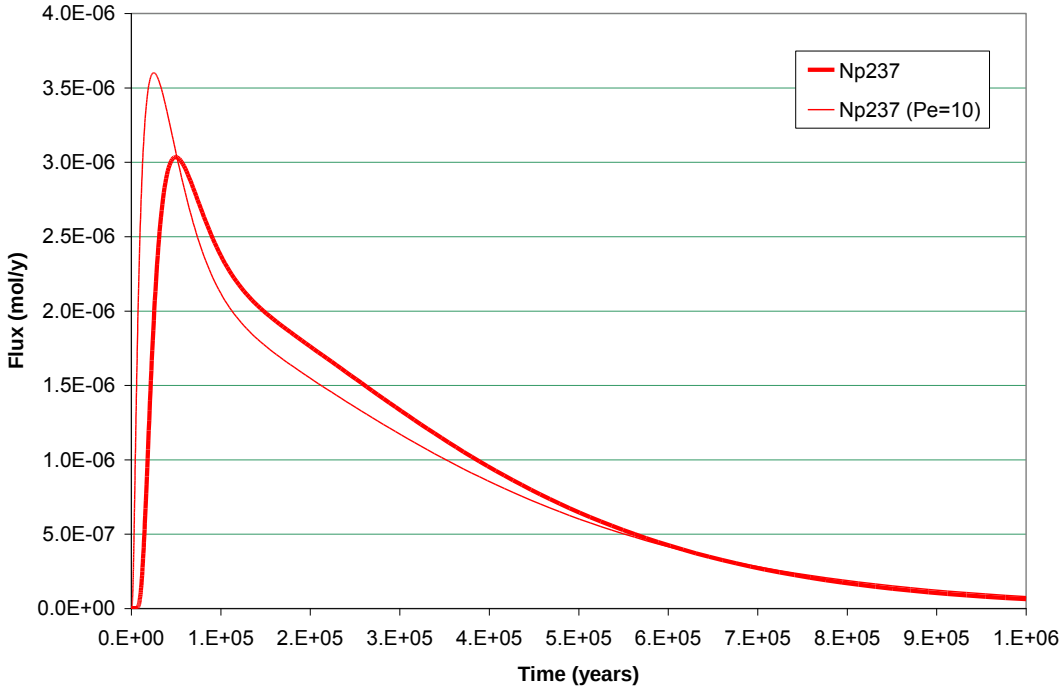

Figure 23: Impact on flux output of Dispersion with Peclet Number 10 for the Np237 Chain Case. U233 Result.

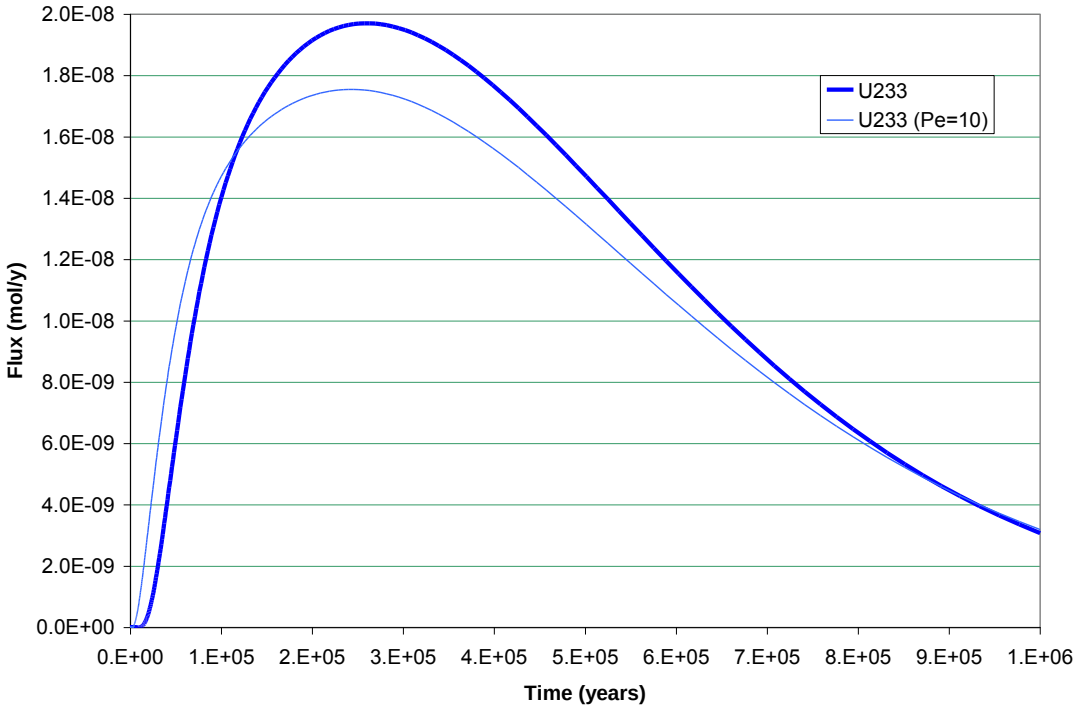

Figure 24: Impact on flux output of Dispersion with Peclet Number 10 for the Np237 Chain Case. Th229 Result.

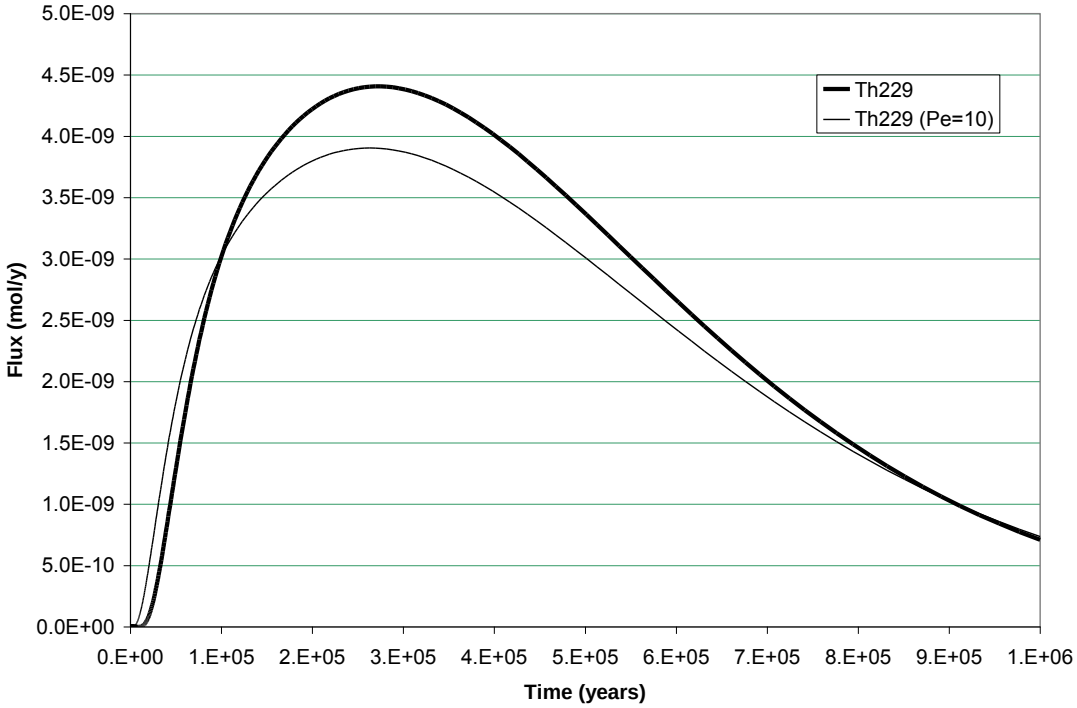

Varying Matrix Properties

The effect of varying matrix properties on the chain members is likely to be more complex than the single nuclide results. A particular case of interest is the effect of the parent retention factor.

Here we run a similar case to the Se79 example. Only the Np237 retention factor is varied, with 5e4 and 4.5e5 being used giving an average of 2e5 for the infinite matrix case. The daughter retention values are unchanged and there is the same F factor in each segment. Two cases were run with the segments in different orders. Figure 25 shows the results. The Np237 result is similar to that with the average retention(it would be exactly the same with an infinite matrix); the ordering is irrelevant. The daughter nuclides are much more affected and the order is important. When the parent nuclide has a high retention at the end of the path the daughters have higher peaks. This is because they are in equilibrium with the parent and this equilibrium is re-established at the end of the path, making the averages irrelevant.

Figure 25: Impact on flux output of Varying Np237 Retention Factor for the Np237 Chain Case

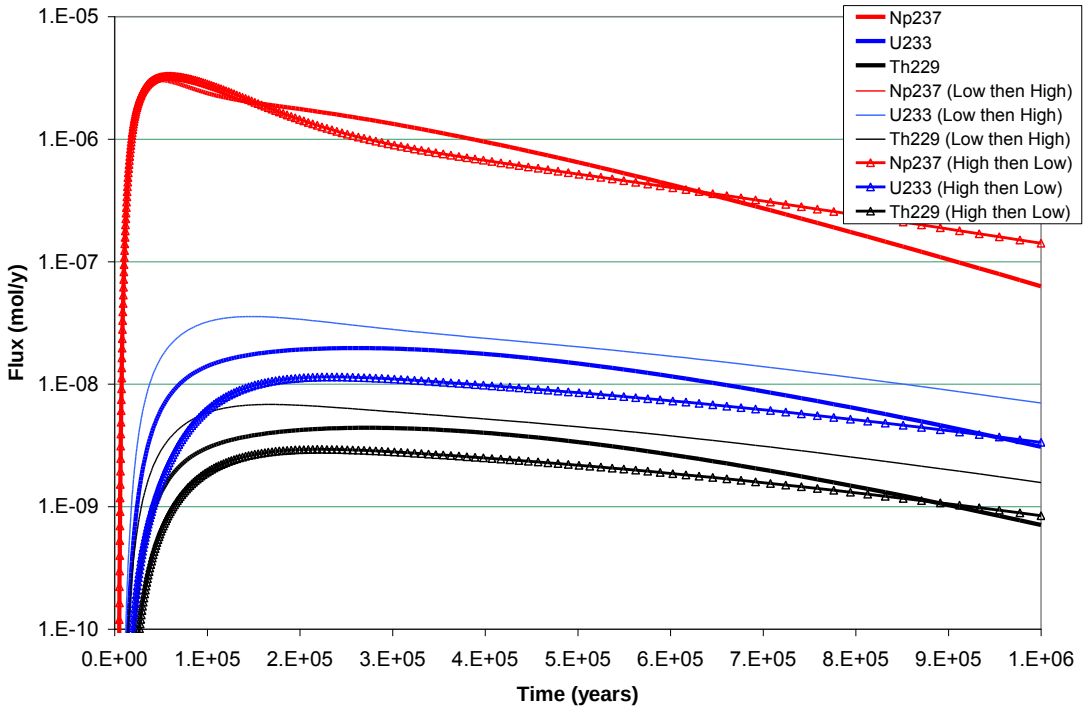

3.5 Examples Using Pathlines

In order to look at some realistic cases, some paths generated using SSM's independent flow modelling capability have been used (Geier, 2008). Step-by–step path information (at 5 m intervals) was supplied by Geier (2009) for a sample set of paths, starting at different points. Four of the paths, chosen at random, are illustrated in Figure 26 to Figure 29. The label Snnn Pnn uniquely identifies the path in the supplied dataset.

Each figure consists of three charts. The top one shows the cumulative F factor (left hand axis) and travel time (right-hand axis) against distance. Note that the time unit here is seconds.

The middle chart shows the half-aperture of the feature that the path is passing though. Four types of feature are distinguished by colour. The EDZ (engineering damaged zone) around the deposition hole and other repository structures is typically the first; then the stochastic features around the repository that are explicitly included in the flow model; next, the rock mass further from the repository is represented by an orthogonal grid with equivalent properties; and finally, paths often reach a deterministic deformation zone.

These show that the initial EDZ can be the dominant contributor to the overall F-factor, as in does in 3 of the 4 cases. Flow in the deformation zones is rapid and they have large aperture, so they contribute little to the F factor or travel time.

It is also notable that the paths travel substantial distances at depth before finding a rapid route to the surface.

In order to explore the implications of this type of path, one of the cases was selected for transport modelling here. The final case was taken, and Figure 29 includes an indication of how this was split into 6 segments represented the different parts of the path.

The length of each segment follows from the geometry. The aperture and velocity were chosen to match the cumulative F factor and travel times at the end of each segment.

Figure 26: Path line S112 P52

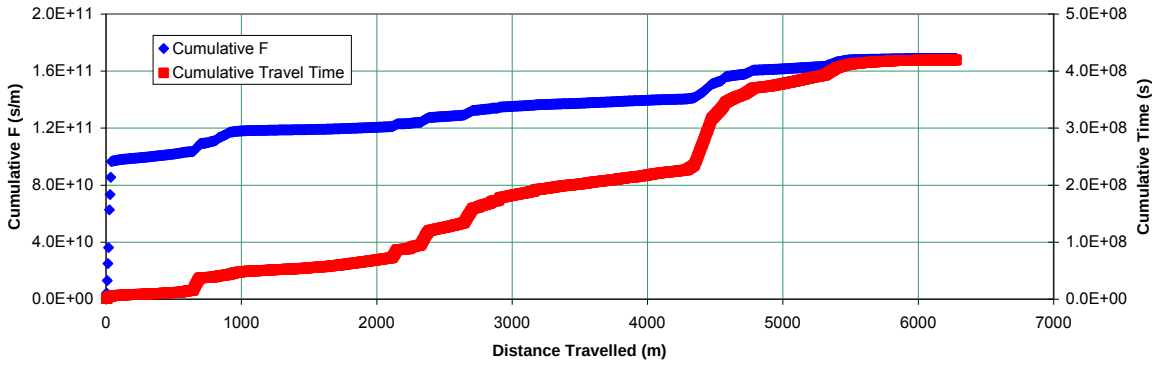

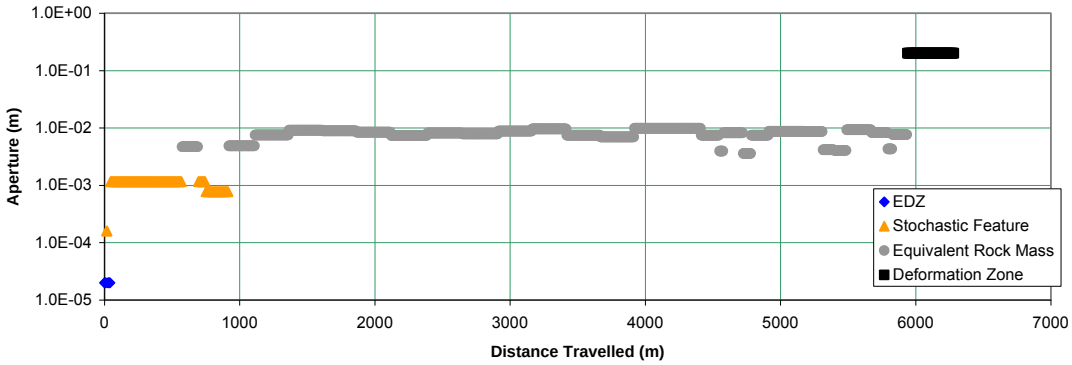

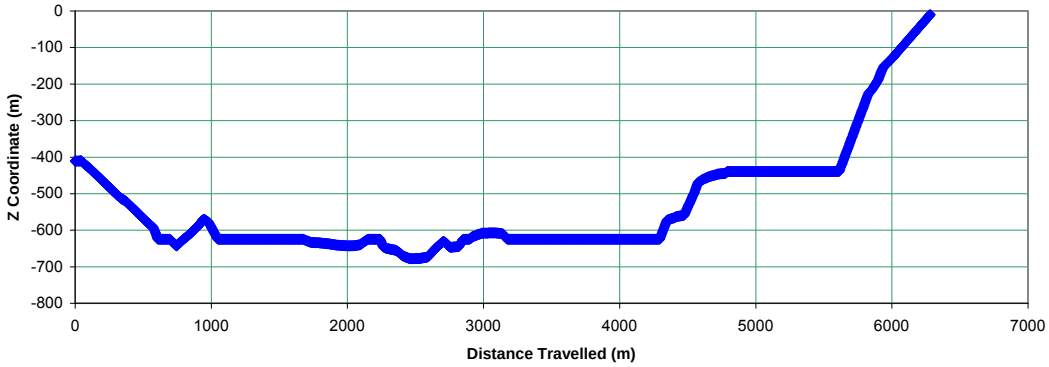

Figure 27: Path line S154 P35

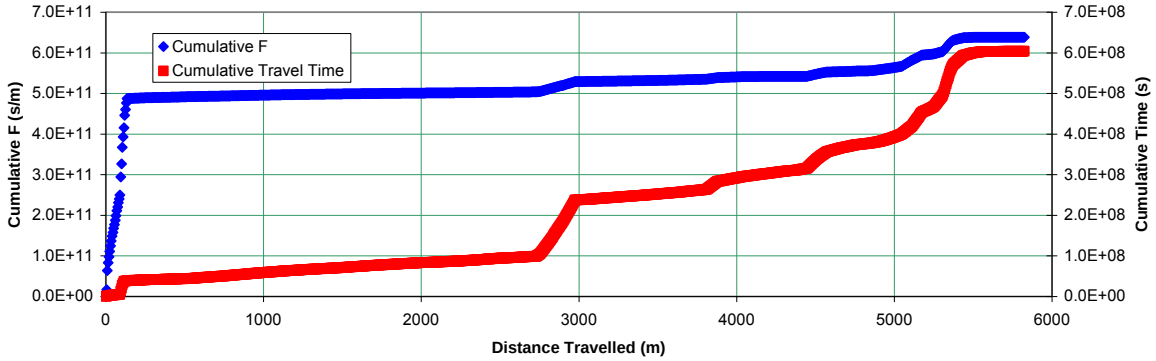

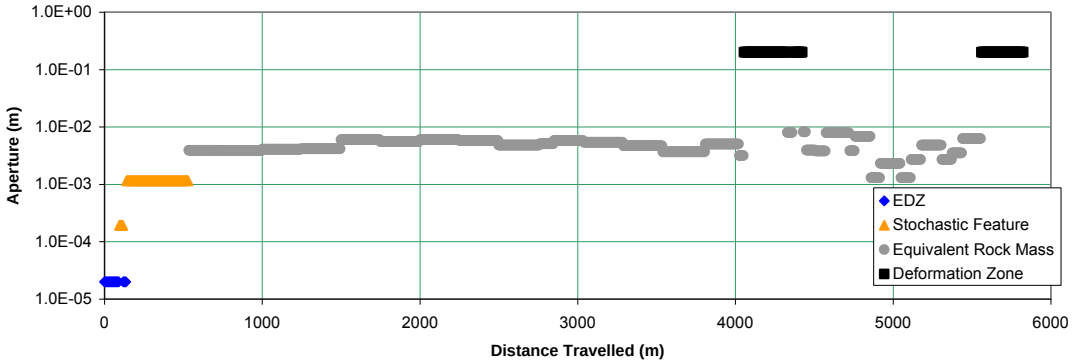

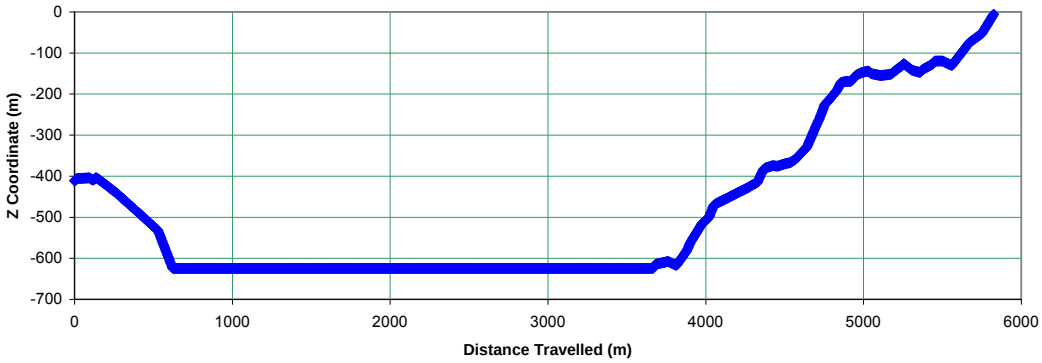

Figure 28: Path line S223 P96

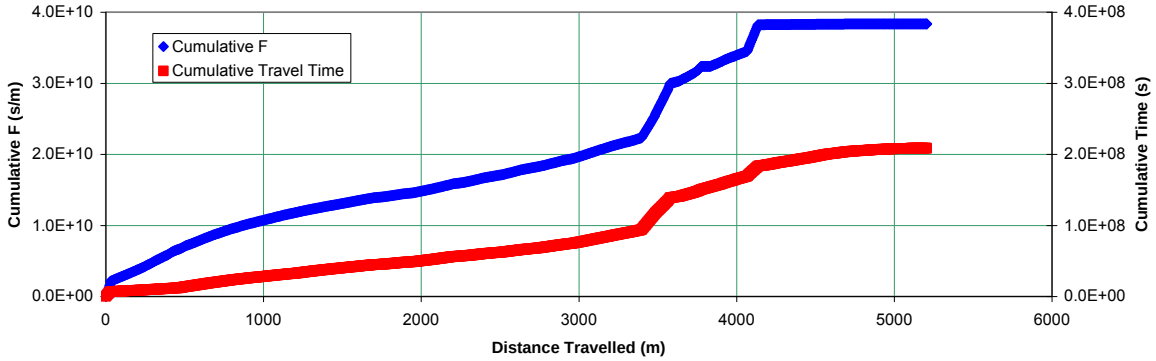

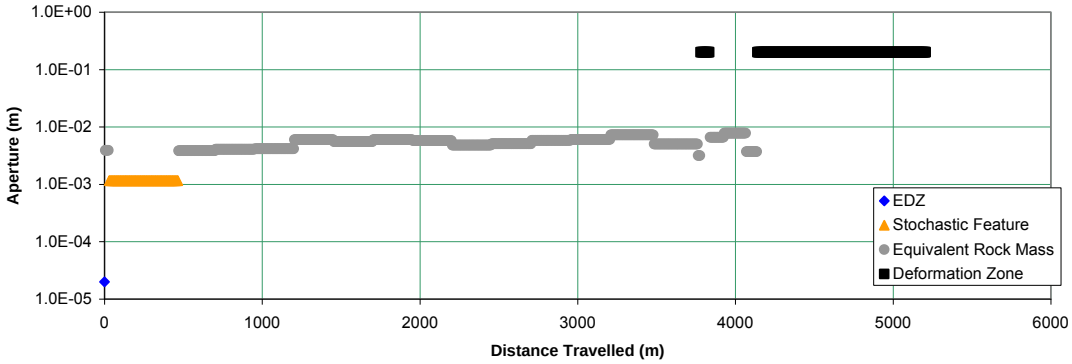

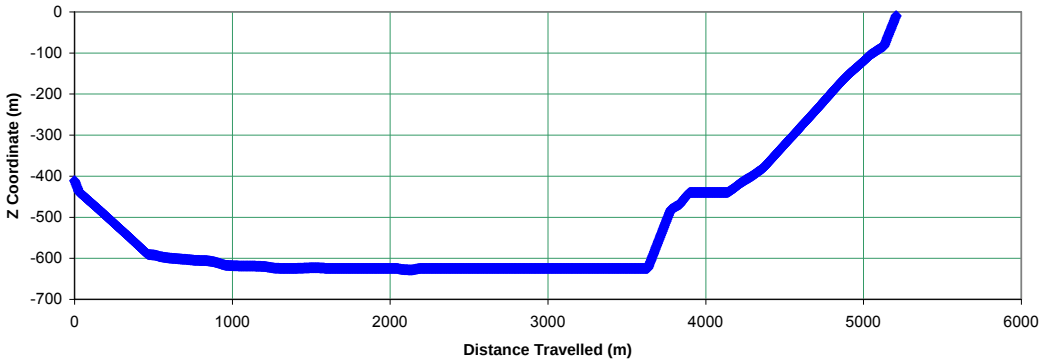

Figure 29: Path line S371 P70

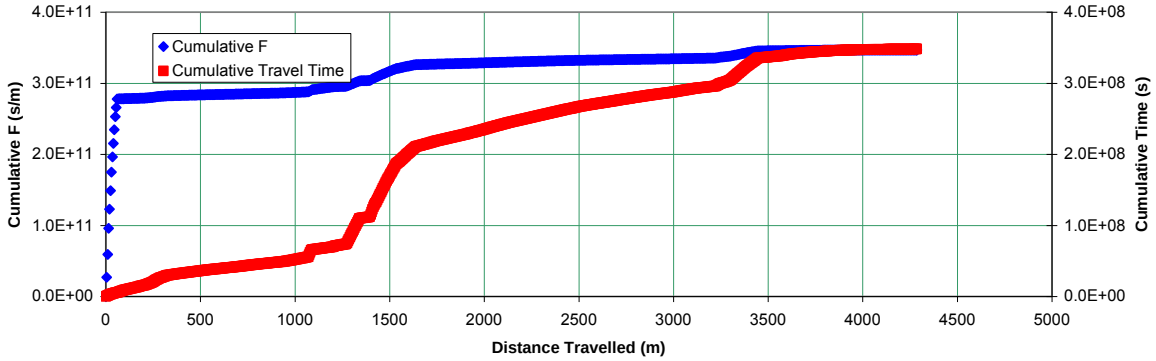

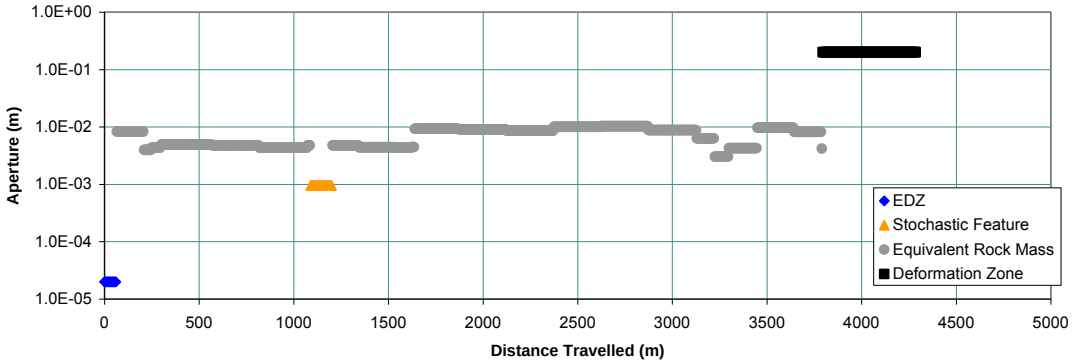

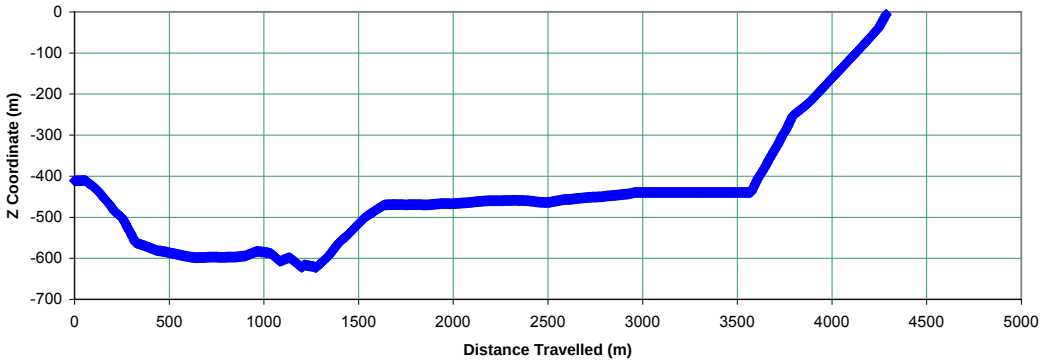

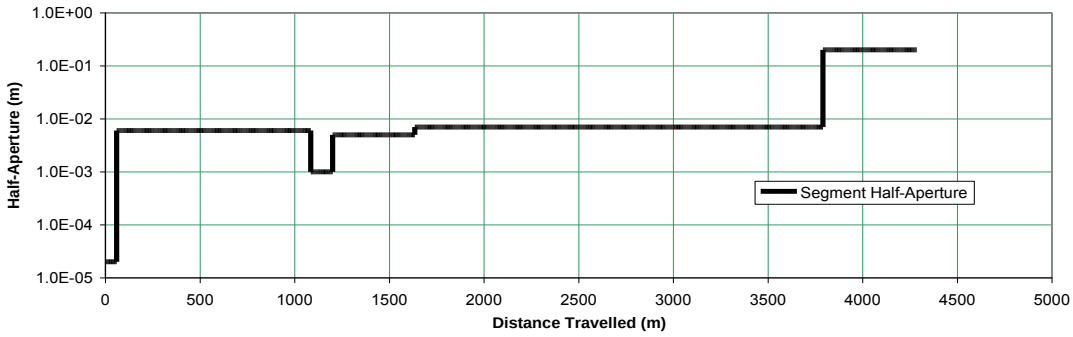

The flow properties used for the transport modelling are given in Table 3.

Table 3: Flow Properties for the Example Pathline (S371 P70)

Segment	Length (m)	Velocity (m/y)	Aperture (m)
1	60	1e-5	4e-5
2	1000	1.7e-5	0.012
3	120	2.4e-5	0.002
4	400	2.8e-6	0.001
5	2000	1.5e-5	0.014
6	500	1.5e-4	0.4

The matrix properties and source term used were as in the numerical study of Section 3.4.

A base case was run for Se79 and the Np237 chain and several variants were explored to look at sensitivity. The focus was on the properties of the EDZ, which are highly uncertain.

Figure 30 shows the Se79 results. It is clear that changing properties of the first section can have a significant impact on the flux at the surface. The high initial aperture case if for an aperture of twice the base case (80 μm instead of 40 μm) and the low initial Kd is for a Kd reduced by a factor of 2. Both of these small changes have a significant effect on the flux, confirming that the overall behaviour is dominated by the transport through the EDZ at the start of the path.

Figure 31 also shows the effect of the higher initial aperture case, this time on the Np237 chain results. The effect of higher Kd for Np in the equivalent rock mass (ERM) section is also explored; this has little effect, despite this being the majority of the path, again confirming the dominance of the EDZ section.

Figure 30: Path line S371 P70 Se79 results

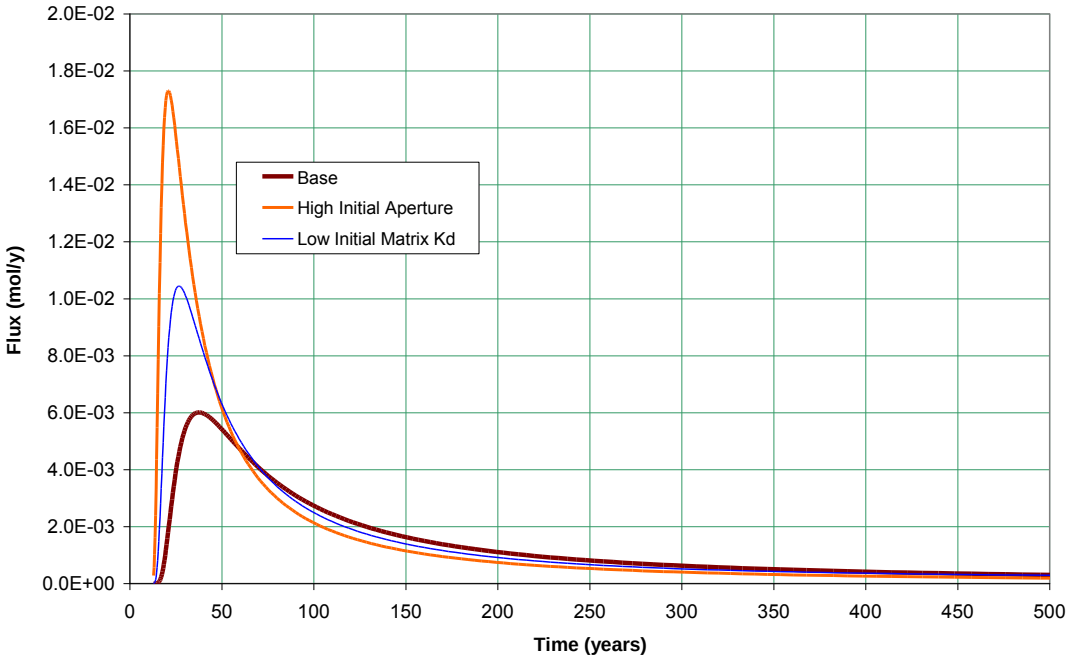

Figure 31: Path line S371 P70 Np chain results

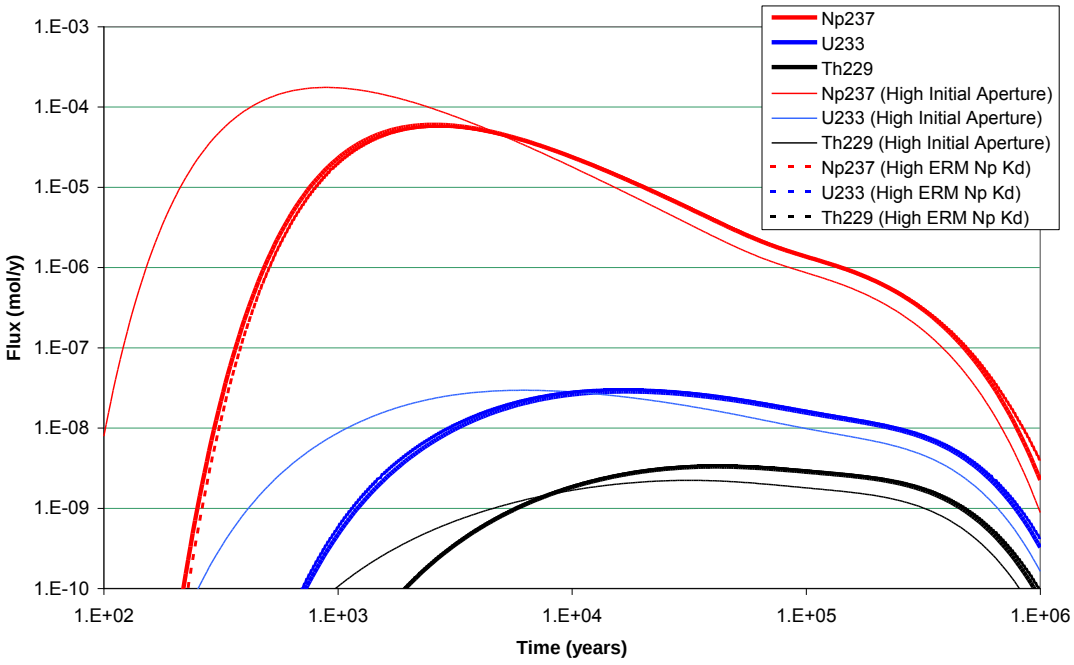

3.6 Conclusions

The SKB approach to radionuclide transport modelling has been to use a one-dimensional path with constant properties. It is expected that this will continue to be their main approach within SR Site. The integrated contact between flowing (fracture) and stagnant (matrix) waters is captured through the F-factor and it is claimed that this provides an adequate representation of the path. This study has explored the extent to which the F-factor approach introduces approximations and the scale of these approximations.

We have re-derived the basic approach to see when the F-factor approach is exact. This is limited to the case with a single nuclide, constant matrix properties and no dispersion. A computer code was developed to calculate the solution for the general case, using the Laplace transform approach that is used by SKB in FARF31.

Sensitivity on the output flux to the F-factor, travel time and matrix property was explored in order to put the scale of approximation into the context of overall uncertainties. Three example cases were considered: a non-sorbed nuclide (I129); a sorbed nuclide (Se79) and a decay chain (Np237, U233, Th229). The non-sorbed nuclide interacts weakly with the rock matrix and essentially passes through the geosphere subject only to the delay caused by the travel time.

Output fluxes are highly sensitive to the F-factor itself, but not to the water travel time. Matrix penetration depth can be important if it is small, but the infinite depth approximation applies to larger depths (10 cm or more in the cases considered here). The retention and porosity in the matrix have a directly proportional effect on peak releases for the single sorbed nuclide.

Compared to other sensitivities, the effect of dispersion for Peclet numbers 10 and higher is small. Also, although the ordering of the properties encountered along a flow path does make a difference to the output flux when dispersion is present, this effect is small. This applies both to the single nuclide and chain cases.

Varying matrix retention properties along a flow path can be handled exactly for a single nuclide, in the infinite matrix case, a result that SKB may be unaware of.

The main approximation that can occur with the F-factor approach is in the use of constant matrix retention properties for a chain case. When there are short-lived daughters, their output fluxes are strongly influenced by the matrix retention properties at the end of the path rather than by any overall average.

Cases using path lines generated using SSM's independent discrete feature model showed that the EDZ can dominate the F-factor for many release points. In such cases,

the properties of this EDZ control the output flux. The approach that SKB take to the EDZ in SR Site should be a focus for review. We note, however, that the relevance of such issues will depend on which canister failure scenarios are considered – if failures can only occur by buffer erosion then this is likely to be where flows are at their highest and path lines from such locations may not pass through the EDZ.

4 PDFs and Parameter Correlations

4.1 Introduction

The regulations in Sweden oblige SKB to undertake risk calculations. This necessitates the specification of probability density functions (PDFs) for uncertain parameters in their consequence analysis models. It also requires consideration to be given to correlations between these uncertain parameters (e.g. to avoid physically incompatible combinations).

The PDFs are by their nature subjective, since they represent lack of knowledge on the precise parameter values that apply. They are, however, motivated by whatever knowledge exists: physical limits; field experiments; laboratory experiments and so on. The subjectivity enters in deciding how relevant these various sources of data are (e.g. the conditions in the experiment will not be precisely those of interest) and in allowing for modelling simplifications or abstractions (e.g. using a single average value requires that this average is what the PDF corresponds to).

Correlations arise because several parameters are actually related to a single underlying process. Where this can be represented explicitly, this approach should be favoured, but in many situations the linkage is less clear. For example, Kds all depend on the local mineralogy and groundwater chemistry and so uncertainty in these aspects impacts on all Kds and makes them correlated.

It is not possible to develop "perfect" PDFs and correlation structures – their subjective nature will always allow for controversy and leave room for refinement. It is, however, reasonable to expect that the PDFs and correlations chosen are defensible and that the arguments supporting them are fully documented. It is SKB's aim to do this in the Data Report (SKB, 2006b).

In the review process for SR-Can (SKI and SSI, 2008), particular instances where the reviewers questioned the choice of PDF can be found, for example for fuel dissolution rates. More generally, the choice between, say, a triangular and a log-triangular PDF needs to be carefully considered, as does the limits for such distributions. For example, if a Kd has a "best estimate" of 1e-3 (m^3 kg^{-1}) but a range from essentially zero to 1e-2, then the choice of PDF can be important for the overall risk calculation: a triangular PDF from 0 to 1e-2 with a peak at 1e-3 has just 10% of the distribution below the best estimate; a log-triangular distribution from a low value of 1e-6 to 1e-2 with a peak at 1e-3 has 75% of the distribution below the best estimate.

Clearly these issues potentially arise throughout the modelling chain – wherever uncertainty is (or should be) acknowledged. In particular, it occurs in the radionuclide transport calculations and this is the focus for this initial study. The near-field (NF) and far-field (FF) components used by SKB are the best place to start. The biosphere needs to be looked at in due course, but this is outside the scope of the current report.

4.2 Triangular and Log-triangular PDFs

SKB generally use triangular or log-triangular PDFs.

For a parameter that has a triangular distribution between the limits $x=a$ and $x=c$ with peak at $x=b$, the mean value of the parameter is $\frac{(a+b+c)}{3}$.

For a parameter that has a corresponding log-triangular distribution the mean value of the parameter is given by:

$$\frac{2}{(\log c-\log a)}\left[\frac{a}{(\log b-\log a)}+\frac{c}{(\log c-\log b)}-\frac{b(\log c-\log a)}{(\log b-\log a)(\log c-\log b)}\right].$$

In this expression the logarithms are natural logarithms.

4.3 Correlated Quantities

Where fully correlated groups of elements are considered a value x is obtained from a uniform distribution [0, 1] and an input value y is then calculated as $y = F^{-1}(x)$, where $F(y)$ is the cumulative distribution function for the input variable in question. In a particular realisation, the same x is used for all elements belonging to the same correlation group.

For a triangular PDF with a lower value a, a peak value b and an upper value c, then the cumulative density function can be written as follows:

$$\begin{aligned} F(y) &= 0 \quad y \le a \\ &= \frac{(y-a)^2}{(b-a)(c-a)} \quad a \le y \le b \\ &= 1-\frac{(c-y)^2}{(c-b)(c-a)} \quad b \le y \le c \\ &= 1 \quad x \ge c \end{aligned}$$

So that for a given value of x, y can be determined as follows:

$$
\begin{aligned}
y = \quad & a + (c-a)\sqrt{x\xi} && 0 \le x \le \xi \\
= \quad & c - (c-a)\sqrt{(1-x)(1-\xi)} && \xi \le x \le 1
\end{aligned}
$$

$$
\xi = \frac{(b-a)}{(c-a)}
$$

4.4 Review of SKB Choices and Assumptions

4.4.1 Source Term and Near-Field Parameters

SKI and SSI (2008) discuss the possibility of higher burnup of fuel that will be sent for disposal. This would affect the radionuclide inventory, but this issue is not considered here.

Table 4 summarises the PDF choices used for source term and near-field (NF) parameter values. The nomenclature follows that employed in Maul et al. (2008). Data Report refers to SKB (2006b).

The following text discusses the key parameters.

Table 4: Source Term and NF Data Values

Parameter	PDF	Comments
Instantaneous release fractions α (-)	'Realistic' values in Table A-4 in Data Report. Triangular distributions employed.	Correlated values for I-129, Cl-36 and Cs-135 could be considered, as well as 'pessimistic' values – see text.
Fuel dissolution rate λ_F (y^{-1})	Data Report Section 3.3: triangular or log-triangular with minimum 1E-8, peak 1E-7 and maximum 1E-6	Both triangular and log-triangular distributions have been considered-see note in the text.
Loss of transport resistance t_{large} (y)	Table 10-3 in the main SR Can report refers to a single value of 1E5 y, but the Data Report indicates that any value between 0 and 1E5 y is possible	This parameter had a single deterministic value in the original AMBER calculations
Solubility limit S (mol m^{-3})	Parameter values employed were in a sample file provided by SKB, not included in SR-Can documentation.	Alternative PDFs could be chosen based on the information given in the Data Report.
Bentonite Effective diffusivity D (m^2 y^{-1})	Data given in Table A-11 of Data Report. Triangular distributions for each element. Correlations represented directly in AMBER calculations.	The range of values is small.
Bentonite Equilibrium sorption coefficients K_d (m^3 kg^{-1})	Table A-13 of Data Report (for highly saline groundwater). Log-triangular distributions for most radionuclides. Correlations derive from grouping radionuclides.	Table A-12 of Data Report gives sorption coefficients for saline and non-saline groundwater. See notes in text.
Backfill Effective diffusivity D (m^2 y^{-1})	Data given in Table A-17 of Data Report. Triangular distributions for each element. Correlations represented directly in AMBER calculations.	
Backfill Equilibrium sorption coefficients K_d (m^3 kg^{-1})	Table A-19 of Data Report (for highly saline groundwater). Log-triangular distributions for most radionuclides.	Table A-20 of Data Report gives sorption coefficients for saline and non-saline groundwater. See notes in text.
Porosity θ (-)	Buffer: Table A-11 of Data Report. Triangular PDFs for anions. Backfill: Table A-17 of Data Report. Triangular PDFs for anions.	See notes in text.
Darcy velocity at deposition hole wall q (m y^{-1})	Sample file provided by SKB, not included in SR-Can documentation	Used in specification of Q_{eq} when spalling is included
Equivalent flow rates at the deposition hole Q_{eq} (m^3 y^{-1})	Sample file provided by SKB, not included in SR-Can documentation	See text.

Fuel Instantaneous Release Fractions

Expert advice in the Data Report was that the instantaneous release fractions for I-129, Cl-36 and Cs-135 are all proportional to the fission gas release and should therefore be correlated. This is not reflected in the data given in Table A-4 in the Data Report.

The parameter values employed in the SR Can calculations employed the 'realistic' values from Table A-4, rather than the 'pessimistic' values that were specified for high fuel burn-up, but these are little different. In addition, the ranges covered are generally small, and so alternative PDF forms would make little difference to the PA calculations.

SKI and SSI (2008) questioned the justification for the parameter values chosen by SKB; more conservative methods have been proposed (for example by Johnson et al., 2005). In particular, the low values employed for Se-76 and Sn-126 were queried.

Fuel Dissolution Rates

As discussed in Maul et al. (2008), the Data Report appears to indicate that the original expert recommendation was for a triangular distribution, but a log-triangular distribution was actually employed in the calculations. This is one of the key parameters for determining overall risks.

For the values chosen by SKB for fuel dissolution, using a triangular distribution gives a mean value of 3.7E-7 y^{-1}. With a log-triangular distribution the corresponding value is 1.5E-7 y^{-1}, which is over a factor of 2 lower.

SKI and SSI (2008) point out that the fuel dissolution rate may be affected by burnup, and that it is possible that the fuel dissolution rate will change with time.

Work undertaken by Quintessa in the EU MICADO project has shown that with an intact buffer, for the range of fuel dissolution rates considered by SKB, the amount of material leaving the near-field (when expressed in terms of mass of total radioactivity) was not sensitive to the fuel dissolution rate (the overriding controlling factor was the flow rate in the fracture). However, if the total near-field dose is plotted instead of the mass of total radioactivity, a correlation can be seen with the peak near-field dose (Figure 32). This figure was produced using the base near-field AMBER case file (case N0), discussed in Section 4.5.

Figure 32: Sensitivity of Near-Field Dose Calculations to Fuel Dissolution Rate using the base near-field AMBER Case File

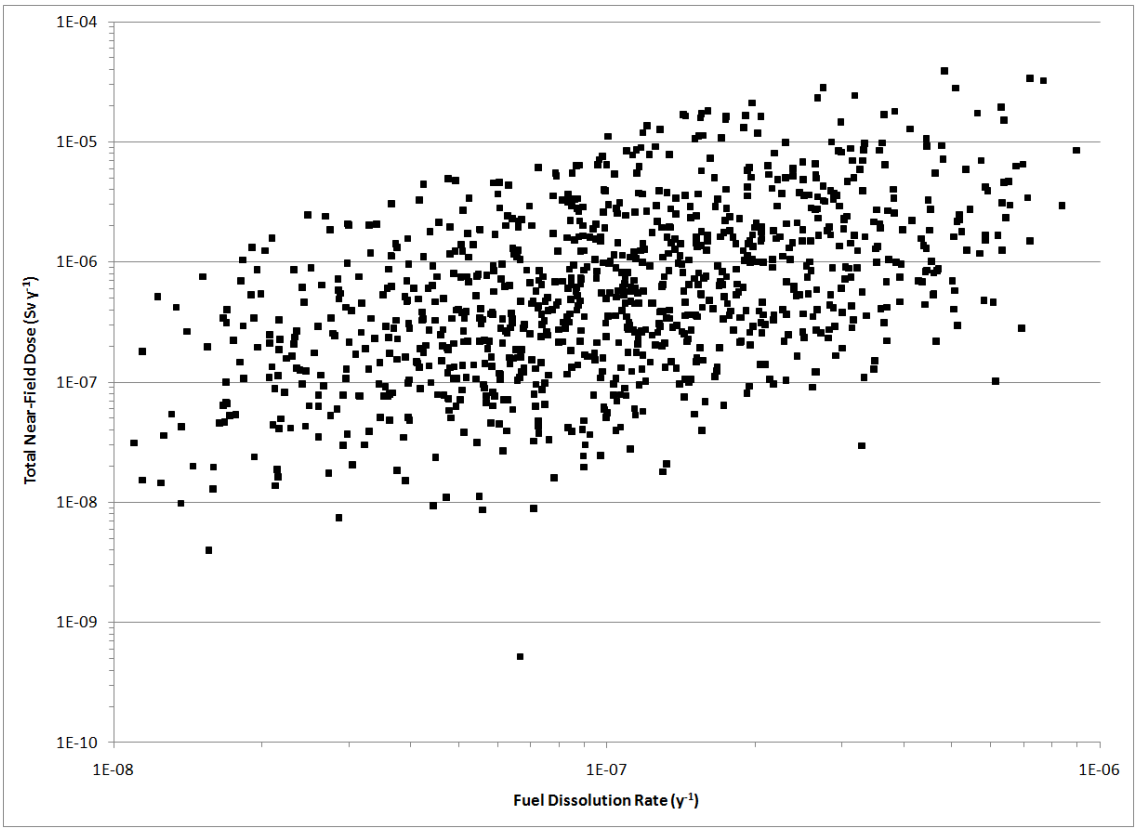

Loss of Transport Resistance

This parameter relates to the period from the onset of a defect to the complete loss of transport resistance between the canister and the buffer. In the Data Report it is stated that this is not an important parameter, but that any value between 0 and 1E5 y is possible. From the Main SR-Can report it appears that a single value of 1E4 y was employed.

Solubility Limits

The Data Report gives PDFs based on assumed groundwater compositions and information from Duro et al. (2006), but the actual parameter values employed were in a sample file provided by SKB, not included in SR-Can documentation. Clearly, alternative PDFs could be specified based on the information given in the SR-Can documentation.

Sorption Coefficients

SKB use correlated sorption coefficients. Values of K_d for elements (in a given redox state) in the same correlation group are fully correlated. As described in Maul et al. (2008), the way that these correlations were implemented by SKB was not been stated explicitly in the SR-Can documentation, but was been clarified in subsequent communications, although SKB indicated that these correlations had little effect on the SR-Can calculations. Log-triangular distributions were employed for most radionuclides.

Alternative calculations are possible with triangular PDFs and/or different groundwater type.

Buffer Porosity and Anion Exclusion

The modelling of the transport of anions through saturated bentonite is currently an important research area (see, for example, Birgesson and Karnland, 2009).

At the time that SR-Can was written SKB assumed that cations 'saw' the full buffer porosity, but anions were excluded from part of this (the interlayer porosity). This resulted in different values being employed for the buffer porosity and for the values of the effective diffusion coefficient for anions.

More recent work by Birgesson and Karnland (2009) suggest that in saturated compacted bentonite, there is very little 'free' porosity, that transport is predominantly through the interlayer regions, and that anions can be transported through these regions, albeit at a slower rate than cations. This change in conceptual model by SKB will certainly lead to a change in the model parameterisation in SR-Site, but is unlikely to have an important effect on the overall Performance Assessment.

Recent work on the THERSA project has led to the development of a new bentonite model (Bond et al, 2009). This also has very little free porosity at saturation for compacted bentonite. The main motivation for the new bentonite model was in the resaturation phase of the repository evolution, but it will be important in the erosion scenario. This will be important for consequence analysis and will provide a basis for checking claims about the number of canisters affected by erosion and the configuration of bentonite in a deposition hole that has suffered significant erosion.

Equivalent Flow Rates at the Deposition Hole

The information used in the SR-Can calculations was taken from detailed groundwater flow calculations and supplied by SKB as a sample file. In Maul et al. (2008) the

sensitivity to the assumptions employed was addressed using alternative independent discrete fracture network (DFN) flow calculations. As discussed in Section 2.3, this is very important for the overall PA; the main issue here is one of conceptual model uncertainty rather than parameter uncertainty.

The sensitivity of the release from the near field to the transport resistance is illustrated in Figure 33 which shows the near-field dose after one million years against the reciprocal of the resistance, Q_{eq}. The dose is broadly proportional to the Q_{eq}, as the regression line suggests. This effect will persist throughout the release calculations as long as an intact buffer is present.

Figure 33: Scatter Plot of Near Field Dose at 1E6 y against Equivalent Flow Rate for Calculations using the Independent DFN Data (no spalling). From SKI 2008:12 (Maul et al, 2008).

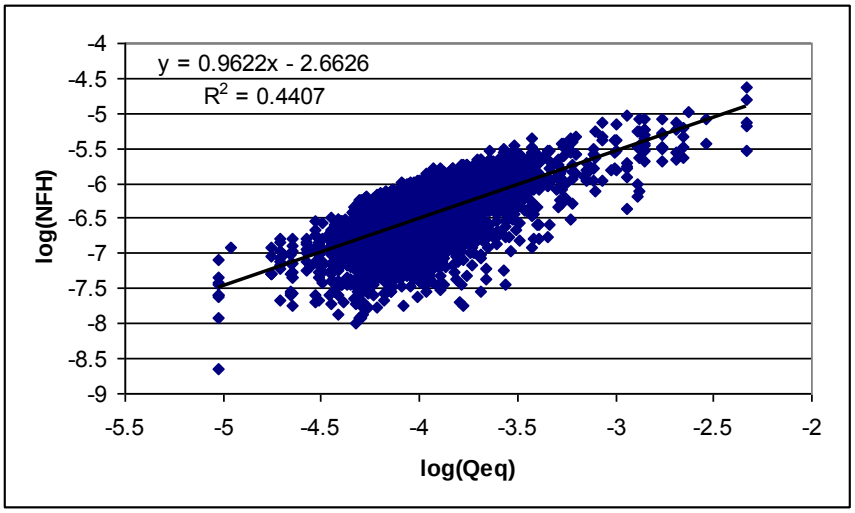

4.4.2 Far-Field Parameters

Table 5 reviews the PDF choices used for the far field (FF). The nomenclature follows that employed in Maul et al. (2008).

Flow Related Parameters

The geosphere transport resistance and the travel time are two of the 'data triples' used in the SR-Can calculations taken from detailed groundwater flow calculations and supplied by SKB as a sample file. In Maul et al. (2008) the sensitivity to the assumptions employed was addressed using alternative independent discrete fracture network (DFN) flow calculations. The main issue here is one of conceptual model uncertainty rather than parameter uncertainty.

Table 5: FF Data Values

Parameter	PDF	Comments
Geosphere transport resistance F (y m^{-1})	Sample file provided by SKB, not included in SR-Can documentation. One of the 'data triples'.	See text
Geosphere travel time t_w (y)	Sample file provided by SKB, not included in SR-Can documentation. One of the 'data triples'.	See text
Effective diffusivity D (m^2 y^{-1})	Rock values given in Data Report Tables A-40 and A-41. Anion exclusion for C, Cl, I and Se with reduction factor of 10. Expressed as the product of a site-specific formation factor (log-normal) and element-dependent diffusivity	
Matrix Porosity ε_m (-)	Table A-42 of data report (Forsmark value): log-normal with mean: -3.03 and standard deviation in the logarithm of 0.20.	
Equilibrium sorption coefficients K_d (m^3 kg^{-1})	Rock values from Table A-43/A-44 of Data report for saline conditions used in original AMBER calculations. Piecewise log-uniform distributions.	Alternative PDFs are possible. Non-saline values could be used in sensitivity studies.
Maximum penetration depth into rock matrix a_m (m)	Data report P194. Triangular distribution	Poorly defined. Other PDFs could be considered.

Sorption Coefficients

In SR Can, sorption coefficients are defined using distributions that are piece-wise uniform in log-space. For some radionuclides (Table A-43) the Data Report gives: the lower bound, LB; the 25th percentile, P25; the best estimate, BE; the 75th percentile, P75; and the upper bound, UB. In this case:

$$\text{If } 0 < x < 0.25 \text{ then } \log(K_d) = \log(LB) + x/0.25 * [\log(P25) - \log(LB)]$$
$$\text{If } 0.25 < x < 0.75 \text{ then } \log(K_d) = \log(P25) + (x - 0.25)/0.5 * [\log(P75) - \log(P25)]$$
$$\text{If } 0.75 < x < 1 \text{ then } \log(K_d) = \log(P75) + (x - 0.75)/0.25 * [\log(UB) - \log(P75)]$$

For other radionuclides (Table A-44) only LB and UB values were given. As for solubility, radionuclides are considered in correlation groups. Values were supplied for both saline and non-saline conditions.

The results from the study of varying properties in Section 3 show that the fluxes, and hence doses, from short-lived daughters are sensitive to the sorption properties at the end of the transport path rather than any average along the path.

SKI and SSI (2008) point out that the sorption coefficient used for Ra-226 is two orders of magnitude greater in SR-Can than SR-97, without a full explanation for this.

Matrix-Related Parameters

As is clear from the analysis presented in Section 3, it is not really appropriate to consider choices for the effective diffusivities, matrix porosity, matrix sorption coefficients, and rock penetration depth in isolation. In many cases the rock penetration depth can be taken to be effectively infinite, and in practice little information is likely to be available for this parameter. In the analytical expressions presented in Section 3 it is frequently the multiplicative combination of the first three parameters that is important, related to the sorption 'capacity' of the matrix.

4.5 Additional Calculations

A set of additional calculations has been defined to address further the issues raised in the review of SKB's choice of parameter PDFs and correlations. The calculations are based on variants of the AMBER calculations for the pin-hole scenario presented in Maul et al. (2008). For simplicity the pathways Q2 and Q3 have been removed from the model: this helps focus attention on the issues being addressed without the complicating factor of different transport pathways. This was found to be useful in the calculations undertaken for the EU MICADO project.

The calculations are shown in Table 6. For the near-field 'N' calculations 'near-field-doses' are calculated (as discussed in SKB, 2006b) in order to investigate the importance of the changes made.

Table 6: Additional Calculations

	Calculation
N0	A **Reference** near-field probabilistic calculation following Maul et al. (2008), but without pathways Q2 and Q3, and without the geosphere. A uniform distribution for the parameter *t_large* between 0 and 1E5 y.
N1	Use of **IRF** (instant release fraction) values based on Johnson et al. (2005).
N2	Independent **solubility** parameters based on the information given in the Data report
N3	Independent **sorption** parameters based on the information given in the Data report
F0	A **Reference** far-field calculation with representative deterministic values for the near-field parameters and the far field flow parameters; only the parameters related to the rock matrix are sampled.
F1	A **small penetration depth**
F2	A reduced **sorption** coefficient for Ra in the matrix. For sorbed nuclides, the parameter combination $\varepsilon_m R_m$ is proportional to the K_d, apart from a small porosity contribution, and this controls matrix effects for infinite penetration depths through $\beta_m = \sqrt{\varepsilon_m R_m D_m}$, and for small penetration depths as the dominant term in the capacity.
F3	Combination of a **small penetration depth** and a reduced **sorption** coefficient for Ra in the matrix

4.5.1 Results from Additional Calculations

Case N0 (Reference)

This reference probabilistic case was concerned only with the near-field, and the Q1 pathway along a fracture intersecting the deposition hole. A total of 1000 samples were used.

A plot of the total near-field dose is shown in Figure 34, with the 5th, 25th, 50th, 75th and 95th percentiles included. In all cases the peak total dose occurs towards the end of the simulation, at about 5e5 years.

Figure 34: Total near-field dose for case N0 (reference).

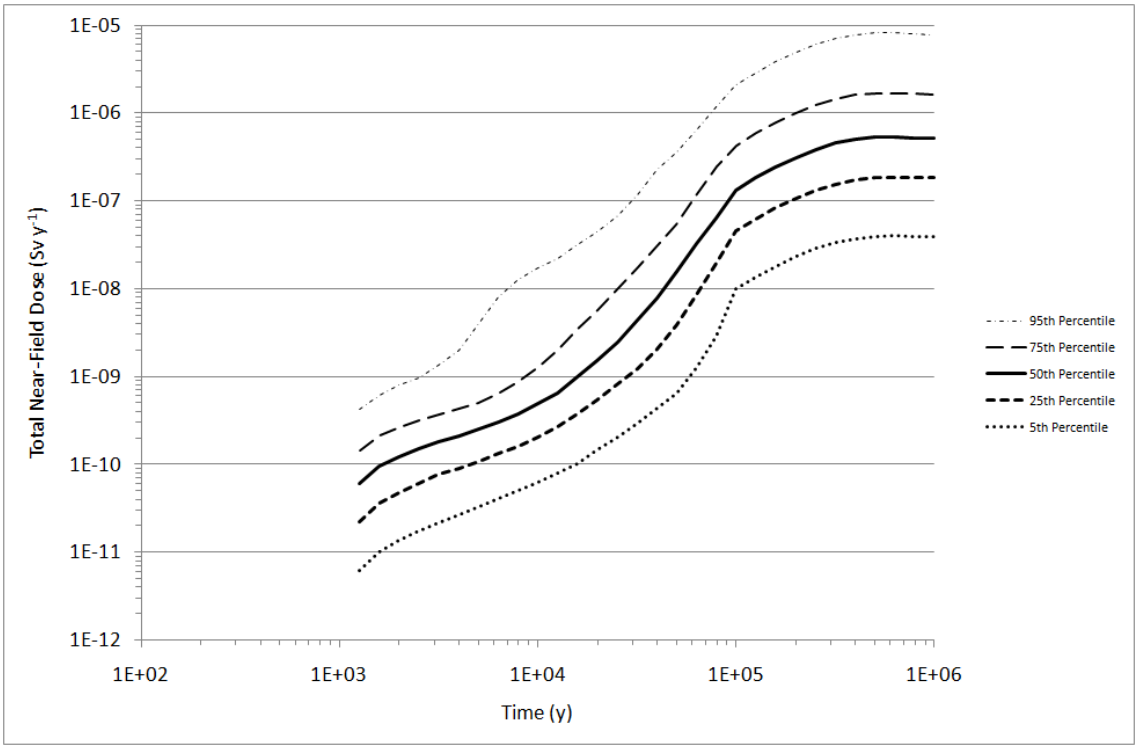

Case N1 (Alternative IRFs)

This deterministic case looked at the effects of using alternative instant release fractions, taken from Johnson et al. (2005). The case was based upon the reference deterministic pinhole scenario case described by Maul et al. (2008), with only the Q1 pathway, representing a fracture intersecting the deposition hole, included. The IRF values used in this case are shown in Table 7, along with the reference SKB values for comparison; in some cases there are four orders of magnitude difference. Although the values quoted by Johnson et al. (2005) are for PWR fuel, they are adopted for this case in the absence of other figures.

Table 7: Comparison of IRF values (as a fraction of the total inventory) used by SKB and for case N1 (Johnson et al., 2005). Where ranges are shown, a triangular distribution is used.

Radionuclide	IRF	
	Reference (SKB, 2006b)	Johnson et al. (2005)
^{79}Se	0.0003 [0, 0.001]	0.11
^{90}Sr	0.0025	0.11
^{99}Tc	0.002 [0, 0.01]	0.11
^{107}Pd	0.002 [0, 0.01]	0.11
^{126}Sn	0.00003 [0, 0.0001]	0.11
^{129}I	0.01 [0, 0.025]	0.16
^{135}Cs	0.01 [0, 0.025]	0.16
^{137}Cs	0.01 [0, 0.025]	0.16

The total near-field dose is shown in Figure 35 along with the reference deterministic case (using the SKB values for the IRFs). The larger IRFs result in an order of magnitude increase in the first peak in the dose at 1e4 years, when the pinhole defect grows. However from 1e5 years onwards, as would be expected, the two variant cases converge as the dominant release mechanism becomes dissolution of the fuel matrix.

For the total dose in the biosphere, the IRFs are more important as the geosphere plays an important role in reducing the long-term release of radionuclides from the repository. The total dose for this case is shown in Figure 36, again with the results from the reference deterministic case. Once again the dose is increased by approximately an order of magnitude; in this case the peak dose is attributable to the IRF.

Figure 35: Total near field dose for case N1 (alternative IRFs).

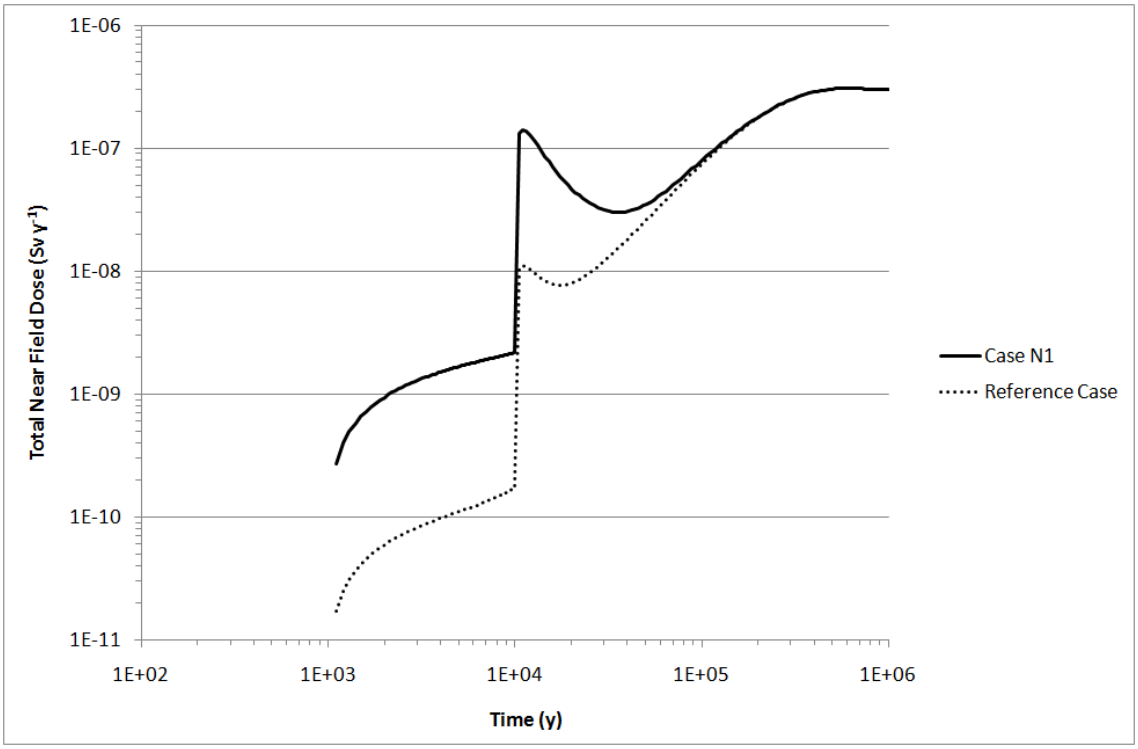

Figure 36: Total dose for case N1 (alternative IRFs).

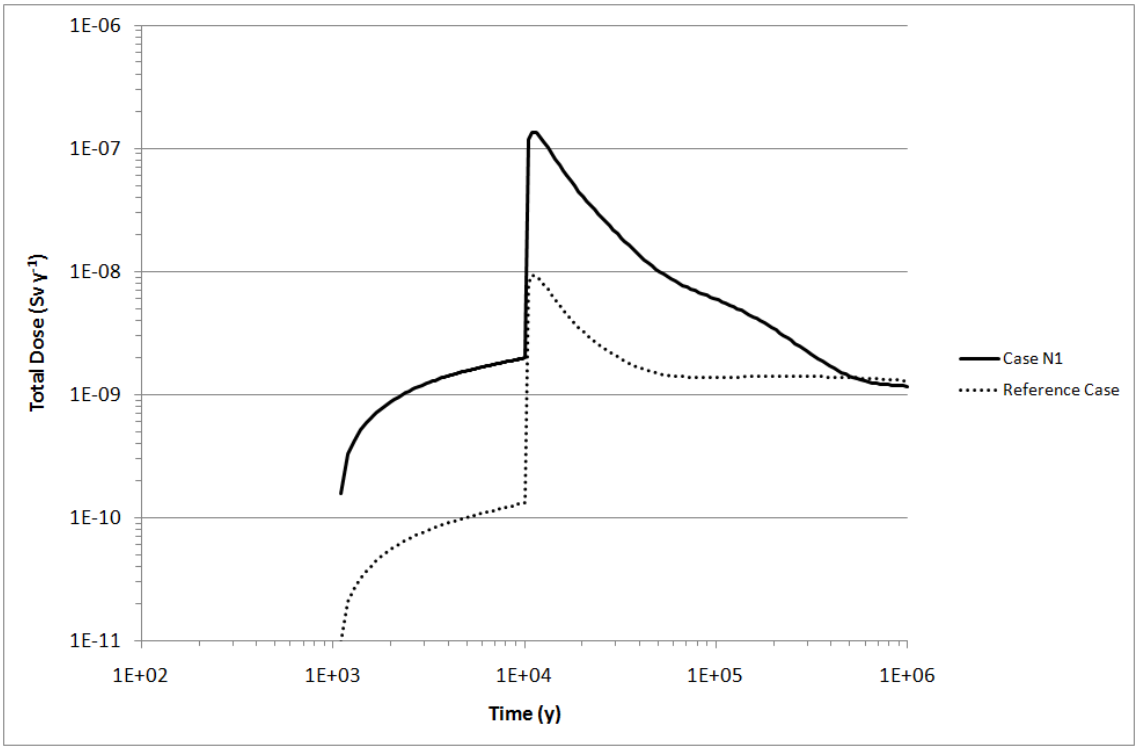

Case N2 (Solubilities)

For the reference probabilistic case solubilities are sampled from a data file provided by SKB, and these appear to be consistent with the histograms given in the appendix of the data report (SKB, 2006b). However in the discussion of solubilities the data report references Duro et al. (2006) which contains suggested uncorrelated ranges for solubilities. Case N2 investigates the effects of using these uncorrelated solubility limits, some of which differ by a large number of orders of magnitude from those in the reference case (notably Ag, U, Se, Pu, and Np). Table 8 compares the reference case values against the values used for this case. As stated in Duro et al. (2006), Cs was assumed to have no solubility limit. Values for the elements Cl, I, and Ca were not given in Duro et al., and were also assumed to have no limit. Pb and Po were taken to have the same limits as Ni, and Ac taken to have the same limit as Ra.

Table 8: Comparison of element solubilities used by SKB and for case N2 (Duro et al., 2006). The "Reference Range" column gives the minimum and maximum values found in the data file provided by SKB, which appears to correlate with the histograms given in the appendix of the data report (SKB, 2006b). The best estimate value quoted for Duro et al. (2006) is the 'RCL' (recommended concentration limit) value, taken from Table 8-1. The ranges were taken from the minimum and maximum values calculated across the scenarios.

Element	Solubility (mol m^{-3})	
	Reference Range	Duro et al. (2006)
Ag	3.34e-17 - 2.50e-10	4.43e-3 [6.9e-4, 5.1e-2]
Am	1.53e-4 - 5.21e-3	8.7e-3 [1.1e-4, 3.7e-2]
C	unlimited	7.1e0 [1.03e-1, 7.1e0]
Cm	2.20e-5 - 9.90e-4	8.7e-3 [1.1e-4, 3.7e-2]
Ho	5.18e-4 - 4.27e-3	1.2e-3 [9.9e-4, 2.6e-2]
Nb	2.08e-2 - 6.08e-1	2.4e-2 [2.4e-2, 2.9e0]
Ni	1.38e-4 - 8.55e-2	5.5e-2 [4.4e-5, 3.4e0]
Np	9.78e-7 - 1.05e-6	1.0e-6 [5.1e-7, 1.7e-2]
Pa	3.17e-4 - 3.33e-4	3.0e-4 [2.0e-4, 3.2e-4]
Pd	3.87e-3 - 3.98e-3	2.9e-3 [2.7e-3, 5.7e-3]
Pu	8.34e-7 - 1.53e-3	1.3e-4 [1.3e-7, 5.9e-1]
Ra	1.31e-4 - 2.33e-3	9.8e-5 [4.0e-5, 8.6e-4]
Se	4.01e-8 - 9.78e-7	1.4e-7 [8.8e-8, no limit]
Sm	3.05e-6 - 4.05e-4	4.4e-4 [2.2e-6, 4.1e-3]
Sn	5.51e-5 - 5.12e-4	8.6e-5 [8.6e-5, 2.7e-3]
Sr	5.77e-2 - 4.86e0	6.7e-1 [1.4e-2, 6.9e-1]
Tc	4.50e-16 - 5.14e-6	4.4e-6 [4.1e-6, 4.5e-6]
Th	2.96e-5 - 2.75e-3	7.9e-4 [2.3e-5, 1.0e-3]
U	4.17e-6 - 2.68e-4	9.5e-6 [3.0e-8, 4.6e-1]
Zr	1.22e-5 - 1.26e-5	9.7e-6 [6.6e-6, 1.0e-5]

The total near field dose for this case is shown in Figure 37, along with the results for the reference case (N0) in grey. There is virtually no difference between the two cases, indicating that the exact value of the solubility limits is not of great importance. This is confirmed by scatter plots of the element solubilities versus the peak total near field dose, which show no correlation.

Figure 37: Total near field doses for case N2 (solubilities).

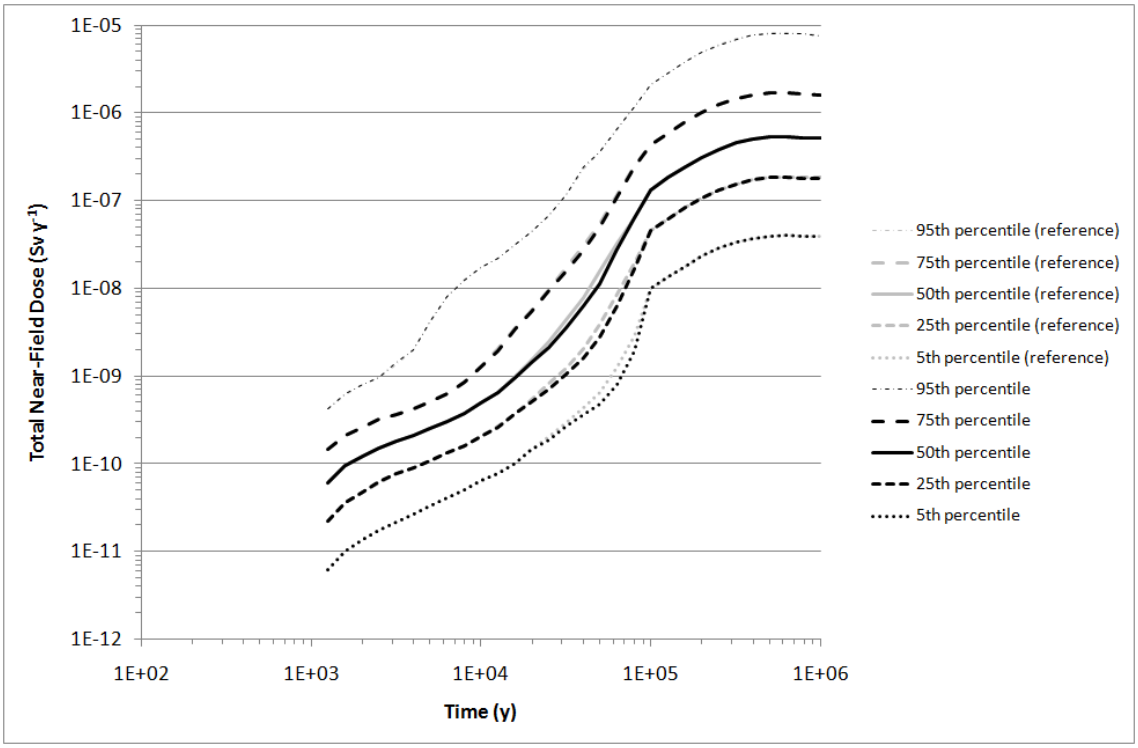

Case N3 (Sorption Coefficients)

The reference case uses buffer sorption coefficients from Table A-13 in the data report, which are valid for highly saline groundwaters. This case uses data from Table A-12, which is for saline and non-saline groundwaters.

The total near-field dose is shown in Figure 38. The results from the reference case are also shown, for comparison. Once again there is little change from the reference case, though the effect of the sorption coefficients increases towards the end of the simulation. Scatter plots of the sorption coefficients for individual elements versus the peak total near field dose do not indicate any strong correlations, confirming the insignificant effect of the buffer transport resistance.

Figure 38: Total near-field doses for case N3 (sorption coefficients).

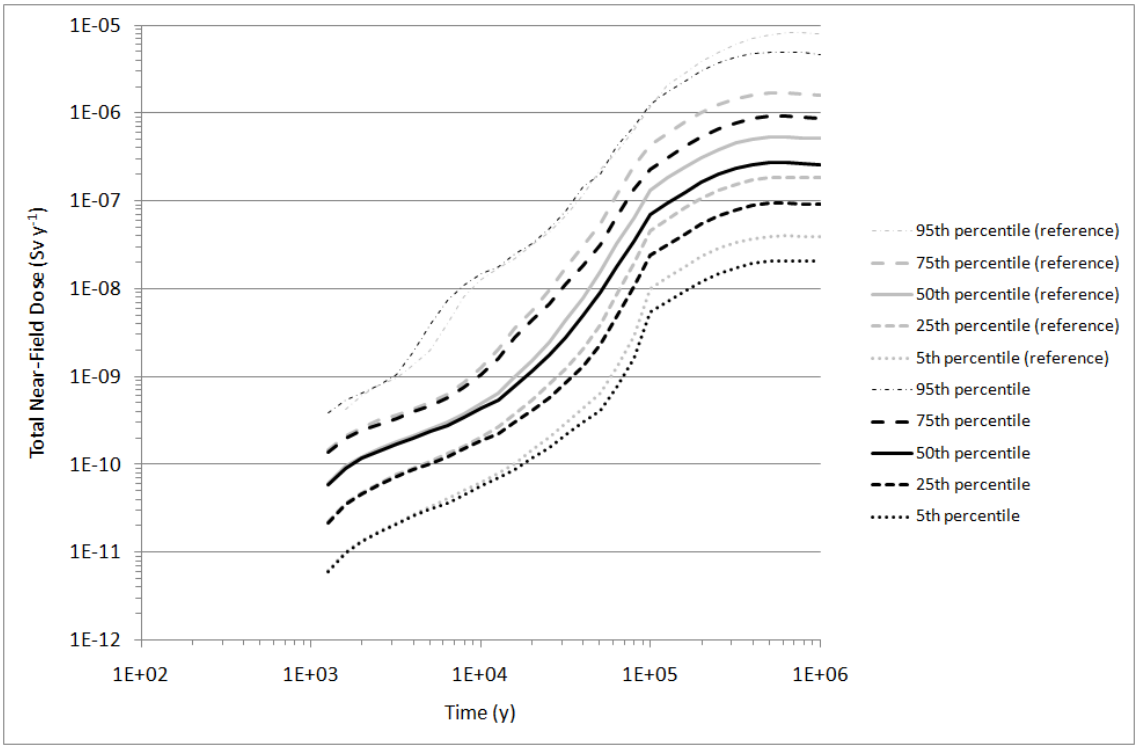

Case F0 Reference Far-Field with Sampled Matrix Penetration Depth

This reference far-field case included the geosphere, but like the other cases, concentrated on the Q1 release pathway from the deposition hole along a fracture. Representative deterministic values were used for the near-field parameters and the far-field flow parameters, thus focussing on the parameters concerned with the physical properties of the rock matrix which were sampled as before.

The rock matrix penetration depth was the same as that used in the original case described in Maul et al. (2008), which is a sampled triangular distribution ranging from 0.02 m to 10 m with a peak at 10 m. In Section 3 it was shown that penetration depths of about 10 cm or larger were equivalent to considering an infinite penetration depth. The distribution used for this case is biased towards larger penetration depths, at the scale of metres rather than centimetres, therefore there will only be a small number of samples where the penetration depth can be considered as finite.

Percentiles of the total dose for this case is shown in Figure 39. After the pinhole widens, the doses from most of the sampled cases fall within a small range, however the 95th percentile is considerably higher than the other percentiles. The U-Th-Ra-Pb decay chain is of particular interest and the contribution to the total dose from this chain is shown in Figure 40. The wide range of doses arises directly from the wide range of F-factors that were sampled.

Figure 39: Total dose for case F0 (reference far-field with sampled penetration depth)

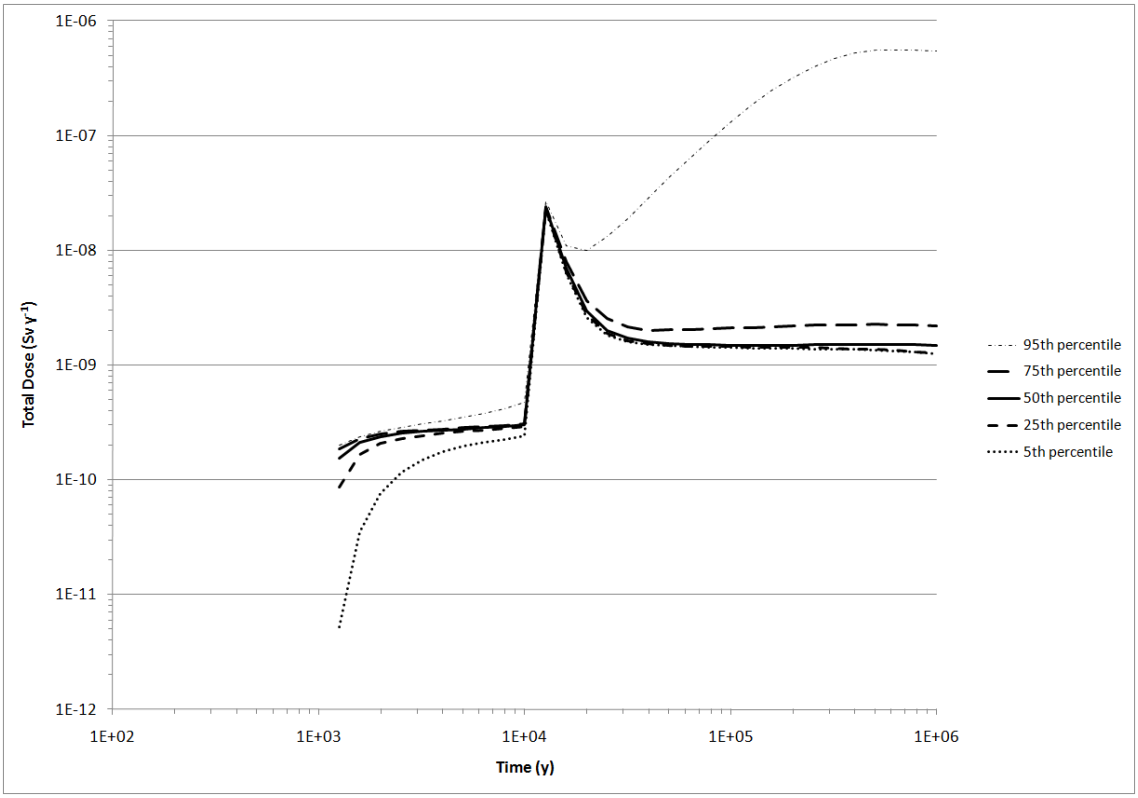

Figure 40: Contribution to the total dose from the U-Th-Ra-Pb decay chain for case F0 (reference far-field with sampled penetration depth)

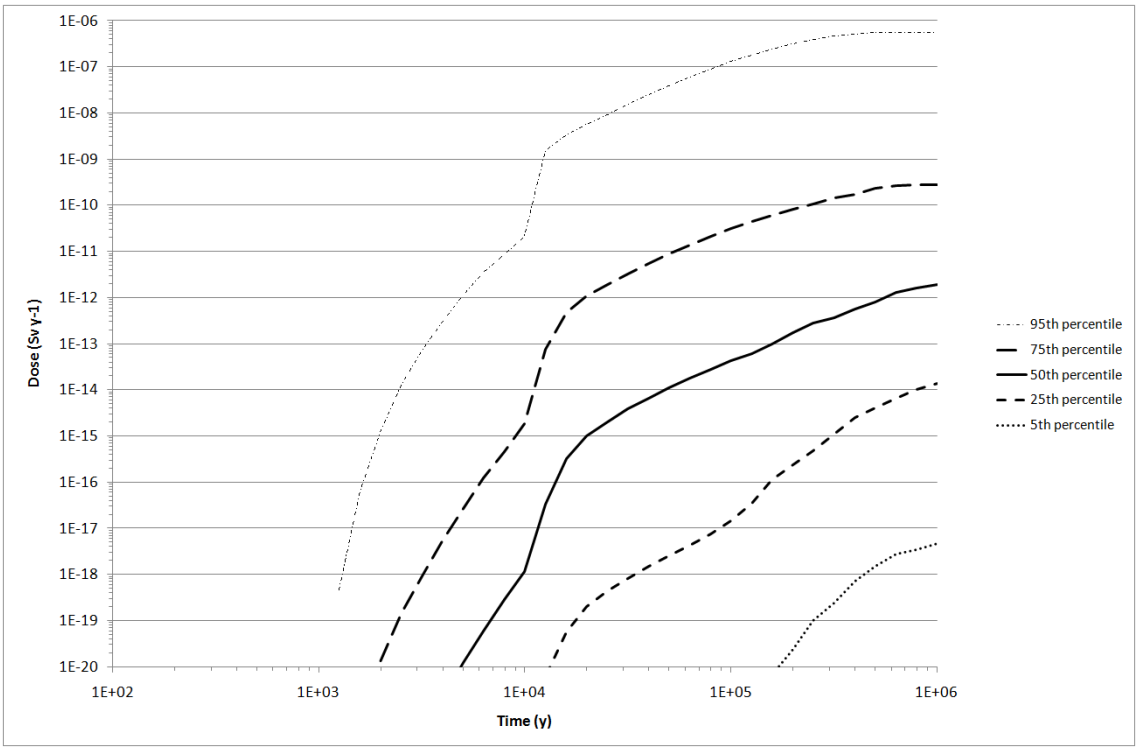

Case F1 Far-Field with Small Penetration Depth

This probabilistic case is identical to the reference case F0, with the exception that the penetration depth is not sampled but set to the fixed small value of 0.02 m. The total dose and the contribution to the total dose from the U-Th-Ra-Pb decay chain are shown in Figure 41 and Figure 42 respectively; there is little difference between this and the reference case (F0), though the 95th percentile is slightly lower for the total dose and all the percentile curves are lower for the U-Th-Ra-Pb dose contribution.

Figure 41: Total dose for case F1 (far-field with small penetration depth)

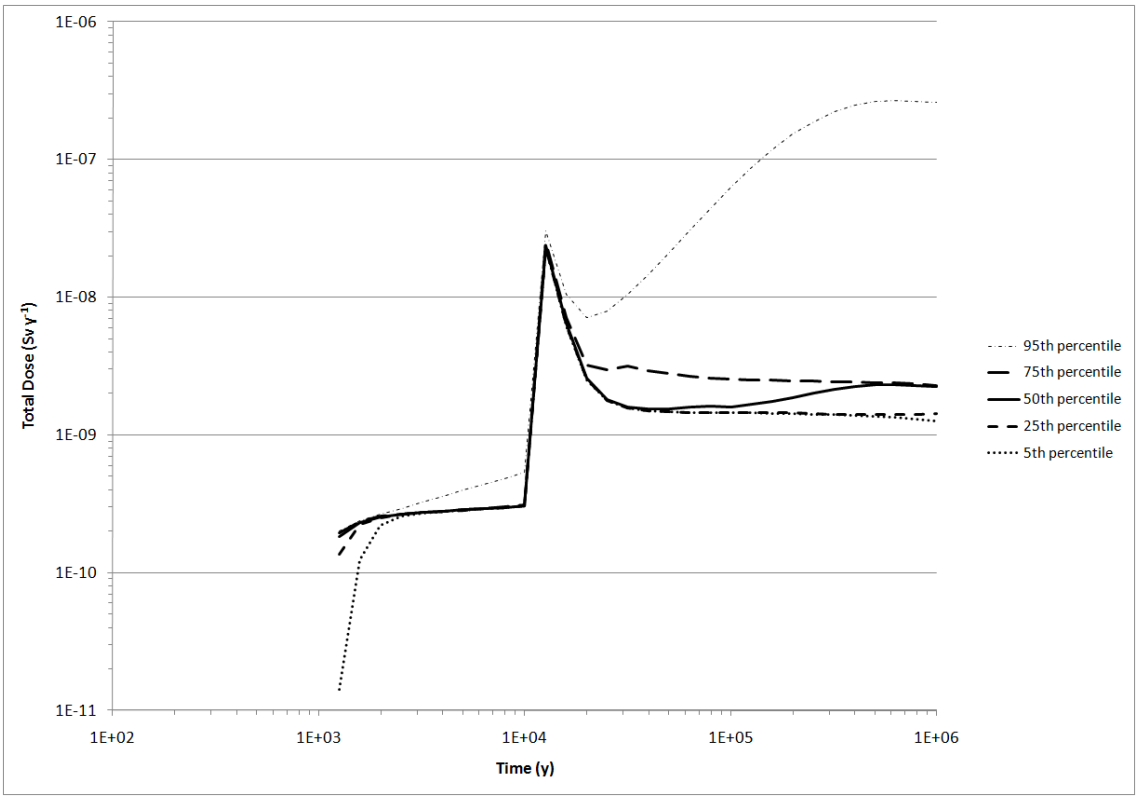

Figure 42: Contribution to the total dose from the U-Th-Ra-Pb decay chain for case F1 (far-field with small penetration depth)

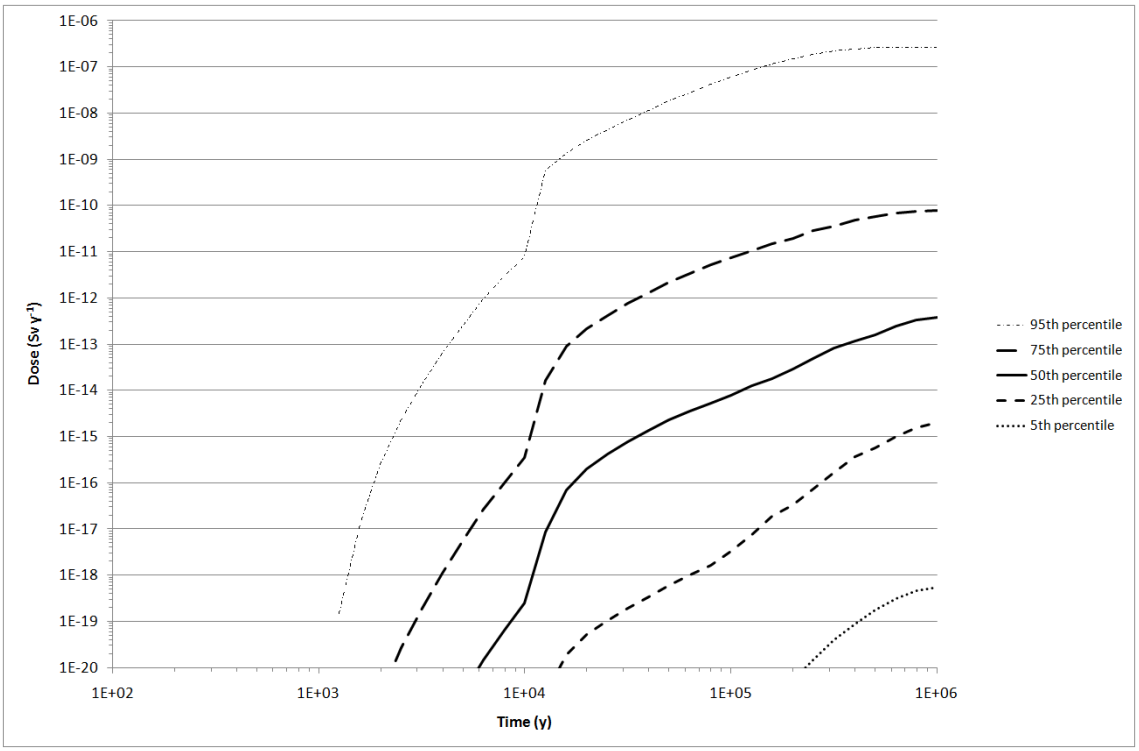

Case F2 Far-Field with Lower Ra Sorption Coefficient and Sampled Penetration Depth

The sorption coefficient for Ra in the rock matrix used by SKB in SR-Can differed quite considerably from that used in SR-97, as shown in Table 9. The ranges employed by SKB for SR-Can were 6.3e-2 to 11 m^3 kg^{-1} for non-saline waters and 6.4e-3 to 2.6 m^3 kg^{-1} for saline waters; the SR-97 values fall within these ranges but since log distributions were used, the peaks are situated at values at least an order of magnitude larger than the SR-97 values. For this case the upper limits of the SR-Can distributions were reduced by an order of magnitude to better represent the SR-97 values. The correlations between nuclides were retained.

Table 9: Comparison of K_d values for granite rock for Ra used in SR-97 and SR-Can; all values are given in m^3 kg^{-1}.

SR-97 (SKB (1999) Table 2-13)		SR-Can (SKB (2006b), Table A-43)	
Reasonable Aberg	**Reasonable Beberg and Ceberg**	**Non-saline best estimate**	**Saline best estimate**
0.02	0.1	1.3	2.1

A percentile plot of the total dose for this case is shown in Figure 43, with the reference case results (case F0) shown in grey for comparison. There is very little difference

between the two cases, although the 95th percentile is raised slightly by the smaller sorption coefficient for Ra.

Figure 43: Total dose for case F2 (far-field with sampled penetration depth and reduced Ra K_d), with the results from case F0 included for comparison.

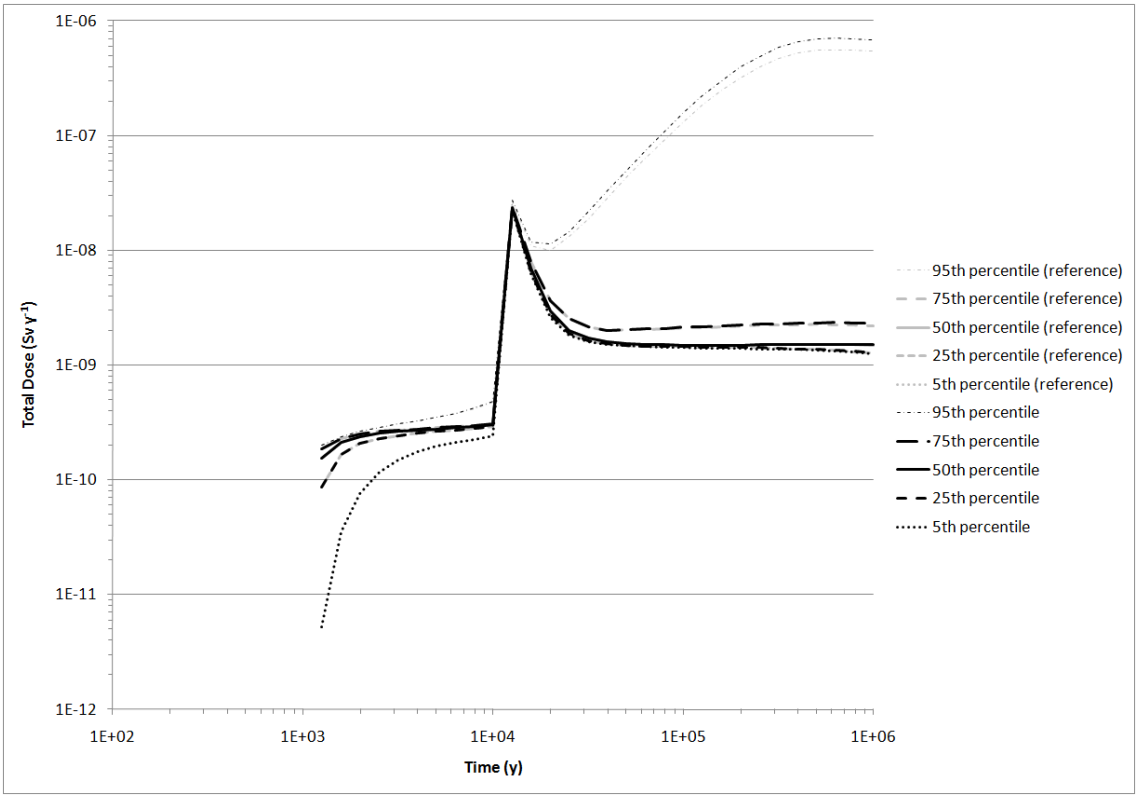

The contribution to the total dose from the U-Th-Ra-Pb decay chain is shown in Figure 44, again with the results from the reference case (F0) shown in grey for comparison. The difference between the doses for the two cases decreases with the higher percentiles; at the 95th percentile the two cases give similar results (on a log scale). Overall it is clear that reducing the sorption coefficient for Ra causes a slightly higher dose.

Figure 44: Contribution to the total dose from the U-Th-Ra-Pb decay chain for case F2 (far-field with sampled penetration depth and reduced Ra K_d), with results from case F0 included for comparison.

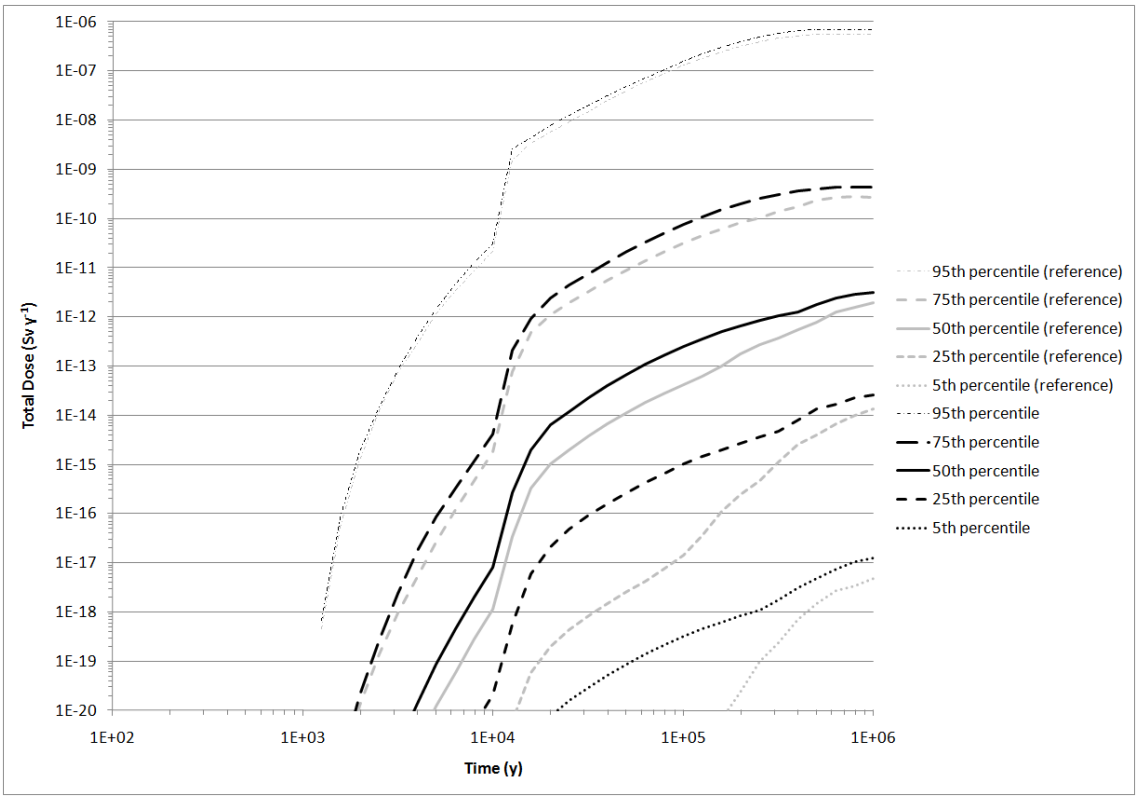

Case F3 Far-Field with Lower Ra Sorption Coefficient and Small Penetration Depth

This case is based on case F1, using a small matrix penetration depth, but employs the reduced range of Ra sorption coefficients described above for case F2. Plots of the total dose and the contribution from the U-Th-Ra-Pb decay chain are shown in Figure 45 and Figure 46 respectively, along with the results from case F1 shown in grey for comparison. The effects of reducing the sorption coefficient for Ra are very similar to those seen in case F2, with slightly higher doses observed.

Figure 45: Total dose for case F3 (far-field with small penetration depth and reduced Ra K_d), with the results from case F1 included for comparison.

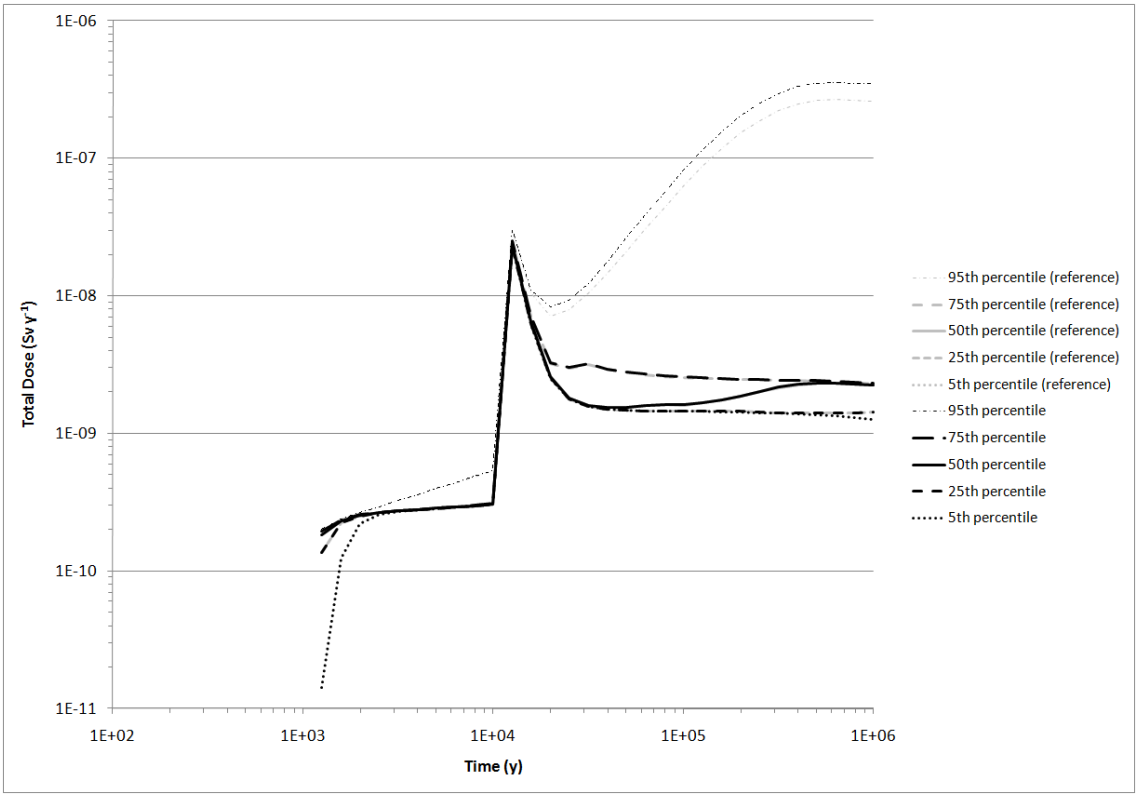

Figure 46: Contribution to the total dose from the U-Th-Ra-Pb decay chain for case F3 (far-field with small penetration depth and reduced Ra K_d), with results from case F1 included for comparison.

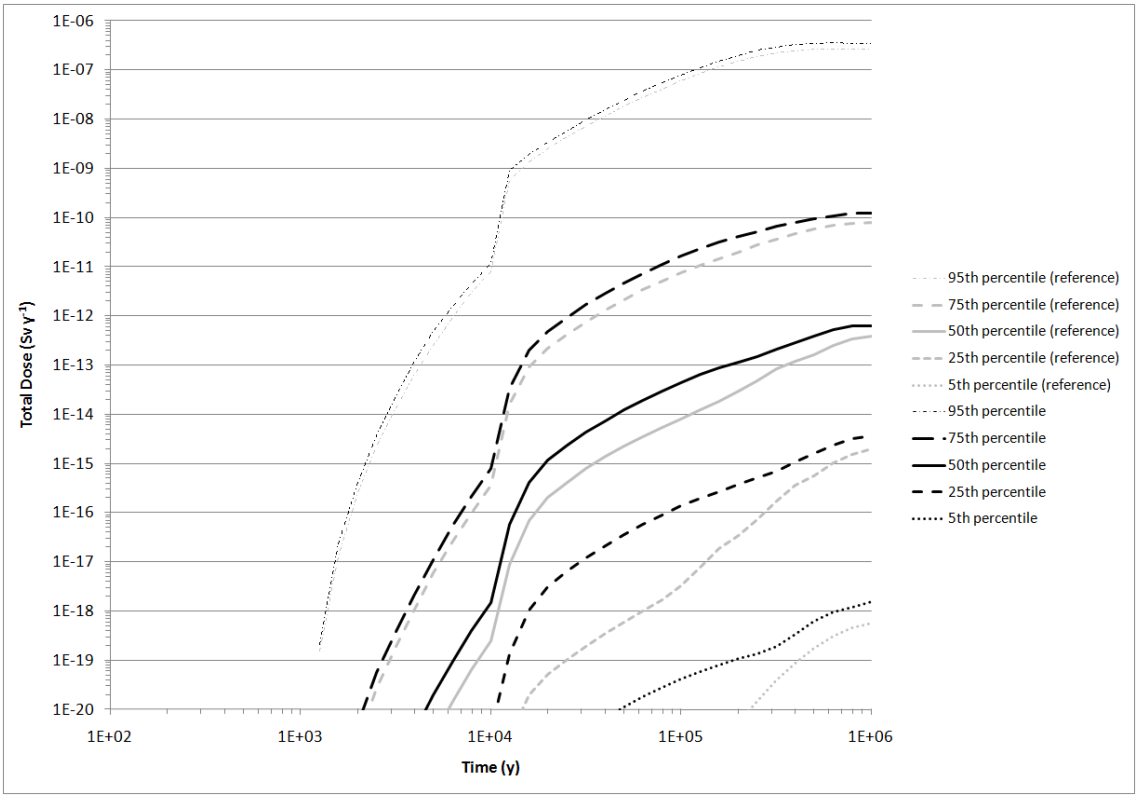

4.6 Conclusions

Parameter PDFs are required in order to undertake risk calculations; these are subjective, as they represent lack of knowledge, but are motivated by the knowledge that is available. Correlations arise because several parameters are related to a common underlying process (e.g. uncertainty in geochemistry affects all nuclides' properties). SKB aim to choose defensible PDFs and correlations and document the justification. The objective of this task was to look for choices that affect the results most and hence where the strongest justification is needed.

The key parameters have been reviewed for the source-term, near-field and geosphere. Several issues have been identified, with some the implications are immediately clear; others required new calculations to be performed.

A key issue for the release overall is the resistance of the buffer-fracture interface. The importance of this interface is well-known and must continue to be a focus for the review. It is more important than the transport resistance offered by the buffer as a diffusive barrier. In particular, results are rather insensitive to details of the near-field sorption properties.

Of the near-field parameters, the larger IRFs had the biggest impact on the result; using the alternative values suggested by Johnson et al. (2005) resulted in an order of magnitude increase in the peak dose (both near-field and total).

Fuel dissolution rates are significant for later releases. Total amounts of radionuclides leaving the near-field are more sensitive to solubility limitation, but the release of shorter-lived nuclides depends on fuel dissolution rates. Near-field doses are more sensitive to the fuel dissolution rate distributions than to solubility limit distributions.

Using uncorrelated solubilities given in Duro et al. (2006) had no discernable effect on the dose; and the use of sorption coefficients for bentonite in saline and non-saline groundwaters caused approximately a factor of 2 reduction in the peak dose.

In the far-field, the uncertainty is likely to be dominated by conceptual uncertainty (e.g. different discrete feature models) leading to different flow distributions.

As highlighted in Section 3, sorption values near the surface may be important for daughter nuclides and the particular case of Ra226 has been considered. The effects of reducing the K_d value for Ra were considered for both a small and a sampled matrix penetration depth. Since the K_d is proportional to the combination $\varepsilon_m R_m$ for sorbed nuclides, when the porosity contribution is negligible, this directly influences the matrix effects. In both cases the smaller sorption coefficient led to a smaller total dose.

5 Quantifying the Role of the Different Barriers

5.1 Introduction

According to the regulations (SKI, 2002), the safety assessment should "…include sequences of events and conditions that are selected and studied independently of probabilities in order to, inter alia, illustrate the significance of individual barriers and barrier functions." The Safety Assessment Methodology (SAM) expert group that reviewed SR Can for SSI and SKI expressed the view that SKB should describe more explicitly how the different barriers contribute to the safety functions isolation and retardation (SKI and SSI, 2008).

Section 10.10 of the main SR Can report is relevant to this issue. To date, the authorities have not attempted to reproduce these calculations or to understand fully the approach that SKB used. The objective of the work described here is to understand the assumptions made by SKB and to attempt to reproduce these calculations.

The calculations presented by SKB are for a number of different cases with different barriers assumed not to be functioning, and these have been reproduced using variants of the AMBER case files employed in the SR-Can review. The probabilistic AMBER calculations are shown in Figure 47. These calculations are for the calculated mean dose and are directly comparable with Figure 10-53 of the main SR Can report. The calculations were undertaken with 1000 samples (3000 for the no copper cases), and so have not fully converged; this results in some 'noise' in some of the curves, particularly for relatively short timescales. The cause of the lack of convergence is the very sharp peak release of I129, occurring shortly after the failure time for the cast iron insert; this gives the potential for some risk dilution if the distribution of such times is too broad.

Based on the discussion in Appendix B of the main SR-Can report it is assumed that for the calculations with 'no buffer' SKB directed the flux of radionuclides out of the canister directly to the geosphere. In the AMBER calculations the original case with the intact buffer was modified to direct the flux from the canister to the geosphere, but using the same parameterisation for the near-field/fracture interface. Alternative, more realistic, approaches to representing radionuclide transport in the absence of a buffer are possible, but the details appear not to be important for consideration of the role played by the different barriers.

Figure 47: Probabilistic Calculations for Barrier Functions

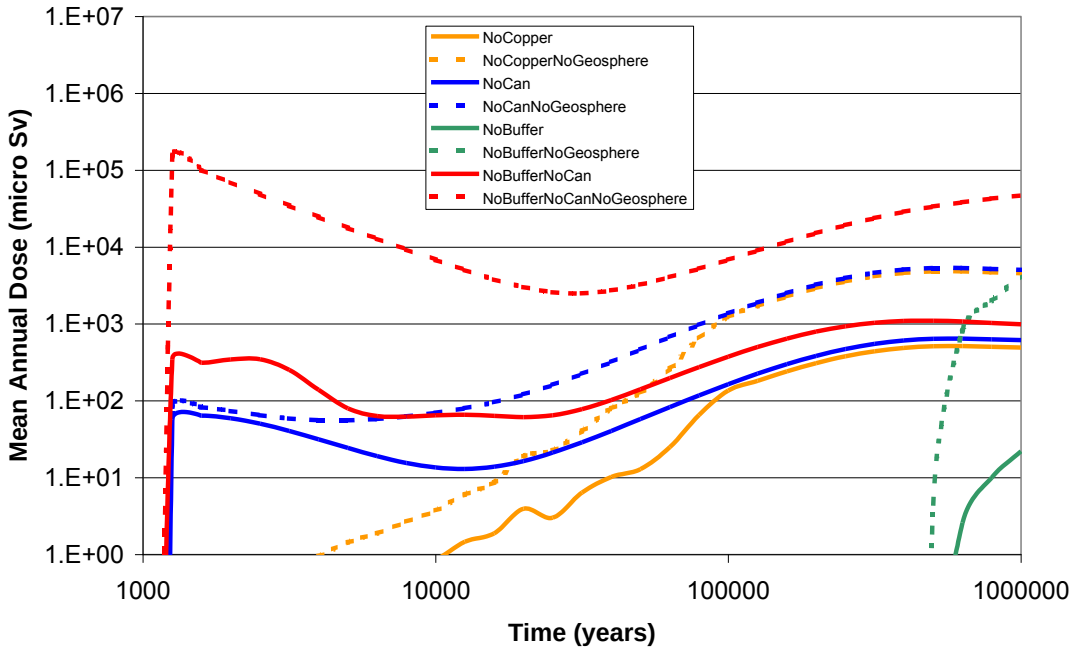

It can be seen that, to all intents and purposes, the SKB calculations have been fully reproduced. The peak doses for all the cases considered are very close to the SKB values with the exception of the NoBufferNoGeosphere case where the AMBER calculations are a couple of orders of magnitude higher at the end of the simulation period; the reason for this difference is not immediately apparent, although, as indicated in Section 2.1.2 there were several areas where the details of the original SKB calculations for this scenario were not clear.

Each of the calculation cases is discussed in turn in the following sections.

5.2 No Copper Shells

This case was considered to investigate the role played by the copper shells. The calculation was based on the pinhole scenario, but applied to all 6000 canisters, with the parameter describing the time taken for the cast iron insert to be penetrated (the AMBER parameter t_{large}) being triangularly distributed with parameters (0, 1E5 y, 1E5 y) so that the peak is at the maximum. As with the pinhole scenario calculations, the peak of the probabilistic calculation exceeds that for representative deterministic calculations (by typically half an order of magnitude) because of the high consequence runs at long times where Ra is the dominant radionuclide.

As indicated by SKB, the resulting peak dose is above the regulatory risk limit by around one-and-a-half orders of magnitude. If retention in the geosphere is neglected, this increases to about three orders of magnitude.

These calculations illustrate the key role played by the copper shells in SKB's safety case, but this depends critically on SKB's arguments for the slow rate of corrosion of copper in repository conditions (see below).

5.3 No Canisters

This calculation follows that for the 'no copper shells' case, but with the time taken for the cast iron insert to be penetrated being neglected. Figure 47 shows that the peak calculated dose is actually the same, because this is calculated to occur on long timescales after all the cast iron inserts have been penetrated in the 'no copper shells case'. The barrier provided by the cast iron inserts is seen to be more important if emphasis is placed on consequences for relatively early timescales.

5.4 No Buffer

SKB argue that the consequences for the case where the buffer does not provide a barrier to radionuclide transport for all 6000 deposition holes is little different from the consequences calculated for the advection scenario (see Section 2.1.2), with calculated peak doses only reaching the regulatory limit after around a million years even if radionuclide retention in the geosphere is neglected. This is because the SKB model for copper corrosion results in the onset of radionuclide release being very late; again only 10 canisters fail in the million year period considered. This calculation again emphasises the key role played by the copper shell in SKB's safety case, and the importance of copper corrosion modelling in the Performance Assessment. Calling this the no buffer case is perhaps misleading as the only aspect of the buffer that is omitted is the transport resistance. The role of the buffer in protecting the canister from flow remains.

5.5 No Canisters or Buffer

This calculation was produced by taking the 'no canisters' calculation and bypassing the transport resistance provided by the buffer. The calculated doses are typically half an order of magnitude higher than those calculated with the buffer intact. When retention in the geosphere is neglected, this difference becomes much larger, over two orders of magnitude, but the value of a calculation that neglects the canister, buffer and geosphere barriers is questionable.

SKB consider that this calculation is important because with only the fuel and geosphere barriers in place, calculated peak consequences are still 'only' comparable with background radiation. However, in this case, as illustrated in the work undertaken by Quintessa in the EU MICADO project, the fuel dissolution rate, which is not generally a key parameter when all the barriers are in place, would then be a critical.

5.6 Conclusions

The following conclusions can be drawn from the calculations considered for quantifying the role of different barriers:

- The SKB calculations presented in SR-Can have been satisfactorily reproduced, confirming that the basis for these calculations is adequately understood.
- The calculations emphasise the key role played by the copper shells in SKB's safety case, but this depends on the calculated slow rate of copper corrosion in repository conditions.
- The no buffer case here simply ignores the transport resistance of the buffer, and as previously documented, confirms that the role of the buffer as a barrier to radionuclide transport is minor compared with the other barriers. A case where there was actually no buffer would perform very differently as is seen in the buffer erosion scenario.
- With other barriers in place radionuclide retention in the geosphere is less important than other barriers, but when other barriers fail, this can be important in keeping calculated consequences to levels that are comparable with background radiation. In these cases the modelling of fuel dissolution can become much more important.
- The conclusions drawn about barrier performance depend critically on the timescales that are being considered. The calculations emphasise again the points made in Section 3 and 4 concerning the importance of the assumptions made about the transport of actinide decay chains members on long timescales.

6 Combining Scenarios

To date, SKB have considered various long-term scenarios in isolation. In particular, the buffer erosion scenario was treated independently from other scenarios. This means that there are no consequences from this scenario unless a canister is actually breached. However, it is entirely conceivable that buffer erosion occurs after some other process or event had led to the failure of a canister. In such a case, any radionuclides sorbed on the buffer material that is eroded would be released.

Here consideration is given to this possibility by combining calculations for the pin-hole and buffer erosion scenarios. The original deterministic AMBER calculation for the pin-hole scenario of Section 2.1.1 has been modified so that all transport rates associated with the buffer are greatly increased at a specified time. This simulates the sudden release of radioactivity sorbed on the buffer at the time in question. Note however that the geosphere behaviour is taken to be as with the intact buffer, in particular no colloidal transport is considered here. Calculations have been undertaken for a release time of 10^4, 10^5 and 10^6 y. The first of these corresponds to the time at which the pin hole is enlarged and the last of which corresponds to the original calculation as the release occurs at the end of the simulation period. The resulting calculated doses are shown in Figure 48.

Figure 48: Deterministic Calculations Combining the Pin-hole and Buffer Erosion Scenarios

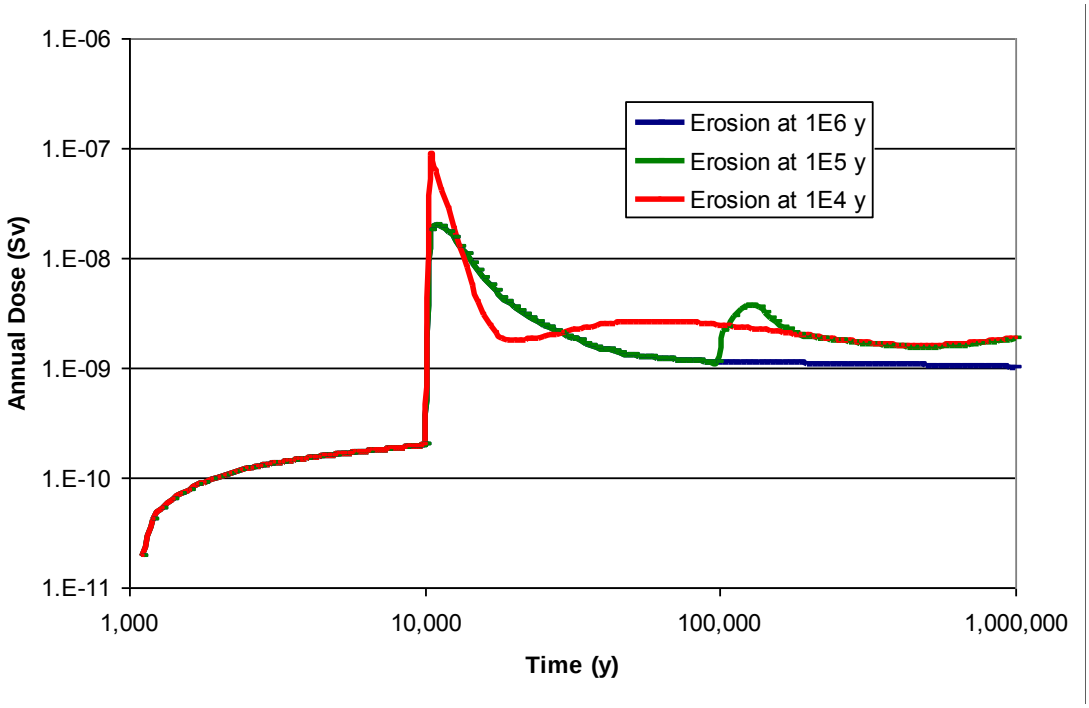

The calculated doses for the loss of buffer at 10^5 years is, as expected, identical to the original calculation up until the time of the loss of buffer event. When the buffer is lost calculated doses rise by about half an order of magnitude, and remain slightly higher for the remainder of the simulation period because of the loss of the buffer sorption capacity.

When the loss of buffer takes place at 10^4 years, the same time that the canister fully fails, dose rates again increase by around half an order of magnitude compared with the original calculation. Over long timescales the resulting doses are very similar to those calculated for the later buffer loss event.

These calculations show that it is straightforward to undertake calculations that combine different scenarios for system evolution. The calculations undertaken here also illustrate the conclusion drawn in Section 5.6 that role of the buffer as a barrier to radionuclide transport is minor compared with the other barriers.

7 Conclusions

Conclusions for each of the topics studied in this work have been presented separately. Here we summarise the most important findings for consequence analysis and the conduct of the SR Site review.

In the study of spatially varying properties, the following conclusions were made.

- The SKB F-factor approach is exact only in the case of a single nuclide, constant matrix properties and no dispersion. Compared to other sensitivities, the effect of dispersion for Peclet numbers 10 and higher is small.

- Output fluxes are highly sensitive to the F-factor itself, but not to the water travel time. Matrix penetration depth can be important if it is small, (less than about 10 cm in the cases considered here). The retention and porosity in the matrix have a direct proportional effect on peak releases for the single sorbed nuclide.

- Varying matrix retention properties along a flow path can be handled exactly for a single nuclide, a result that SKB may be unaware of.

- The main approximation that can occur with the F-factor approach is in the use of constant matrix retention properties for a chain case. When there are short-lived daughters, their output fluxes are strongly influenced by the matrix retention properties at the end of the path rather than by any overall average.

- Cases using path lines generated using SSM's independent discrete feature model showed that the EDZ can dominate the F-factor for many release points. In such cases, the properties of this EDZ control the output flux. The approach that SKB take to the EDZ in SR Site should be a focus for review. The relevance of such issues will depend on which canister failure scenarios are considered – if failures can only occur by buffer erosion then this is likely to be where flows are at their highest and path lines from such locations may not pass through the EDZ.

For the study of PDFs, key parameters have been reviewed for the source-term, near-field and geosphere. The following conclusions were reached.

- A key issue for the release overall is the resistance of the buffer-fracture interface. The importance of this parameter is well-known and must continue to be a focus for the review. It is more important that the transport resistance offered by the buffer as a diffusive barrier. In particular, results are rather insensitive to details of the near-field sorption properties.

- Of the near-field parameters, the larger IRFs had the biggest impact on the result; using the alternative values suggested by Johnson et al. (2005) resulted in an order of magnitude increase in the peak dose (both near-field and total).

- Fuel dissolution rates are significant for later releases. Near-field doses are more sensitive to the fuel dissolution rate distributions than to solubility limit distributions.

- The use of uncorrelated radionuclide solubilities given in Duro et al. (2006) had no discernable effect on the dose; and the use of sorption coefficients for bentonite in saline and non-saline groundwaters caused approximately a factor of 2 reduction in the peak dose.

- In the far-field, the uncertainty is likely to be dominated by conceptual uncertainty (e.g. different discrete feature models) leading to different flow distributions.

- The effects of reducing the matrix K_d value for Ra were considered for both a small and a sampled (effectively infinite) matrix penetration depth. In both cases the smaller sorption coefficient led to a smaller total dose.

The SKB calculations for the role of the various barriers presented in SR-Can have been satisfactorily reproduced, confirming that the basis for these calculations is well understood. In particular, the following conclusions were reached.

- The calculations emphasise the key role played by the copper shells in SKB's safety case, but this depends on the calculated slow rate of copper corrosion in repository conditions.

- As previously documented, the role of the buffer as a barrier to radionuclide transport is minor compared with the other barriers. The case presented has just the transport resistance of the buffer neglected; a case with no buffer would behave very differently.

- With other barriers in place radionuclide retention in the geosphere is less important than other barriers, but when other barriers fail, it can be important in keeping calculated consequences to levels that are comparable with background radiation. In these cases, modelling of fuel dissolution can become much more important.

Looking at the impact of combined scenarios, the following conclusion was reached.

- A combined pinhole and erosion scenario could give spike release of factor 3 higher than pinhole alone, even without enhanced transport in the geosphere that might occur due to colloids arising from the buffer erosion.

References

Andersson J, Hermanson J, Elert M, Gylling B, Moreno L and Selroos J-O (1998). Derivation and treatment of the flow-wetted surface and other geosphere parameters in the transport models FARF31 and COMP23 for use in safety assessment, SKB report R-98-60, Svensk Kärnbränslehantering AB.

Bateman H (1910). Solution of a System of Differential Equations Occurring in The Theory of Radioactive Transformation. Proc. Cambridge Phil. Soc. 15:423-427.

Birgersson M and Karnland O (2009). Ion Equilibrium between Montmorillonite Interlayer Space and an External Source – Consequences for Diffusional Transport. Geochimica et Cosmochimica Acta 73, 1908-1923. Doi:10.1016/j.gca.2008.11.027.

Bond A E, Maul PR, Savage D, Wilson J (2009). The Use of QPAC-EBS for Project THERESA Full-Scale Tests. Quintessa Report to SSM, QRS-3009A-2, version 2.0.

Carslaw H S and Jaeger J C (1959). Conduction of Heat in Solids, 2nd Edition, Oxford University Press.

Duro L, Grivé M, Cera E, Domènech C and Bruno J (2006). Determination and Assessment of the Concentration Limits to be used in SR-Can. SKB TR-06-32, Svensk Kärnbränslehantering AB.

Elert M, Gylling B and Lindgren M (2004). Assessment Model Validity Document FARF31. SKB R-04-51, Svensk Kärnbränslehantering AB.

Geier J (2008). Discrete Feature Modelling (DFM) User Documentation. SKI Report 2008:57.

Geier J (2009). Sample particle tracks for SSM transport modelling. E-mail dated 6th September 2009.

Hedin A (2003). Probabilistic Dose Calculations and Sensitivity Analyses using Analytic Models. Reliability Engineering and System Safety 79(2), 195-204.

Johnson L, Ferry C, Poinssot C and Lovera P (2005). Spent Fuel Radionuclide Source-term Model for Assessing Spent Fuel Performance in Geological Disposal. Part 1: Assessment of the Instant Release Fraction. Journal of Nuclear Materials, 346, 56-65.

Maul P R and Robinson P C (2008). Radionuclide Transport Calculations in Preparation for the Review of SR-Site. Quintessa Report to SSM QRS-1097K-1 version 1.0.

Maul P R, Robinson P C, Bond A E and Benbow S J (2008). Independent Calculations for the SR-Can Assessment: External Review Contribution in Support of SKI's and SSI's Review of SR-Can, SKI Report 2008:12.

RETROCK (2005). Treatment of radionuclide transport in geosphere within safety assessments (Retrock), European Commission, Nuclear science and technology, EUR 21230 EN.

Robinson PC and Maul PR (1991). Some experience with the numerical inversion of Laplace transforms. Math. Engng Ind. Vol3 No 2, VSP 1991.

Selroos J-O (1996). Mass Transfer Effects on Tracer Tests in a Heterogeneous Rock Fracture. Nordic Hydrology 27 (4) 215-230.

Selroos J-O and Cvetkovic V (1996). On the characterisation of retention mechanisms in rock fractures. SKB report TR-96-20, Svensk Kärnbränslehantering AB.

SKB (2006a). Long-term Safety for KBS-3 Repositories at Forsmark and Laxemar – a First Evaluation: Main Report of the SR-Can project, SKB TR-06-09, Svensk Kärnbränslehantering AB.

SKB (2006b). Data report for the safety assessment SR-Can, SKB TR-06-25, Svensk Kärnbränslehantering AB.

SKI (1991). SKI Project-90: Volume 1. SKI Technical Report 91:23.

SKI (2002). The Swedish Nuclear Power Inspectorate's Regulations concerning Safety in connection with the Disposal of Nuclear Material and Nuclear Waste, SKIFS 2002:1.

SKI and SSI (2008). SKI's and SSI's Review of SKB's Safety Report SR-Can. SKI Report 2008:23. SSI Report 2008:04 E.

Smith P, Nordman H, Pastina B, Snellman M, Hjerpe T and Johnson L (2007). Safety Assessment for a KBS-3H Spent Nuclear Fuel Repository at Olkiloto: Radionuclide Transport Report. Posiva Report 2007-07, Posiva Oy.

Talbot A (1979). The Accurate Numerical Inversion of Laplace Transforms. J. Inst. Math. Appl. 23.

Wilmot R D (2009). Report on a Meeting: Consequence Analyses February 2009. Galson Sciences Report to SSM 0908-1 version 1.0.

Worgan K J and Robinson PC (1995), The CRYSTAL Geosphere Transport Model: Technical Documentation Version 2.1. SKI Report 95:55.

Appendix A Nomenclature

An overbar denotes the Laplace transform throughout the report.

Symbol	Description
a_m	limited matrix diffusion depth [m]
C_f^n	concentration of nuclide *n* in the flowing water [moles/m^3]
C_m^n	concentration of nuclide *n* in the matrix water [moles/m^3]
D_{eff}^n	effective diffusion coefficient for nuclide *n* [m^2/year]
D_f^n	dispersion/diffusion coefficient for nuclide *n*. $D_f^n = \frac{vL}{Pe} + D_{eff}^n$ [m^2/y]
D_m^n	matrix effective diffusion coefficient for nuclide *n*. [m^2/y]
F	F factor $= L\delta_f / v$ [y/m]
G_{in}^n	specified flux at *x=0* for nuclide *n* [mol/y]
G_{out}^n	output flux for nuclide *n* [mol/y]
$H()$	Heaviside function
h	fracture aperture [m]
$K_{a,m}^n$	area-based sorption coefficient of nuclide *n* for the matrix [m^3/m^2]
$K_{d,m}^n$	matrix sorption coefficient of nuclide *n* [m^3/kg]
L	leg length [m]
Pe	Peclet number (for dispersion) [-]
Q	flow rate in a flow tube [m^3/y]
Q_{eq}	equivalent flow rate [m^3/y]
q	Darcy velocity [m/y]
R_f^n	retardation (due to surface sorption if any) of nuclide *n* [-]
R_m^n	retention factor in the matrix of nuclide *n* [-]
s	Laplace variable [y^{-1}]
S	solubility limit [mol/m^3]
t	time [y]
t_{large}	time for enlargement of canister pin hole [y]
t_w	water travel time [y]

t'_w	travel time with retardation in the flowing feature [y]
w	flow tube width [m]
x	distance along the flow tube [m]
v	water velocity [m/year]
z	distance into the rock matrix [m]
α	instantaneous release fraction [-]
β_m	factor in solution of matrix transport equation , = $\sqrt{\varepsilon_m R_m D_m}$ [m/y$^{1/2}$]
δ_f	surface area of matrix per unit volume of flowing water [m^2/m^3]
γ_{adv}	exponent in solution of non-dispersive transport equation [-]
ε_m	matrix porosity [-]
λ^n	decay constant for nuclide n [per year]
λ_F	fuel dissolution rate [per year]
μ	term in solution of dispersive transport equation [-]
ϕ	factor in solution of matrix transport equation, = $\sqrt{\frac{\varepsilon_m R_m (\lambda + s)}{D_m}}$ [m^{-1}]
ρ_m	matrix grain density [kg/m^3]

Appendix B General Solution for a Decay Chain for a Single Segment

Here, we present the general solution for advection and dispersion in the fracture and a finite matrix with constant properties. The basic approach follows Worgan and Robinson (1995) with a simpler approach to the rock matrix solution.

For completeness, we restate the equations and boundary conditions from the main text.

$$R_f^n \frac{\partial C_f^n}{\partial t} = D_f^n \frac{\partial^2 C_f^n}{\partial x^2} - v\frac{\partial C_f^n}{\partial x} - \lambda^n R_f^n C_f^n + \lambda^{n-1} R_f^{n-1} C_f^{n-1} + \delta_f D_m^n \left.\frac{dC_m^n}{dz}\right|_{z=0} \tag{B.1}$$

$$\varepsilon_m R_m^n \frac{\partial C_m^n}{\partial t} = D_m^n \frac{\partial^2 C_m^n}{\partial z^2} - \lambda^n \varepsilon_m R_m^n C_m^n + \lambda^{n-1} \varepsilon_m R_m^{n-1} C_m^{n-1} \tag{B.2}$$

$$hw\left[vC_f^n - D_f^n \frac{dC_f^n}{dx} \right]_{x=0} = G_{in}^n \tag{B.3}$$

$$\left[pC_f^n + q\frac{dC_f^n}{dx} \right]_{x=L} = 0 \tag{B.4}$$

$$\left[C_m^n\right]_{z=0} = C_f^n \tag{B.5}$$

$$\left[\frac{dC_m^n}{dz} \right]_{z=a_m} = 0 \tag{B.6}$$

Where we have introduced p and q in (B.4) to generalise the downstream boundary condition – one of them will be zero and the other unity.

The result of interest is the flux at the far end:

$$G_{out}^n = hw\left[vC_f^n - D_f^n \frac{dC_f^n}{dx} \right]_{x=L} . \tag{B.7}$$

We start by Laplace-transforming and solving (B.2) with the boundary conditions (B.5) and (B.6).

We write the Laplace-transformed solution as a matrix times the fracture concentrations:

$$\overline{C}_m^n = \sum_{r=1}^{n} M_m^{nr} \overline{C}_f^r \,. \tag{B.8}$$

Then, the solution for each matrix can be written

$$M_m^{nr} = \sum_{k=r}^{n} U_m^{nk} V_m^{kr} \frac{\cosh[\phi^k (a_m - z)]}{\cosh[\phi^k a_m]}, \tag{B.9}$$

where

$$\phi^k = \sqrt{\frac{\varepsilon_m^k R_m^k (\lambda^k + s)}{D_m^k}} \,. \tag{B.10}$$

It then follows that

$$U_m^{nn} = 1, \tag{B.11}$$

$$U_m^{nr} = \frac{\lambda^{n-1} \varepsilon_m^{n-1} R_m^{n-1} U_m^{n-1,r}}{\varepsilon_m^n R_m^n (\lambda^n + s) - \dfrac{D_m^n}{D_m^r} \varepsilon_m^r R_m^r (\lambda^r + s)} \tag{B.12}$$

$$V_m^{rk} = 0 \quad \text{if} \quad r < k \,, \tag{B.13}$$

$$V_m^{kk} = 1, \tag{B.14}$$

$$V_m^{rk} = -\sum_{l=k}^{r-1} U_m^{rl} V_m^{lk} \quad \text{if} \quad r > k \,. \tag{B.15}$$

The required contribution to the fracture equation can then be written

$$\delta_f D_m^n \left. \frac{d\overline{C}_m^n}{dz} \right|_{z=0} = -\sum_{r=1}^{n} E_m^{nr} \overline{C}_f^r \,, \tag{B.16}$$

$$E_m^{nr} = \delta_f D_m^n \sum_{k=r}^{n} U_m^{nk} V_m^{kr} \phi^k \tanh[\phi^k a_m] \,. \tag{B.17}$$

In the infinite matrix case the final tanh term simply becomes unity.

Substituting this into a transformed version of (B.1) gives the equation

$$g^n \overline{C}_f^n = D_f^n \frac{d^2 \overline{C}_f^n}{dx^2} - v \frac{d\overline{C}_f^n}{dx} + \lambda^{n-1} R_f^{n-1} \overline{C}_f^{n-1} - \sum_{r=1}^{n-1} E_m^{nr} \overline{C}_f^r \,, \tag{B.18}$$

where

$$g^n = R_f^n (\lambda^n + s) + E_m^{nn} \,. \tag{B.19}$$

The solution to this system can be written

$$\overline{C}_f^n = \frac{1}{hw}\sum_{r=1}^{n} U_f^{nr}\left[a_+^r \exp(-\alpha_+^r x) + a_-^r \exp(-\alpha_-^r x)\right], \tag{B.20}$$

where

$$\alpha_\pm^r = \frac{-v \pm \sqrt{v^2 + 4D_f^r g^r}}{2D_f^r}, \tag{B.21}$$

$$U_f^{nn} = 1, \tag{B.22}$$

$$(g^n - g^r)U_f^{nr} = R_f^{n-1}\lambda^{n-1}U_f^{n-1,r} - \sum_{k=r}^{n-1} E_m^{nk}U_f^{kr}, \tag{B.23}$$

and the $a_\pm^r$ coefficients are chosen to match the boundary conditions. This results in another recurrence relationship

$$V_f^1 = \overline{G}_{in}^1, \tag{B.24}$$

$$V_f^n = \overline{G}_{in}^n - \sum_{k=1}^{n-1} U_f^{nk}V_f^k, \tag{B.25}$$

and then

$$\begin{pmatrix} v + D_f^r\alpha_+^r & v + D_f^r\alpha_-^r \\ \left(p + q\alpha_+^r\right)e^{-\alpha_+^r L} & \left(p + q\alpha_-^r\right)e^{-\alpha_-^r L} \end{pmatrix}\begin{pmatrix} a_+^r \\ a_-^r \end{pmatrix} = \begin{pmatrix} V_f^r \\ 0 \end{pmatrix}, \tag{B.26}$$

Finally

$$\overline{G}_{out}^n = \sum_{r=1}^{n} U_f^{nr}\left[a_+^r\left(v + D_f^r\alpha_+^r\right)\exp(-\alpha_+^r L) + a_-^r\left(v + D_f^r\alpha_-^r\right)\exp(-\alpha_-^r L)\right]. \tag{B.27}$$

In the case of no diffusion or dispersion in the fracture only the a_+^r terms survive and we can write

$$\overline{G}_{out}^n = \sum_{r=1}^{n} U_f^{nr}V_f^r \exp(-\alpha_+^r L). \tag{B.28}$$

Strålsäkerhetsmyndigheten
Swedish Radiation Safety Authority

SE-171 16 Stockholm
Solna strandväg 96

Tel: +46 8 799 40 00
Fax: +46 8 799 40 10

E-mail: registrator@ssm.se
Web: stralsakerhetsmyndigheten.se